

**UNCLASSIFIED**

---

**AD 273 495**

*Reproduced  
by the*

**ARMED SERVICES TECHNICAL INFORMATION AGENCY  
ARLINGTON HALL STATION  
ARLINGTON 12, VIRGINIA**



---

**UNCLASSIFIED**

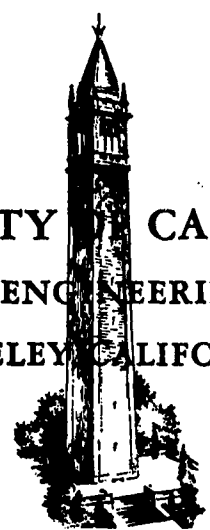
NOTICE: When government or other drawings, specifications or other data are used for any purpose other than in connection with a definitely related government procurement operation, the U. S. Government thereby incurs no responsibility, nor any obligation whatsoever; and the fact that the Government may have formulated, furnished, or in any way supplied the said drawings, specifications, or other data is not to be regarded by implication or otherwise as in any manner licensing the holder or any other person or corporation, or conveying any rights or permission to manufacture, use or sell any patented invention that may in any way be related thereto.

62273495

RECEIVED  
15 JAN 1962

TECHNICAL REPORT  
HE-150-182

UNIVERSITY OF CALIFORNIA  
INSTITUTE OF ENGINEERING RESEARCH  
BERKELEY CALIFORNIA



---

AN EXPERIMENTAL INVESTIGATION OF FREE MOLECULE  
MOMENTUM TRANSFER BETWEEN GASES  
AND METALLIC SURFACES

---

by

Robert Erwin Stickney

(145) 1962  
11.0-8

RECEIVED  
HARVARD  
N-62-2-6  
JAN 25 1962

SERIES NO. 20  
ISSUE NO. 134  
DATE January 25, 1962

CONTRACT N-onr-222(45)  
REPORT NO. HE-150-182  
SERIES NO. 20-134  
JANUARY 25, 1962

JOINTLY SPONSORED BY THE  
OFFICE OF NAVAL RESEARCH AND  
THE OFFICE OF SCIENTIFIC RESEARCH

---

AN EXPERIMENTAL INVESTIGATION OF FREE MOLECULE  
MOMENTUM TRANSFER BETWEEN GASES  
AND METALLIC SURFACES

---

by

Robert Erwin Stickney

Submitted in partial satisfaction of the  
requirements for the degree of Doctor of  
Philosophy in Mechanical Engineering

Reproduction in whole or in part is permitted  
for any purpose of the United States Government

FACULTY INVESTIGATORS:

S. A. SCHAAF, PROFESSOR OF ENGINEERING SCIENCES  
L. TALBOT, ASSOCIATE PROFESSOR OF AERONAUTICAL SCIENCES  
G. J. MASLACH, PROFESSOR OF AERONAUTICAL ENGINEERING

Approved



# ABSTRACT

Measurements of the normal momentum transfer between gases and metallic surfaces were obtained under conditions of free molecule flow by means of a torsion balance and molecular beam apparatus. Helium, hydrogen, neon, nitrogen, argon, and carbon dioxide were investigated on tungsten, platinum-blackened-tungsten, platinum, and aluminum surfaces which were most likely contaminated with oxides and adsorbed gases. In the majority of the tests a thermal beam of gas molecules was directed against a heated test surface at normal incidence; a small number of tests were performed at oblique angles of incidence. Momentum transfer measurements were obtained with the surface at various temperatures, the range being from 25° to 550° C.

The experimental results indicate that the efficiency of the momentum transfer process increases with the molecular weight of the test gas and the roughness of the test surface, but is relatively independent of the surface material under the present conditions. The momentum transfer rates for helium and hydrogen are significantly less than those measured for the heavier gases at the same surface temperature. The accommodation of the test gases to the surface temperature appears to be incomplete except, possibly, for argon and carbon dioxide. The results obtained for each gas-surface combination are used to estimate the values of two different accommodation coefficients, the coefficient of translational energy transfer and a modified form of the coefficient of normal momentum transfer.

## TABLE OF CONTENTS

	<u>Page</u>
ABSTRACT	i
1.0 INTRODUCTION	1
1.1 Investigations of Particle-Surface Interactions	1
1.2 Objectives of the Proposed Investigation	2
2.0 PRELIMINARY CONSIDERATIONS	4
2.1 Introductory Remarks	4
2.2 The Basic Features of Molecular Beams	4
2.3 General Considerations of Momentum Transfer Measurements	6
2.4 The Use of a Torsion Balance for Momentum Transfer Measurements	7
2.5 Discussion of Preliminary Designs and Experiments	9
3.0 THE PROPOSED EXPERIMENTAL PROGRAM	15
3.1 General Considerations	15
3.2 Analysis of the Constant Pressure Procedure	17
3.3 Analysis of the Constant Torque Procedure	18
4.0 EXPERIMENTAL APPARATUS	21
4.1 General Description	21
4.2 Vacuum System	22
4.3 Auxiliary Apparatus	23
4.3.1 The Lamp and Scale	23
4.3.2 The Projector	24
4.3.3 The Gas Supply System	24
4.3.4 The McLeod Gauge	25

4.4	Molecular Beam Apparatus	25
4.5	Torsion Balance Apparatus	27
4.5.1	General Remarks	27
4.5.2	The Dummy Surface	29
4.5.3	Test Surface Materials	30
5.0	THE EXPERIMENTAL PROGRAM	32
5.1	The Experimental Procedures	32
5.1.1	Constant Torque Procedure	33
5.1.2	Constant Pressure Procedure	35
5.2	Direct Measurements of Surface Temperature	37
5.3	Methods for Interpreting the Experimental Data	39
5.3.1	The Normal Momentum Interpretation (Normal Incidence)	39
5.3.2	The Translational Energy Interpretation (Normal Incidence)	45
5.3.3	The Translational Energy Interpretation (Oblique Incidence)	48
5.4	Experiments at Normal Incidence: Results and Conclusions	50
5.4.1	General Comments	50
5.4.2	Tungsten Surfaces	53
5.4.3	Blackened Tungsten Surfaces	54
5.4.4	Aluminum Surfaces	55
5.4.5	Platinum Surfaces	56
5.4.6	Overall Results and Conclusions	57
5.5	Experiments at Oblique Incidence: Results and Conclusions	58

6.0	CONCLUDING CONSIDERATIONS AND COMMENTS	61
6.1	Precision and Sensitivity	61
6.2	Accuracy and Sources of Error	61
6.3	Proposed Future Investigations	67
6.4	Comments on Particle-Surface Interaction Parameters Used in Rarefied Gas Dynamics	68
6.4.1	Introductory Remarks	68
6.4.2	The Energy Accommodation Coefficient	71
6.4.3	The Coefficient of Normal Momentum Transfer	75
6.4.4	The Coefficient of Tangential Momentum Transfer	78
6.4.5	Concluding Remarks on Accommodation Coefficients	79
APPENDIX 1.	AN ANALYSIS OF NORMAL MOMENTUM TRANSFER BASED ON AN "IDEAL MODEL". (Normal Incidence)	80
A1.1	Summary	80
A1.2	The Intensity of an "Ideal" Molecular Beam	84
A1.3	The Mean Speed of an "Ideal" Molecular Beam	86
A1.4	The Momentum Transported by an "Ideal" Molecular Beam	87
A1.5	The Mean Normal Velocity Component for Re-Emission from an Equilibrium Gas	89
A1.6	The Re-Emitted Normal Momentum for an Equilibrium Gas	89
APPENDIX 2.	THE APPLIED TORQUE AT ARBITRARY ANGLE OF INCIDENCE	91
A2.1	Introduction	91
A2.2	Theoretical Formulation of the Problem	91
A2.3	An Approximate Solution	93
A2.4	Results and Conclusions	95
	REFERENCES	97
	TABLES	102
	FIGURES	115



## 1.0 INTRODUCTION

### 1.1 Investigations of Particle-Surface Interactions

Increasing interest in the overlapping fields of rarefied gas dynamics, upper atmospheric physics, surface physics, and high-vacuum technology has served to stimulate research concerning particle-surface interactions, the study of the interaction between atomic or molecular particles and the surfaces of solid materials. One of the most important tasks is to gain a better understanding of the energy and momentum transfer processes associated with the interaction, and to determine how these processes are influenced by the velocity, angle of incidence, and chemical and physical nature of the gas molecule, as well as by the temperature, surface conditions, and chemical and physical nature of the solid material.

The first experimental investigations of particle-surface interactions were performed near the beginning of this century and are described in some of the basic kinetic theory textbooks<sup>1-3</sup>. A comprehensive discussion of more recent investigations has been prepared by Hurlbut<sup>4</sup>, and the obvious conclusion is that only a limited quantity of reliable results has been obtained.

A most interesting observation has been made in numerous experiments<sup>1-3</sup>: The molecules of a rarefied gas at temperature  $T_i$  which collide with a heated surface at temperature  $T_w$  do not necessarily attain complete thermal equilibrium with the surface and may therefore be re-emitted with an average energy which lies between the states  $T_i$  and  $T_w$ . This problem has been the subject of many investigations, the results of which indicate that the efficiency of

energy transfer is usually smaller for gases of low molecular weight and generally increases as the surface becomes more contaminated with adsorbed gases and oxides.

The fact that the energy transfer associated with particle-surface interactions is often an inefficient process leads one to inquire about the momentum transfer, a problem which has received much less attention. Since momentum is a vector quantity, investigators have divided the problem into two parts, one dealing with the transfer of momentum in directions which are tangent to the plane of the surface ("tangential momentum") and the other with the transfer of momentum in directions normal to the test surface ("normal momentum"). Some informative investigations of tangential momentum transfer have been performed using the rotating cylinder technique<sup>5</sup>; it seems, however, no significant work has been accomplished concerning normal momentum transfer, although recently there has been increased interest in such work because of its importance to the problem of determining the aerodynamic forces on bodies traveling through rarefied atmospheres<sup>6</sup>.

### 1.2 Objectives of the Proposed Investigation

The general purpose of the present investigation is to study the normal momentum transfer, or the normal stresses, in particle-surface interactions involving various gases and surface materials. The specific objective is to develop and utilize an experimental technique which is suitable for determining the dependence of normal momentum transfer on the following variables or conditions:

- (1) the chemical and physical nature of the surface materials

- (2) the nature of the surface contaminants, including oxides, adsorbed gases, etc.
- (3) the temperature of the surface material
- (4) the chemical and physical nature of the test gases
- (5) the angle of incidence of the impinging gas molecules
- (6) the velocity distribution of the impinging gas molecules.

This objective was not completely realized in the present investigation because the program was limited to experiments which could be accomplished with a relatively simple and inexpensive apparatus. Of the variables listed above, the first, third, and fourth were considered in some detail, while the fifth received only a small amount of attention due to lack of time and deficiencies in the apparatus (see Section 5.5). Both the fifth and sixth variables will be incorporated into a program which is planned for the near future using a modified form of the existing apparatus (see Section 6.3); it is not possible to include the second variable because the existing vacuum system does not provide the ultra-clean high vacuum conditions which are necessary for determining and controlling the contamination level of the test surfaces.

## 2.0 PRELIMINARY CONSIDERATIONS

### 2.1 Introductory Remarks

A system consisting of a molecular beam and a torsion balance was chosen for the present investigation. Some of the reasons for this selection are presented in Sections 2.2 to 2.4, along with a brief consideration of the basic features of molecular beams and torsion balances. The results of the developmental program and preliminary experiments are discussed in Section 2.5.

### 2.2 The Basic Features of Molecular Beams

In simplest terms a molecular beam is a directional flow of gas in which there is a negligible amount of collisions or interactions between molecules. A molecular beam is formed by allowing gas to flow, or more exactly, to effuse thermally from a low pressure chamber (the "source chamber") through an aperture (the "source slit") into a second chamber which is maintained at a still lower pressure. As illustrated in Fig. 1, a second aperture (the "defining slit") is used to form a molecular beam in the test chamber by allowing only a specific fraction of the molecules to pass.

There are two requirements which must be satisfied in order to obtain an "ideal" molecular beam, i.e., a collision-free maxwellian beam. First, the length of the mean free path of the gas in the source chamber must be larger than the dimensions of the source slit; this is accomplished by maintaining the source pressure at a sufficiently low value. The second requirement is that the defining chamber and the test chamber be evacuated to the extent that the residual gases cause a negligible amount of scattering, or attenuation, of the molecular beam.

The limits of these two requirements are not known with precision, and are discussed in more detail in references 7, 8, and 9. This matter will be considered again in later sections of this report.

Molecular beam techniques which have been developed and utilized by workers in various areas of physics and chemistry have proven to be well suited for investigations of particle-surface interactions. The major advantages gained by using a molecular beam in these studies are:

- (1) the experiment may be conducted under high vacuum conditions which permit one to have better control over the degree of surface contamination resulting from adsorbed gases.
- (2) the particle-surface interaction may be studied independent of the gas phase molecule-molecule interactions since it is possible to reduce the latter to a negligible effect (i.e., free molecule flow conditions).
- (3) the number flux, mean velocity, momentum, and energy of the molecules in the beam may be accurately calculated by kinetic theory if the requirements for an "ideal" molecular beam are sufficiently fulfilled.
- (4) the direction of the molecular beam particles is known and controlled by the geometry of the source and defining slits.

In particle-surface interaction studies it is desirable to know the state and flow properties of the molecular beam to a high degree of accuracy, and this information is provided by points (3) and (4) above if the beam is "ideal".

A kinetic theory analysis of an "ideal" molecular beam is presented in Appendix 1. An expression is derived for the rate at which molecules from a source slit of area  $S$  strike a test surface of area  $S'$  which is located a distance  $l$  from  $S$ . For the special case of a small test surface perpendicular to the centerline of the molecular beam this rate, generally known as the molecular beam intensity, is given by Eq. (A1.25):

$$N = \frac{P S S'}{2 \pi l^2} \left[ \frac{2}{m \pi k T_1} \right]^{1/2} \quad (2.1)$$

where  $m$  is the molecular mass,  $k$  is the Boltzmann constant, and  $P$  and  $T_1$  are pressure and temperature of the gas in the source chamber. It should be emphasized that this equation is restricted to the case of normal incidence, i.e., the direction of the molecular beam is normal to the test surface. The validity of Eq. (2.1) is discussed in Section 2.5 and in Appendices 1 and 2.

### 2.3 General Considerations of Momentum Transfer Measurements

One of the first questions to be considered in the design of an experiment is whether it is more advantageous to use direct or indirect measurements techniques. In the present case this means a choice between:

- (1) measuring the quantity of interest, the momentum transfer, directly by a physical technique
- (2) inferring the momentum transfer from the results of indirect measurements.

The first method requires a force measurement which might be achieved by mounting the test surface on a suitable balance; the second method could be accomplished by measuring the velocity and angular distribution of the molecules before and after scattering from the surface as this information would be sufficient to determine the momentum transfer (and also the energy transfer in most cases).

Both of the above methods are being considered at present in the University of California Aeronautical Sciences Laboratory; this report presents the results obtained using a direct measurement technique.

#### 2.4 The Use of a Torsion Balance for Momentum Transfer Measurements

The direct measurement of momentum transfer in particle-surface interactions has historically proven to be very difficult because of the extremely small magnitude of the force to be measured. Several different designs of force (or torque) measuring balances appear to be suitable<sup>10-12</sup>, but the "radiometer-type" torsion balance was selected for this experiment because of its simplicity. This type of torsion balance has been used to study radiometer forces<sup>1,2</sup>, vapor pressures<sup>13</sup>, and molecular beam velocities<sup>14</sup> and flow fields<sup>15</sup>. It has been applied to investigations of particle-surface interactions by Mitani, et. al.<sup>16</sup>, Bassett<sup>7</sup>, Holister, et.al.<sup>17</sup>, and Carpenter<sup>18</sup>. The results of these experiments have been very limited due to the fragile nature of the torsion fibers and instabilities resulting from mechanical vibrations and electrostatic charge effects, as well as to the extremely small magnitudes of the forces to be measured. Since valid results could not be obtained until these problems were solved, the first portion of the present experimental program was devoted to this end. (Section 2.5).

The "radiometer-type" torsion balance generally consists of a small vane, the "test surface", which is suspended on a thin, vertical fiber (Fig. 2). If a force  $F$ , such as that resulting from an impinging beam of molecules, is applied to the test surface at a distance  $R$  from the fiber (Fig. 1), the balance will be subjected to an applied torque  $\tau$ :

$$\tau = R F_n \quad (2.2)$$

where  $F_n$  is the component of  $F$  which is normal to the test surface. (Note that only the normal component contributes to the torque.) The fiber acts as a torsion member and will undergo an angular deflection  $\theta$  according to the relation for the restoring torque,

$$\tau = K \theta \quad (2.3)$$

where  $K$  is the torsional rigidity or torsional spring constant of the fiber. A standard means of determining  $K$  is based on the period of oscillation  $t$  for simple harmonic motion,

$$t = 2\pi \sqrt{I/K} \quad (2.4)$$

where  $I$ , the moment of inertia, is calculated from the mass and dimensions of the balance.

If the applied force is due exclusively to the interaction of a molecular beam with the test surface, then  $F$  is equal to the rate at which momentum is transported to and from the surface by the gas molecules. Therefore the normal force  $F_n$  is equivalent to

$$F_n = p_i + p_r = p \quad (2.5)$$



where  $p_i$  is the magnitude of the "normal momentum" (i.e., the momentum component normal to the surface) which is transported to the surface per unit time by the incident molecules,  $p_r$  is the magnitude of the normal momentum transported away from the surface per unit time by the re-emitted molecules, and  $p$  is defined as the sum of  $p_i$  and  $p_r$ .

Since the magnitude of the applied torque is equal to that of the restoring torque, the above equations may be used to derive an expression for the total normal momentum transfer per unit time,  $p$ :

$$p = \frac{\tau}{R} = \frac{K \theta}{R} \quad (2.6)$$

From this it is apparent that measurements of  $K$ ,  $\theta$ , and  $R$  are sufficient to determine the normal momentum transfer rate associated with the particle-surface interaction.

## 2.5 Discussion of Preliminary Designs and Experiments

In past experiments the intensity of the molecular beam, i.e., the number of molecules striking the test surface per second, has usually been severely limited by the pumping speed of the diffusion pumps. In order to utilize the full strength of the beam investigators were forced to use a defining slit which caused the entire beam to be intercepted by the test surface (Fig. 1a). A detrimental attribute of this technique is that it is very difficult to obtain an accurate measurement of  $R$ , the distance from the fiber to the center of impact of the molecular beam on the surface.

Problems associated with the measurement of  $R$  and with low intensity molecular beams were alleviated in the present experiment by

using a high-speed diffusion pump. This permitted the use of the arrangement shown in Fig. 1b, where the defining slit is designed to form a beam which completely covers one-half of the test surface. The forces to be measured are therefore at least one order of magnitude greater than in past experiments. The length of the torque-arm  $R$  is now simply one-half of the distance from the fiber axis to the edge of the exposed surface if the alignment is accurate and if the molecular beam has parallel particle paths and uniform intensity at the surface.

Another advantage of a high-speed diffusion pump is that it can be used to evacuate simultaneously both the defining region and the test region (Fig. 1b). This modification of the conventional design leads to a more compact and simple system, but does so at the expense of the test chamber pressure.

Preliminary tests showed that mechanical vibrations could be reduced to a tolerable level if:

- (1) the apparatus was securely mounted on an independent concrete foundation
- (2) the apparatus was isolated from the vibration of the mechanical pump by using flexible connections
- (3) a viscous damping technique was designed to eliminate balance vibrations which often occur both accidentally and unavoidably.

Various attempts were made to develop a suitable magnetic or eddy-current damping mechanism but the paramagnetic properties of the test surface caused them to assume a preferred orientation with respect to the applied magnetic field. Therefore, this technique was abandoned for a viscous

damping arrangement consisting of a small cup of diffusion pump oil which could be brought into contact with the lower end of the balance rod when desired (see Fig. 7 and Section 4.5.1).

The first balances were made with quartz fibers and their erratic behavior indicated the presence of electrostatic charges. Various shielding methods such as copper screens, stannus oxide coatings, and graphite paints proved to be unsuccessful. The solution was to dissipate the static charge on the test surface by grounding it through an electrical conductor. This could be accomplished by either coating the quartz fiber with a conductive material or by using a torsion fiber which is itself a conductor. The latter method was adopted and the balances are now made with 0.0002 inch diameter tungsten fibers. This completely eliminated the erratic behavior and no shielding was necessary.

The tungsten fibers proved to be exceedingly strong, both in tension and torsion, for their size. They also appeared perfectly elastic and immune to aging under existing conditions because there were no appreciable changes in the zero points or periods of oscillation of the balances.

Although the period of oscillation was constant in the absence of a molecular beam, its magnitude was observed to decrease noticeably with increases in the magnitude of the applied torque. Since the measured torque varied in an approximately linear manner with respect to the source pressure, it is concluded that this decrease in the period is not due to a change in the torsional rigidity of the balance; it may result from the dynamics of the oscillating surface when it is subjected to an applied torque which is a complicated function of the angular position of the surface.

Various schemes for raising the temperature of the test surface were considered. The technique of radio-frequency induction heating proved to be unsatisfactory because the balance exhibited a strong tendency to assume a preferred orientation in the non-uniform field. Radiant heating by a focused light source located outside the vacuum chamber was much more successful and therefore was adopted.

It was found that the initial heating of newly installed test surfaces had to be carried out slowly in order to avoid violent deflections of the balance which could result in breakage. This erratic behavior, most probably due to "explosive" out-gassing, disappeared after the first heating cycle; it was then possible to raise the surface temperature from 25 to 600°C in a few seconds without any adverse effects.

The most undesirable feature of the apparatus results from the fact that it is practically impossible to mount the balance on the support shaft in such a way that the centerline of the shaft coincides accurately with that of the torsion fiber. This unavoidable mis-alignment, or eccentricity, of several thousandths of an inch causes the lateral position of the fiber, and therefore of the test surface also, to change as the support shaft is rotated, thereby affecting the alignment of the balance with respect to the defining and source slits (i.e., the amount of surface area exposed to the molecular beam will vary as the shaft is rotated unless the slit alignment is continually adjusted). This problem is a difficult one to remedy and therefore has not been completely corrected, but the constant torque procedure described in Sections 3.3 and 5.1.1 was devised as a means of bypassing the problem since it permits the shaft position to remain fixed during an experimental test.

An interesting observation was made during the preliminary experiments with the test surface at room temperature: in order to apply the same amount of torque to the balance, the source chamber pressure for helium had to be approximately 2.5% greater than that for argon. It is possible to explain this effect by assuming that near free molecule flow, not fully-developed free molecule flow, exists at the source slit due to the fact that the mean free path may not be sufficiently large compared to the slit dimensions under the present conditions. One characteristic of near free molecule flow is that the flow rate increases more rapidly with pressure than the linear relation predicted by free molecule flow theory<sup>9</sup>. Therefore, at a given source pressure the flow rate for argon will be greater than that for helium because the atomic mean free paths of these gases differ by a factor of 3, approximately, meaning that argon is farther into the region of near free molecule flow than helium. It is concluded from preliminary tests over a range of source pressure levels that the transition from near free molecule to free molecule flow is an extremely gradual process for rectangular slits; e.g., the 2.5% pressure difference between argon and helium appeared to be fairly constant for Knudsen numbers ranging from 1 to 70 (the Knudsen number used here is defined as the ratio of the argon mean free path to the slit width). For circular apertures the transition is much more rapid in this range of Knudsen numbers<sup>9</sup>.

It was found that experimental measurements of the torque were approximately 12% larger than the theoretical predictions of Eq. (A1.13) in Appendix 1, the source gas and test surface being at room temperature. The primary cause of this discrepancy is that the actual beam intensity

$N$  is greater than that for an "ideal" beam because of near free molecule flow through the source slit, as mentioned above. It is therefore necessary to introduce a correction factor  $\zeta$  into Eq. (2.1):

$$N = \frac{\zeta P S S'}{2 \pi d^2} \left( \frac{2}{m \pi k T_1} \right)^{1/2} \quad (2.7)$$

This correction factor must be added to all equations which contain  $N$ , such as Eq. (A1.13). It is convenient to consider  $\zeta$  to be a dimensionless flow coefficient which is a function of the Knudsen number, its value becoming unity in the limiting case of fully-developed free molecule flow through the source slit. (Note:  $\zeta$  is related only to that flow region near the centerline, or axis of symmetry of the molecular beam; therefore it is not identical to the conventional flow coefficient such as that measured by Liepmann<sup>9</sup>). At the present time there is no proven theoretical method for evaluating  $\zeta$  at arbitrary Knudsen numbers for rectangular slits; it is also very difficult to determine  $\zeta$  accurately by experimental measurements.

### 3.0 THE PROPOSED EXPERIMENTAL PROGRAM

#### 3.1 General Considerations

With the molecular beam-torsion balance system described in the preceding sections it should be possible to study the efficiency of normal momentum transfer between different gases and surface materials at various angles of incidence as a function of the temperature of the test surface and/or the velocity distribution of the impinging gas molecules. It was decided that only the test surface temperature would be varied in the present experimental program because the apparatus for accomplishing this appeared to be less complex than that required to vary the velocity distribution. (Several possible methods of varying the velocity distribution are discussed in Section 6.3). A simple radiant heating technique (Sections 2.5 and 4.3.2) was selected as the means of elevating the surface temperature; the molecular beam source chamber is to be maintained at room temperature at all times, meaning that the mean speed of the incident molecule is essentially constant and may be easily determined by kinetic theory if the molecular beam is "ideal" (see Section A1.3 of Appendix 1).

A major problem of an experimental program employing a heated test surface is that one must devise a suitable method for determining the surface temperature. Direct measurements by means of thermocouples on the test surface appear to be impractical because the connecting wires would probably have an adverse effect on the torsional properties of the balance. It is possible to estimate the test surface temperature from measurements obtained with thermocouples on a "dummy" or replica of the surface (Section 5.2) but this is a rather laborious process. The use

of an optical pyrometer also does not appear to be a feasible method due to the fact that the temperature is relatively low, the range being from 25 to 550° C. Therefore it was decided that the surface temperature would be estimated indirectly from experimental momentum transfer measurements made with a "reference" gas which is assumed to be completely accommodated\* to the surface temperature (Section 5.1). The validity of this method was verified approximately by direct measurements made with a "dummy surface" (Section 5.2).

Preliminary tests indicate that in the present apparatus it would be extremely difficult to make highly accurate measurements of the absolute, or total magnitude of the normal momentum transfer, or torque, because

- (1) the precise value of the flow coefficient  $\zeta$  is neither known nor easily determined (Section 2.5).
- (2) an inherent source of error is associated with the measurements of the torsional rigidity  $K$  and the geometrical dimensions which are required for absolute measurements (see Eq. (A1.12) in Appendix 1).

Therefore the present experimental program was based primarily on relative measurement techniques which appear to circumvent these difficulties. A procedure of constant source pressure and variable torque is discussed in Section 3.2, while the opposite procedure, that of constant torque and variable source pressure, is presented in Section 3.3. In both procedures

---

\* A gas is "completely accommodated" to a surface having temperature  $T_w$  if it attains a state of thermal equilibrium with the surface. In this case the gas molecules are re-emitted diffusely with a maxwellian velocity distribution which is characteristic of an equilibrium gas at a temperature  $T_w$ .



the measurements made with the surface heated (i.e., elevated surface temperatures) are expressed in terms of, or relative to, the corresponding measurements made with the surface unheated (i.e., the surface temperature at room temperature).

It should be mentioned that although the experimental program was based primarily on relative measurement methods, absolute measurements of the torque were made in order to substantiate approximately the general validity of the molecular beam-torsion balance technique, and to study the dependence of  $\zeta$  on the source pressure and the source slit design (see Section 2.5).

### 3.2 Analysis of the Constant Pressure Procedure

The constant pressure procedure seems to be the most straightforward means of obtaining data as it is based on the following simple scheme: for each value of surface temperature the balance support shaft is rotated an amount sufficient to return the test surface to that position where the desired angle of incidence is attained; the source pressure remains constant throughout this procedure. For example, assume that initially the source gas and test surface are at room temperature, the source pressure is fixed at the constant value  $P = P_0$ , and the desired angle of incidence has been attained by rotating the balance support shaft through an angle  $\theta_0$  from that position which causes the surface to have this same orientation in the absence of a molecular beam, i.e., zero source pressure. (The subscript "0" will be used to denote those quantities which are measured when the test surface is unheated.) Now if the surface is heated the momentum of the re-emitted molecules will most likely increase, meaning that the applied torque will be larger

and therefore cause the balance to deflect. It is possible to cancel this deflection, and thereby attain the desired angle of incidence again, by rotating the balance support shaft to a new position  $\theta$  which increases the restoring torque by the exact amount required to counterbalance the additional applied torque. This procedure may be repeated for different values of the surface temperature and  $\theta$  recorded in each case.

The results of the constant pressure procedure may be expressed as relative measurements in the convenient form of a ratio of the shaft angular positions,  $\theta/\theta_o$ . From Eq. (2.6) it is evident that  $\theta/\theta_o$  is equal to the ratio of the normal momentum transfer rate for the heated surface,  $p$ , to that for the unheated surface,  $p_o$ :

$$\frac{\theta}{\theta_o} = \frac{p}{p_o} = \frac{p_i + p_r}{p_i + p_{r_o}} \quad (3.1)$$

Note that  $p_i$  is the same in both the heated and unheated cases since the source pressure and temperature are held constant.

Equation (3.1) constitutes a convenient means of investigating the normal momentum transfer since it does not require measurements of  $P$ ,  $\zeta$ ,  $K$ , and the geometrical dimensions; however it does assume that these quantities are constant and unaffected by the heating process.

### 3.3 Analysis of the Constant Torque Procedure

The constant torque procedure is based on the following scheme: for each value of surface temperature the source pressure is adjusted so as to maintain the torque and angle of incidence at fixed values.

The initial details of this procedure are identical to those of the constant pressure procedure (Section 3.2), but in the present case the

balance deflection which results from heating the test surface is cancelled by an appropriate reduction of the source pressure rather than by an increase in the restoring torque. The normal momentum transfer and the applied torque are proportional to the molecular beam intensity, which is in turn proportional to the source pressure; therefore, by proper adjustment of this pressure it is possible to reduce the normal momentum transfer by the same amount that it is increased by heating the test surface, meaning that the torque and angle of incidence will be maintained at their original values. This procedure may be repeated for several surface temperatures and the pressure recorded in each case.

The results of the constant torque procedure may be expressed as relative measurements in the convenient form of the ratio of the source pressure for the unheated surface,  $P_o$ , to that for the heated surface,  $P$ . From Eq. (2.7) one can show that this pressure ratio is equivalent to the corresponding ratio of intensities:

$$\frac{P_o}{P} = \frac{N_o}{N} \quad (3.2)$$

This statement is based on the assumption that  $\xi$  is equal to  $\xi_o$ , which appears to be valid for the present apparatus (see Section 2.5).

Since the torque is constant in this procedure, it follows that the normal momentum transfer rate for the unheated surface,  $p_o$ , is equal to that for the heated surface,  $p'$ . (The prime superscript is added to denote that this quantity is associated with a molecular beam intensity which is different than that for  $p_o$ .)

Therefore Eq. (3.2) may be expressed as

$$\frac{P_o}{P} = \frac{p'}{p_o} \frac{N_o}{N} = \frac{(p' N_o/N)}{p_o} \quad (3.3)$$

since  $p'/p_o = 1$ . Now since  $p'$  is proportional to  $N$  (see Section A1.4 of Appendix 1), the quantity  $(p' N_o/N)$  corresponds to that normal momentum transfer rate which would occur for an intensity  $N_o$  (i.e., for a source pressure  $P_o$ ). Therefore,

$$\frac{P_o}{P} = \frac{p}{p_o} = \frac{p_i + p_r}{p_i + p_{r_o}} \quad (3.4)$$

where  $p$  is equal to  $(p' N_o/N)$ .

Note that the right-hand side of Eq. (3.4) is equal to that of Eq. (3.1). This means that the experimental values of  $\theta/\theta_o$  and  $P_o/P$  obtained by the respective procedures should be numerically equal for the same test conditions, i.e., for the same gas, surface material, angle of incidence, and surface temperature. (The results of such a comparison are given in Section 5.1.2). Therefore,

$$\left( \frac{\theta}{\theta_o} \right)_{\text{const. } P} = \left( \frac{P_o}{P} \right)_{\text{const. } \tau} \quad (3.5)$$

meaning that the experimental results obtained by one procedure may be converted into equivalent values for the other procedure.

#### 4.0 EXPERIMENTAL APPARATUS

##### 4.1 General Description

The general layout of the equipment is shown in Figs. 3 and 4.

The basic components of the primary system are:

- (1) a mechanical vacuum pump located outside the building.
- (2) an oil diffusion pump mounted on a steel framework which is securely fastened to a concrete foundation.
- (3) a water-cooled baffle located on top of the diffusion pump.
- (4) a flanged stainless steel cylinder which connects the baffle to the test chamber.
- (5) a glass cylinder which serves as the test chamber.
- (6) a top flange on which the molecular beam, defining slit, and balance assemblies are mounted.

The secondary components may be divided into the following general classifications:

- (1) the gas supply system which provides the molecular beam source chamber with the various test gases at regulated pressure levels.
- (2) the McLeod gauge for measuring the source chamber pressure.
- (3) the cathetometer which is used in aligning the source slit, defining slit, and balance.
- (4) the projector for heating the test surface by radiation.
- (5) the galvanometer light sources and circular scale which are used to determine the position of the test surface.

A more detailed description of the apparatus is presented in the following sections.

#### 4.2 Vacuum System

The mechanical vacuum pump, a 5 H.P. Kinney DVD 8-8-10, is located outside the building on a concrete foundation and is connected to the diffusion pump by means of a 1-1/2-inch diameter tubing with flexible Dresser couplings. This pump is much larger than required by the diffusion pump, but is convenient as it can evacuate the system to a pressure of 100 microns in approximately one minute.

As mentioned in Section 2.5, it is most important to have a high pumping speed in this experiment. This was satisfactorily accomplished with an NRC HS6-1500 oil diffusion pump. A 6-inch CEC water-cooled baffle was used to reduce the amount of oil vapor that "back-streams" from the diffusion pump into the test chamber. It was decided that a liquid nitrogen trap was not necessary because the test chamber was not designed for "bake-out" or for "clean" high vacuum conditions.

A flanged stainless steel cylinder, 6-5/8 inches in diameter, is located between the baffle and the test chamber. It contains the damper mechanism (Section 4.5.1) and the vacuum gauges.

A 15-inch length of extruded pyrex glass pipe serves as the test chamber. The inside and outside diameters of this cylinder are approximately 7 and 8 inches, respectively. The optical qualities of the glass were satisfactory even though there were some irregularities and distortions.

All temporary vacuum seals were designed to use either O-rings or Sealastic fittings (M. H. Heustis Company). The sealing of rotating and translating shafts by means of standard O-rings was extremely successful.

Approximate measurements of the test chamber pressure were obtained by a flanged Hughes VTP 6578 ionization gauge. The ultimate vacuum was of the order of  $5 \times 10^{-6}$  mm Hg when no gas was supplied to the source chamber. Under the same conditions a value of  $\sim 1.4 \times 10^{-6}$  mm Hg was measured by a glass-enclosed Hughes VTP-7169 ionization gauge; this figure dropped to  $\sim 1.5 \times 10^{-7}$  mm Hg when the entrance tube of the gauge was immersed in liquid nitrogen, indicating the presence of condensible gases and vapors in the test chamber.

Under typical operating conditions, such as for nitrogen in the source chamber at a pressure of 100 microns, the test chamber pressure is  $\sim 7 \times 10^{-5}$  mm Hg according to the VTP-6578 gauge, and the pumping speed is  $\sim 7$  micron-liters per second or  $\sim 100$  liters per second. (The indicated pumping speed would be considerably higher if it were based on the pressure read with the VTP-7169 gauge trapped with liquid nitrogen.)

#### 4.3 Auxiliary Apparatus

##### 4.3.1 The Lamp and Scale

The angular position of the test surface is determined by means of the lamp and scale technique which is often used with galvanometers. A beam of light from a Leeds and Northrup #2099 galvanometer lamp is reflected from a mirror on the balance and focused on the scale. The circular scale (Fig. 3) has a 1 meter radius and consists of a long strip of graph paper stretched around a lucite cylinder which is supported by a wooden frame. The scale was extended for  $360^\circ$  so that it would be suitable for investigations in which the angular orientation of the test surface relative to the molecule beam is varied.

#### 4.3.2 The Projector

An ancient slide projector provided the radiant energy which was used to heat the test surfaces. The performance of this simple device using standard lens and bulbs was very satisfactory; surface temperatures of more than 600° C could be achieved with a 500-watt bulb in a matter of seconds.

The projector was placed on a horizontal platform (Fig. 4) so that its position could be varied easily when focusing the radiation on the test surface. The power supplied to the bulb is controlled by a variable autotransformer (Powerstat Type 236) and measured with a Weston Tester, Model 785. Since the total area of the filaments in the bulb is approximately the same size as the test surface, it was usually possible to focus the radiation in such a way that only the surface would be heated.

#### 4.3.3 The Gas Supply System

The molecular beam requires a gas supply system capable of providing the source chamber with different gases at various, steady pressure levels. This was accomplished in the following manner: gas from a high-pressure cylinder is first reduced by a standard regulator to ~ 10 psi, then by a Fisher S100-4 regulator to ~ 7 inches of water (~ 0.25 psi), and finally by a type VL Veeco variable leak to the source pressure  $P$  which ranges from 25 to 250 microns (i.e., from 0.025 to 0.25 mm Hg).

Commercial grade cylinder gases were used because it was felt that the present experiment did not require ultra-high purity gas. The supply line included a liquid nitrogen trap for removing



condensable contaminants, but the data appeared to be the same whether this trap was filled or not.

#### 4.3.4 The McLeod Gauge

A McLeod Gauge designed for measuring pressures in the range of 1 to 280 microns was built in this laboratory several years ago. The difference in the heights of the mercury columns is read, with the help of a magnifying glass, on a scale which is scribed on a mirror. This reading is related to the pressure by the expression

$$P = 1.10 (\Delta H)^2 \quad (4.1)$$

where  $\Delta H$  is the height difference in centimeters; the constant 1.10 is the gauge calibration factor. Since the smallest division on the scale is 0.05 cm, the reading error is probably no greater than  $\pm 0.025$  cm, meaning that it is theoretically possible to measure a pressure of 100 microns to  $\pm 0.5\%$ .

The McLeod Gauge was connected to the molecular beam source chamber by 1/2-inch flexible copper tubing and Sealastic fittings. A glass U-tube was installed between the gauge and the source chamber in order to trap the mercury vapor. The U-tube was immersed in a dewar of either ice water or liquid nitrogen; the experimental results appeared to be the same in both cases.

#### 4.4 Molecular Beam Apparatus

The molecular beam source chamber is a hollow brass bar mounted on the top flange (Fig.5). On its front face there is a 1/2-inch diameter opening which is covered by the source slit. Two different rectangular slit designs were used in order to determine their effect on the data (no

significant effect was noticed). Slit #1 was constructed from four strips of 0.001 inch steel shim stock and is approximately 0.0025 inches (0.00635 cm) wide by 0.394 inches (1.00 cm) high (Fig. 6a). It is fastened to the source chamber by a brass plate with four screws. Slit #2 was made in a 1/8 inch stainless steel plate by milling a slot in the center section which had been previously machined to reduce its thickness (Fig. 6b). The dimensions of this slit have been measured with an optical comparator: width = 0.0069 inches (0.0175 cm), height = 0.1366 inches (0.3470 cm), thickness or channel length = 0.010 inches (0.0254 cm). A circular aperture was used on one occasion (Section 5.3.3); it consisted of an 0.040 inch (0.1016 cm) diameter hole drilled in a piece of 0.001 inch shim stock. The magnitude of  $l$ , the distance from the source slit to the test surface, was approximately 6.20 cm for Slit #1, 6.50 cm for Slit #2, and 6.30 cm for the circular aperture.

The purpose of the partition wall and defining slit (Fig. 7) is to reduce the amount of background flow in the test chamber and to control the alignment of the molecular beam with respect to the test surface. The partition wall consists of a sheet of 0.005 inch stainless steel supported by a brass framework. Note that the defining region and the test region are not separate compartments because they share the same diffusion pump; this is contrary to normal molecular beam practice but of little consequence in the present experiment (see Section 2.5).

The defining slit consists of a 3/4 cm wide by 1 cm high aperture in a 5 inch diameter stainless steel disc (Fig. 7). It is possible to rotate this disc from outside the vacuum chamber by means of a crank which is connected to a worm and gear by a flexible cable (Fig. 8). A small

amount of lateral adjustment is provided by a lever and push-rod mechanism which causes the disc to swing about an eccentric pivot point. The combined use of these two adjustments enables one to align the defining slit with the source slit and the balance centerline.

#### 4.5 Torsion Balance Apparatus

##### 4.5.1 General Remarks

All of the balances were constructed according to the design shown in Fig. 2. A test surface of dimensions 1.0 by 2.0 cm is cemented to an 0.015 cm (0.006 inch) diameter quartz rod by means of Eccobond 58C, an epoxide based adhesive produced by Emerson and Cuming, Inc. This bonding agent must be cured at 150° C for 2 hours. It was selected because it is an electrical conductor and has adequate adhesive qualities at elevated temperatures.

The quartz rod is bonded by means of silver paint to a 5/16 by 1/2 inch piece of 0.005 inch aluminum sheet. Silver paint is also used to bond the galvanometer mirror (Leeds and Northrup #Std 1142-2) and the tungsten fiber to this plate, and to bond the other end of the fiber to a 1/16 by 1/4 by 1/2 inch stainless steel mounting plate.

The low thermal conductivity of the quartz rod is a valuable feature because it minimizes the undesirable conductive heat transfer from the heated test surface to the mirror and fiber, and to the oil cup. (Balances using tungsten rods experienced enough heat transfer to vaporize the oil in the cup and to melt the silver paint connections.) Since quartz is also an electrical insulator, it was necessary to use a 0.001-inch diameter tungsten wire between the test surface and the aluminum plate in order to provide a means of grounding

static charges. (It is this problem of static charge which requires the bonding agents to be electrical conductors.)

The tungsten torsion fiber is 10 cm long and has an approximate diameter of 0.0002 inches ( $\sim 5$  microns, or 0.0005 cm). They are available from the Sigmund Cohn Corporation, Mount Vernon, New York. Although the fibers are very rugged for their size, it is still necessary to handle them with extreme care. Fibers made from other materials, such as platinum and gold, were not tried because tungsten proved to be entirely satisfactory.

As mentioned previously, a viscous damping technique was devised to reduce the vibrations and oscillations of the balance. It consists of a small cup of diffusion pump oil which may be raised, when desired, so that it comes into contact with the bottom end of the quartz rod (see Fig. 7). The mechanism for adjusting the vertical position of the oil cup is located in the stainless steel cylinder and controlled from outside the vacuum by means of a movable shaft.

The balance mounting plate is fastened by a small screw into a slot milled in the end of a  $3/8$  inch diameter brass shaft which is positioned vertically in the center of the test chamber. As mentioned previously in Section 2.5, it is important that this mounting operation be done in a manner which achieves good alignment of the fiber axis with the centerline of the shaft.

The balance support shaft passes through an O-ring seal in the top flange and is clamped by a collet to a precision machine-divided wheel (Fig. 5). The perimeter of this 10 inch diameter wheel has been divided into 100 equal major graduations, each of which is

subdivided into tenths. Therefore, since 100.0 graduations correspond to one revolution, the relation between the wheel reading  $W$  and the angular displacement  $\theta$  of the balance shaft is

$$\theta = 2 \pi \frac{W}{100.0} \quad (4.2)$$

meaning that the smallest wheel division is equivalent to  $6.28 \times 10^{-3}$  radians. A vernier was provided on the fixed reference wheel in order to improve this precision by a factor of 16. Great care was required during the machining of the divided wheel, the reference wheel, and the shaft housing in order to achieve a high degree of concentricity.

#### 4.5.2 The Dummy Surface

The use of a "dummy surface" to obtain direct measurements of surface temperatures at various projector voltages is described in Section 5.2. The dummy surface assembly (Fig. 9) consists of a 1 cm by 2 cm tungsten surface, 0.001 inches thick, cemented to a quartz rod which is mounted on a piece of micarta. This assembly is fastened to a hollow support shaft which extends through an O-ring seal in the top flange, enabling one to adjust its position from outside the vacuum chamber.

Two thermocouples made from 0.001 inch platinum and platinum-10% rhodium wire have been spot-welded to the surface. The extension leads are copper wires which have been joined to the thermocouple wires by soft solder. These leads are brought outside the vacuum chamber through the hollow support shaft, the vacuum seal being made with Eccobond 26, an epoxy resin. The thermocouple output was measured with a Brown potentiometer.

#### 4.5.3 Test Surface Materials

As previously stated, all of the balances were constructed in the same manner (Section 4.5.1). The test surfaces are 1 cm by 2 cm, and are washed in methyl ethyl ketone; no other cleaning or polishing operation was used.

The material for tungsten surfaces was obtained from the H. Cross Company of New York in the form of an 0.001 inch sheet. The structure of this material was of a fibrous nature, but the surface was still relatively shiny. Other than being difficult to cut, tungsten was nice to work with because its rigidity prevented accidental bending and thermal distortions.

The blackened tungsten surfaces were prepared by electrochemical deposition of platinum on a regular tungsten balance. The resulting surface is microscopically "rough", probably consisting of spires or ridges of platinum. This technique is commonly used to produce "black bodies" for radiation studies. The preparation of the blackened tungsten surfaces was guided by C. P. Butler of the Naval Radiological Defense Laboratory.

The aluminum surfaces were made from an 0.005 inch sheet having a very smooth and shiny finish. Preliminary tests indicated that 0.001 inch foil was not satisfactory because it distorted, or curled up, when heated. It should be mentioned that because of aluminum's strong affinity for oxygen, these test surfaces are completely covered by an oxide layer.

An 0.001 inch sheet of platinum was purchased from the Braun-Knecht-Heimann Company. The surface finish was not extremely shiny.

Some permanent thermal distortion occurred so it was concluded that thicker material should be used for future balances.

It was not possible to use ferromagnetic materials for test surfaces because of their interaction with stray magnetic fields. It is expected that non-conducting materials, such as some crystalline substances, could not be used because of static electricity problems (see Section 2.5).

## 5.0 THE EXPERIMENTAL PROGRAM

### 5.1 The Experimental Procedures

The constant torque procedure (Section 3.3) was used to obtain the majority of the experimental data because in the present apparatus it appears to be a more reliable method than the constant pressure procedure (Section 3.2). The disadvantages of the latter procedure are related mainly to the difficulty of maintaining a constant source pressure and to the unavoidable eccentricity of the fiber axis relative to the axis of the balance support shaft, causing a slight change in the alignment of the fiber with respect to the source and defining slits upon rotation of the shaft (see Section 2.5). On the other hand, the constant pressure procedure does offer two definite advantages: the required manual operations may be executed more easily, and the shaft position  $\theta$  may be measured with more precision than the source pressure. Therefore it is important that the above-mentioned disadvantages be corrected in the future so that this procedure may be used more extensively.

As stated in Section 3.1, it was decided that the temperature of the test surface would be estimated indirectly from experimental momentum transfer measurements made with a "reference" gas which is assumed to be completely accommodated to the surface temperature. The details of this indirect procedure are described in Section 5.3.1. Argon was selected as the reference gas for the following reasons:

- (1) The energy transfer measurements of Michels<sup>19</sup> indicate that argon is completely accommodated on unflashed\*

---

\* an "unflashed" material is one which has not been elevated (or "flashed") to an extremely high temperature in order to remove the surface contaminants, such as adsorbed gases.



tungsten. In these measurements the surface temperature was only 10° C higher than that of the gas, and the molecules impinged at all angles of incidence; therefore the validity of these results under the present experimental conditions is questionable because the temperature difference is as large as 550° C and the impinging molecules are restricted to a specific angle of incidence.

- (2) Indirect temperature estimates calculated from argon data are in approximate agreement with those measured with a "dummy surface" (see Section 5.2).
- (3) Experimental results obtained with argon, nitrogen, and carbon dioxide are generally in close agreement, indicating that these gases are accommodated approximately to the same extent. Such a fortuitious occurrence for gases of different physical and chemical natures is most likely to exist only if the accommodation is nearly complete for each gas.

In the following two sections the operational details of the experimental procedures are described.

#### 5.1.1 Constant Torque Procedure

The majority of the experimental tests were performed according to the following steps:

- (1) A balance is installed and the system evacuated to a pressure of approximately  $5 \times 10^{-6}$  mm Hg.
- (2) The vertical position of the balance and the lateral position of the defining slit are adjusted to align them properly with the source slit.

- (3) By rotating the balance support shaft, the test surface is positioned so that the desired angle of incidence is attained (there is no molecular beam until Step 5). This position is called the "zero point" and readings are taken of the scale, the wheel position  $W'$ , and the period of oscillation.
- (4) The location of the projector is adjusted so that the radiation causes a minimum deflection (usually less than 2 cm on the scale) of the balance from its "zero point".
- (5) Gas is introduced into the source chamber, forming a molecular beam which deflects the surface from its "zero point".
- (6) With the surface and source gas at room temperature the support shaft is rotated an amount sufficient to return the scale reading to its "zero point" value. (This insures that the original angle of incidence is attained again.) Readings are then taken of the source pressure  $P_0$ , and the wheel  $W_0$ .
- (7) The projector voltage is set at a value which will cause the surface to be heated to a temperature of approximately 500° C. The source pressure is reduced to a value  $P$  so as to maintain the same wheel and scale readings as measured in Step 6. (This insures that the torque remains constant if the torsional rigidity of the fiber does not change.) Readings are taken of  $P$  and the projector voltage  $V$  and current  $I$ .

- (8) Step 7 is repeated for several lower voltage settings at approximately ten minute intervals.
- (9) Step 6 is repeated and then Step 8, but in the opposite direction, finishing with Step 7. (See Table I)
- (10) Step 6 is repeated again.

It is usually desirable to damp out excessive balance vibrations after each pressure measurement. The simple pendulum oscillations may be damped with the oil cup; the torsion pendulum oscillations may be damped either with the oil cup or by manipulating the wheel in such a manner that the oscillations are cancelled or "bucked out". Although it is possible to reduce the balance motion to such a degree that the oscillations will have an amplitude of less than 1 cm on the scale, most measurements are made at an amplitude of ~ 10 cm and the scale reading is determined by taking an average of the extreme readings for several oscillations.

A typical data sheet for the case of normal incidence is shown in Table I. It should be noted that the calculation of  $P_o/P$  uses the value of  $P_o$  obtained by averaging the three source pressure measurements taken at zero voltage, i.e., with the test surface at room temperature. The argon data may be considered as a calibration run since it is used only in the approximate calculation of the surface temperature (Section 5.3.1).

#### 5.1.2 Constant Pressure Procedure

The steps of this procedure are identical to all of those stated in the preceding section except for Step 7:

- (7) The projector voltage is set at a value which will cause the surface to be heated to a temperature of approximately 500° C. The resulting increase in applied torque is balanced by rotating the wheel an amount sufficient to return the scale reading to its "zero point" value. Readings are taken of the wheel position  $W$  and the projector voltage  $V$  and current  $I$ .

As an attempt to keep the source pressure constant throughout the test, the variable leak was immersed in a flask of water which served to isolate it from thermal effects.

A typical data sheet for the case of normal incidence is shown in Table II. This test was more successful than the average because the source pressure remained extremely steady throughout the run and the shaft-fiber eccentricity discussed in Sections 2.5 and 5.1 appeared to be negligible for this particular balance.

The applied torque is proportional to  $(W - W')$ , the change in the wheel reading due to the effect of the molecular beam. By means of Eq. (4.2) it is possible to evaluate  $\theta$ , the angular displacement, or rotation, of the balance support shaft:

$$\theta = 2 \pi \frac{W - W'}{100.0} \quad (5.1)$$

It is convenient to normalize this expression with respect to  $\theta_0$ , the angular displacement that occurs when the test surface is at room temperature (i.e., zero projector voltage). The resulting form is

$$\frac{\theta}{\theta_0} = \frac{W - W'}{W_0 - W'} \quad (5.2)$$

As discussed in Section 3.3, the numerical value of  $\theta/\theta_0$  is equal, theoretically, to  $P_0/P$  and may therefore be plotted on the same graph. This procedure was followed for the data presented in Table II; the results are included in Fig. 13 and indicate excellent agreement between the constant pressure procedure and the constant torque procedure.

## 5.2 Direct Measurements of Surface Temperature

The "dummy surface" described in Section 4.5.2 was used to obtain direct measurements of the surface temperature. For this measurement the "dummy surface" was approximately positioned in the region where the test surface is usually located, and the thermocouple readings were recorded at various power settings of the projector. After completing this procedure the "dummy surface" was swung out of the way so that the torsion balance could be returned to its original position. Then experimental measurements of  $P_0/P$  were performed for argon by means of the constant torque procedure; the results were used to obtain indirect estimates of the surface temperature (these estimates were made using Eq. (5.6) which appears in Section 5.3.1).

The "dummy surface" measurements and the indirect temperature estimates are compared in Fig. 10. The imperfect agreement may be due to one or more of the following reasons:

- (1) the accommodation of argon may not be complete; the indirect values will agree very well with the direct measurements if it is assumed that  $\alpha \approx 0.94$ . (Note:  $\alpha$  is the energy accommodation coefficient defined in Section 5.3.2)

- (2) the value of the flow coefficient  $\zeta$  may not remain exactly constant when the source pressure is varied; for a surface at 500° C, the indirect measurement would be in error by ~ 30° if  $\zeta/\zeta_0$  differed from unity by only 0.5%.
- (3) the value of the torsional rigidity  $K$  may not be constant if the temperature of the fiber is accidentally increased when the surface is heated.
- (4) the direct temperature measurement may be incorrect because of faulty thermocouples or errors in the reading and conversion techniques.
- (5) the test surface and the dummy surface may have slightly different values of reflectivity and emissivity, although they were made from the same sheet of tungsten.

These and other possible sources of error are discussed in Section 6.2

It should be mentioned that subsequent tests, performed in the same manner, produced increasingly poor agreement between direct and indirect measurements. No definite explanation for this has been found but there is a remote possibility that it results from a change of the radiation properties, i.e., reflectivity and emissivity, of the test surface due to prolonged exposure at more than 500° C to oil vapor and other contaminants; the "dummy surface" was subjected to these conditions for a much shorter period of time so its radiation properties would not have been affected to the same extent.

### 5.3 Methods for Interpreting the Experimental Data

Two methods for interpreting the experimental data will be presented: the first method considers the problem from the general viewpoint of normal momentum transfer, while the second treats the problem in terms of translational energy transfer.

The expressions developed in Sections 5.3.1 and 5.3.2 are restricted to the case of normal incidence. Section 5.3.3 contains expressions for oblique angles of incidence in terms of the translational energy interpretation.

#### 5.3.1 The Normal Momentum Interpretation (Normal Incidence)

A tabulation of the experimental data obtained for the specific case of normal incidence is given in Table III. A primary objective of the present investigation is to determine the dependence of the re-emitted normal momentum,  $p_r$ , on the surface temperature  $T_w$ ; therefore it is appropriate to plot the experimental results using a coordinate system of  $p_r$  versus  $T_w$ . A "normalized" form of  $p_r$  has been used in Figs. 11 through 15, i.e.,  $p_r/p_i$ . The value of  $p_r/p_i$  is assumed to be given by

$$\frac{p_r}{p_i} = \frac{5}{3} \left[ \frac{p_o}{P} \right] - 1 \quad (5.3)$$

which is derived in the following manner: Eq. (3.4) is solved for  $p_r/p_i$ , giving

$$\frac{p_r}{p_i} = \frac{p_o}{P} \left[ 1 + \frac{p_{r_o}}{p_i} \right] - 1 \quad (5.4)$$

If it is assumed that when the surface is unheated, i.e., when  $T_w = T_i$ ,

the test gas is re-emitted with a diffuse maxwellian velocity distribution having temperature  $T_i$ , one can show by means of kinetic theory that  $p_{r_o}/p_i$  is equal to  $2/3$  (see Eq. (A1.10) of Appendix 1). With this assumption Eq. (5.3) may be obtained from Eq. (5.4). Note that no assumption has been made for the velocity distribution function associated with  $p_r$  when the surface is heated.

If a gas is completely accommodated to the heated surface, the re-emitted gas will have a definite velocity distribution function; this enables one to derive the following expression:

$$\frac{p_r}{p_i} = \frac{p_w}{p_i} = \frac{2}{3} \sqrt{T_w/T_i} \quad (5.5)$$

(The kinetic theory derivation of this equation appears in Section A1.1 of Appendix 1.) An expression for the surface temperature may now be obtained by substituting Eq. (5.5) into (5.3) and solving for  $T_w$ :

$$T_w = T_i \left[ \frac{5}{2} \left( \frac{p_o}{p} \right) - \frac{3}{2} \right]^2 \quad (5.6)$$

The above equation was used to estimate indirectly the surface temperature from the argon data, assuming that argon is completely accommodated. (A detailed discussion of the underlying assumptions associated with Eqs. (5.3) and (5.6) is given in Section 6.2.)

The following question will be considered now: Is there a parameter which would be suitable for the general description of the present results? Only one normal momentum transfer parameter has been introduced to date, and it is defined as<sup>20</sup>



$$\sigma' = \frac{p_i - p_r}{p_i - p_w} \quad (5.7)$$

where  $p_r$  and  $p_i$  are defined as in Section 2.4, and  $p_w$  is the rate at which normal momentum is transported from the surface by a completely accommodated gas. This "normal momentum transfer coefficient" expresses the degree to which the incident normal momentum is accommodated to the equilibrium value associated with the surface temperature  $T_w$ . It should be emphasized that this parameter, like most "accommodation coefficients", was designed primarily for a specific set of test conditions, i.e., the interaction between a surface at temperature  $T_w$  and a gas which is essentially in thermodynamic equilibrium with it, the departure from equilibrium being infinitesimal. In such a state of near-equilibrium the directions of the incident molecules are random, meaning that the re-emission will be diffuse for specular reflection as well as for complete accommodation. Since diffuse re-emission is predicted for both limiting conditions, specular reflection and complete accommodation, it may be assumed to occur in general; in this case  $\sigma'$  is essentially an energy accommodation coefficient because it depends only to the absolute magnitudes of the molecular velocities, their directions being pre-determined.

It is worthwhile to consider the validity of applying  $\sigma'$  to a flow situation, i.e., a situation in which the incident molecules have a preferred direction. In this case a specific model of the particle-surface interaction is unintentionally assumed when one employs  $\sigma'$ ; this model is not capable of representing the actual interaction realistically, as will be clearly demonstrated in the following paragraphs and in Section 6.4.3.

In the present experiments at normal incidence, Eq. (5.7) may be assumed to have the form

$$\sigma' = \frac{1 - p_r/p_i}{1 - p_w/p_i} = \frac{1 - p_r/p_i}{1 - \frac{2}{3}\sqrt{T_w/T_i}} \quad (5.8)$$

where Eq. (5.5) has been substituted for  $p_w/p_i$ . This equation may be solved for  $p_r/p_i$ , giving

$$\frac{p_r}{p_i} = 1 - \sigma' \left(1 - \frac{2}{3}\sqrt{T_w/T_i}\right) \quad (5.9)$$

The above expression has been plotted for several representative values of  $\sigma'$  in Fig. 16 using the same coordinate system as employed in Figs. 11 through 15. (Note:  $T_i$  is taken to be 25° C (298° K) in all cases).

For the moment the reader should focus his attention on Fig. 16:

- (1) For  $\sigma'$  equal to zero,  $p_r$  is equal to  $p_i$  from Eq. (5.9), meaning the gas is reflected specularly. This condition is represented by the appropriately labeled horizontal line in Fig. 16. (Note that in this case  $p_r$  is constant, being independent of  $T_w$ .)
- (2) For  $\sigma'$  equal to unity,  $p_r$  is equal to  $p_w$ , meaning the gas is completely accommodated to the surface. This condition is represented by the diagonal line which indicates that  $p_r$  is a function of  $T_w$ .
- (3) For arbitrary values of  $\sigma'$  in the range zero to unity,  $p_r$  is restricted by Eq. (5.9) to values between the limits of  $p_r = p_i$  and  $p_r = p_w$ . This is illustrated

in Fig. 16 by the lines of constant  $\sigma'$  which are contained in the region bounded by  $\sigma' = 0$  and

$$\sigma' = 1.$$

An important observation should now be made in Figs. 11 through 15: the experimental values of  $p_r$  are usually less than  $p_w$ , and therefore are often outside the range which is consistent with the parameter  $\sigma'$  in Eq. (5.9). The unpredicted behavior of  $p_r$  may be explained by the hypothesis that the actual re-emission is essentially diffuse while the energy accommodation is, at the same time, incomplete (i.e., the "temperature" of the re-emitted gas is less than  $T_w$ ). This hypothesis is based in part on the fact that scattering experiments conducted under conditions similar to the present ones (i.e., a thermal beam at normal incidence on contaminated metallic surfaces) give results which exhibit no tendency toward specular reflection, the re-emission being highly diffuse<sup>21</sup>. It is also based on the results of experimental investigations of energy accommodation which indicate that the "temperature" of the re-emitted gas may be substantially less than the surface temperature<sup>1-3</sup>.

From the preceding observation and hypothesis it appears that it may be more realistic, although probably not entirely accurate, to modify the parameter  $\sigma'$  in such a way that the limiting case of specular reflection is replaced by one of diffuse re-emission with no energy accommodation (i.e., the molecules are re-emitted as though they came from a gas in a state of thermal equilibrium at the temperature  $T_1$ ). Therefore a new interaction model based on the following assumptions is adopted:

- (1) In the limiting case of complete accommodation the molecules are re-emitted as though they came from an equilibrium gas at temperature  $T_w$ , the surface temperature. (Therefore,  $p_r = p_w$ .)
- (2) In the limiting case of no accommodation\* the molecules are re-emitted as though they came from an equilibrium gas at temperature  $T_i$ , the temperature of the incident gas. (Therefore,  $p_r = \frac{2}{3} p_i$  from Eq. (A1.10) of Appendix 1.)\*\*
- (3) In the general case of partial accommodation no definite assumptions are made concerning either the directional and velocity distributions or the temperature of the re-emitted gas (although the nature of the limiting cases implies that the re-emission is probably diffuse maxwellian in the general case also, i.e., the molecules are re-emitted as though they came from an equilibrium gas at temperature  $T_r$ , where  $T_r = T_i + \alpha(T_w - T_i)$  as will be shown in Section 5.3.2).

This model may be used as the basis of a modified coefficient of normal momentum transfer,  $\sigma''$ , which is derived directly from  $\sigma'$  by substituting  $\frac{2}{3} p_i$  in the place of  $p_i$  in Eq. (5.7):<sup>#</sup>

---

\* Although there is no energy accommodation in this case, there is a substantial accommodation of normal momentum due exclusively to the assumption of diffuse re-emission.

\*\*<sup>#</sup> The relation  $p_r = \frac{2}{3} p_i$  is valid for normal incidence only; a more general relation, which is valid for any angle of incidence, is  $p_r = \frac{2}{3}(p_i + \tau_i)$ , where  $(p_i + \tau_i)$  is the total incidence momentum,  $\tau_i$  being the tangential component.

$$\sigma'' = \frac{\frac{2}{3} p_i - p_r}{\frac{2}{3} p_i - p_w} \quad (5.10)$$

Note that if one assumes diffuse re-emission for the general case of partial accommodation, then  $\sigma''$  depends only on the absolute magnitudes of the molecular velocities; in this case  $\sigma''$  is essentially an energy accommodation coefficient, just as  $\sigma'$  is in the case of near-equilibrium.

The attributes of  $\sigma''$  may be studied by means of the following equation which is analogous to Eq. (5.9):

$$\frac{p_r}{p_i} = \frac{2}{3} \left[ 1 + \sigma'' \left( \sqrt{T_w/T_i} - 1 \right) \right] \quad (5.11)$$

This expression has been plotted for several representative values of  $\sigma''$  in Fig. 16. Note that  $p_r$  is restricted by Eq. (5.11) to values between the limits of  $p_r = \frac{2}{3} p_i$  for  $\sigma'' = 0$  (diffuse re-emission with no energy accommodation), and  $p_r = p_w$  for  $\sigma'' = 1$  (complete accommodation); this new range is generally sufficient to envelop the present experimental results.

Lines of constant  $\sigma''$  have been included on Figs. 11 through 15; therefore it is possible to make estimates of the value of  $\sigma''$  for each gas-surface combination. These values are presented and discussed in Section 5.4 along with other results. The momentum parameters  $\sigma'$  and  $\sigma''$  are discussed again in Section 6.4.3.

### 5.3.2 The Translational Energy Interpretation (Normal Incidence)

It is possible with the introduction of one additional assumption to interpret the experimental data in terms of the molecular translational energy. This assumption is incorporated in the following

model of the particle-surface interaction: the gas molecules are re-emitted from the heated test surface with the diffuse directional distribution and the maxwellian velocity distribution of a gas in thermal equilibrium at the temperature  $T_r$ ; the magnitude of  $T_r$  depends on the degree of energy accommodation and is therefore not necessarily equal to either  $T_i$  or  $T_w$ . (The validity of such a model is discussed in Section 6.2.)

The main attribute of this model is that it enables one to express  $p_r$  in terms of the temperature  $T_r$ , thereby transforming the consideration from momentum transfer to energy transfer. From Eq. (A1.8) in Appendix 1,  $p_r/p_i$  may now be expressed as

$$\frac{p_r}{p_i} = \frac{2}{3} \sqrt{T_r/T_i} \quad (5.12)$$

which may be substituted into Eq. (3.4) to obtain

$$\frac{p_o}{p} = \frac{3}{5} \left( 1 + \frac{2}{3} \sqrt{T_r/T_i} \right) \quad (5.13)$$

The experimental data for normal incidence has been plotted in Figs. 17 through 21 using a coordinate system of  $p_o/p$  for the "test gas" versus  $T_w$ , where  $T_w$  has been estimated from the argon data by means of Eq. (5.6). (The value of  $T_i$  is again taken to be 25° C (298° K). Note that an abscissa of  $p_o/p$  for argon has been included at the top of each figure.

At this time it is convenient to introduce an energy accommodation coefficient defined as<sup>20</sup>

$$\alpha = \frac{E_r - E_i}{E_w - E_i} \quad (5.14)$$

where  $E_i$  is the rate at which energy is transported to the surface by the incident molecules,  $E_r$  is the rate at which energy is transported from the surface by the re-emitted molecules, and  $E_w$  is the rate at which energy would be transported from the surface if complete accommodation occurred (i.e., if the molecules attain a state of complete thermal equilibrium with surface temperature  $T_w$  before being re-emitted).

Since the torsion balance is affected only by the translational energy of the molecules, the following considerations will be limited to an accommodation coefficient of translational energy which is denoted by the symbol  $\alpha_t$ . The definition of this coefficient is identical to Eq. (5.14) except that the terms  $E_i$ ,  $E_r$ , and  $E_w$  are now restricted to translational energy. If the incident and re-emitted molecules have the directional and velocity distributions of an equilibrium gas, as assumed throughout this section, their mean translational energies are equal to their respective temperatures multiplied by  $2k$ , where  $k$  is the Boltzmann constant (see Section 37 of reference 3). In this case Eq. (5.14) may be expressed as

$$\alpha_t = \frac{T_r - T_i}{T_w - T_i} \quad (5.15)$$

where  $T_r$  represents the kinetic temperature of the re-emitted gas defined by the relation

$$\frac{3}{2} k T_r = \frac{1}{2} m \overline{v_r^2} \quad (5.16)$$

Although the assumed re-emission model may be invalid, Eq. (5.15) will

still have meaning if  $T_r$  is considered as a hypothetical "effective kinetic temperature" which is defined as a measure of the mean translational energy of the re-emitted molecules.

Equation (5.15) may be solved for  $T_r$  and the result substituted into Eq. (5.13) to obtain

$$\frac{p_o}{p} = \frac{3}{5} \left( 1 + \frac{2}{3} \left[ 1 + \alpha_t (T_w/T_i - 1) \right]^{1/2} \right) \quad (5.17)$$

This expression has been plotted on Figs. 17 through 21 for several values of  $\alpha_t$ , making it possible to estimate the value of  $\alpha_t$  for each gas-surface combination. These values are presented and discussed in Section 5.4 along with those of  $\sigma''$ .

### 5.3.3 The Translational Energy Interpretation (Oblique Incidence)

The equations of Sections 3.2 and 3.3 are applicable for both normal and oblique angles of incidence because they are expressed in the general terms of normal momentum transfer. Therefore, the relation

$$\left( \frac{p_o}{p} \right)_{\text{const. } \tau} = \left( \frac{\theta}{\theta_o} \right)_{\text{const. } p} = \frac{p}{p_o} = \frac{p_i + p_r}{p_i + p_{r_o}} \quad (5.18)$$

is valid for any angle of incidence.

A similar statement cannot be made concerning the equations of Sections 5.3.1 and 5.3.2 because they are based on assumptions which restrict them to the special case of normal incidence. A more general "ideal" model which is applicable for any angle of incidence is developed in Appendix 2; it takes into account the facts that the beam



intensity is actually not completely uniform over the test surface, and the molecular beam disperses radially from the source slit, meaning that the particle paths are not exactly parallel at the test surface. In this case the magnitude of  $p$  is not constant over the surface since it is a function of the intensity and direction of the beam molecules, and therefore the applied torque is no longer equal to the simple product of  $R$  and  $p$  given in Eq. (2.6), but now equal to the integral of the product  $Rp$ . Appropriate integral expressions have been derived for  $\tau_i$ , the torque due to the normal momentum of the incident molecules, and  $\tau_r$ , the torque due to the normal momentum of the re-emitted molecules. Numerical solutions were obtained and the computer results are tabulated in Table V.

The validity of these results was checked experimentally by measuring the variation of torque with angle of incidence for an unheated test surface. In this investigation the partition wall was omitted and a circular source aperture was used (Section 4.4). A modified form of the constant pressure procedure was employed: wheel readings were taken for various orientations of the test surface relative to the molecular beam (i.e., various angles of incidence), the approximate value of the angle of incident being estimated from the scale reading. The experimental results are in excellent agreement with the theory, as shown in Fig. 22.

The equations of Appendix 2 may be used to derive the following expression:

$$\frac{P_o}{P} = \frac{\frac{\tau_i}{\tau_r} + \sqrt{T_r/T_i}}{\frac{\tau_i}{\tau_r} + 1} \quad (5.19)$$

In order to obtain an explicit expression of  $P_o/P$  at a specific angle of incidence, the appropriate numerical values of  $\tau_i$  and  $\tau_r$  given in Table V must be substituted into Eq. (5.19). For example, the following is obtained for angle of incidence of  $45^\circ$ :

$$\frac{P_o}{P} = \frac{0.988 + \sqrt{T_r/T_i}}{1.988} \quad (5.20)$$

Solving this for  $T_r$  gives

$$T_r = 298 \left( 1.988 \frac{P_o}{P} - 0.988 \right)^2 \quad (5.21)$$

where  $T_i$  has been assumed equal to  $25^\circ \text{ C}$  ( $298^\circ \text{ K}$ ). These equations will be utilized in Section 5.5.

#### 5.4 Experiments at Normal Incidence: Results and Conclusions

##### 5.4.1 General Comments

The agreement of data obtained for a specific gas-surface combination was in general quite satisfactory even though the experimental runs were conducted with different balance assemblies, source slits, projector locations, alignments, and at different room temperatures and source pressures. Therefore it is concluded that the results are not strongly dependent on any of these factors.

The following interesting observation concerning the scatter which appears in the data should be mentioned: the magnitude of  $P_0/P$  for the gases of low molecular weight was often smaller and less reproducible in the first half of an experimental run (i.e., in Step 7 of Section 5.1.1) than the corresponding value measured in the second half (i.e., in Step 9). This behavior was most pronounced for helium and hydrogen on tungsten. The data for gases of higher molecular weight was much more consistent and did not exhibit any definite patterns. A possible explanation is that the state of the surface contamination is initially unstable and slowly changes to a more stable state. This change in the surface contamination could account for the scatter appearing in the results; it should be pointed out that each plotted point is the average of two measurements, meaning that the scatter has been artificially reduced to some extent.

In the following paragraphs the estimated values of  $\sigma''$  and  $\alpha_t$  are summarized for each gas-surface combination. One of the main reasons for including a translational energy interpretation of the present data is that the results may be compared with those determined by other researchers using different measurement techniques (no such comparison may be made for the  $\sigma''$  values since this appears to be the first investigation of normal momentum transfer). The comparison of energy accommodation coefficients is of questionable validity because:

- (1) the majority of the published values are for clean, or semi-clean surfaces; the surfaces in the present experiment are contaminated with oxides and adsorbed gases,

therefore the results should be compared only to those obtained with similar unflashed conditions.

- (2) most of the investigations have been made in a thermal conductivity cell with small temperature differences (i.e., with  $T_w$  approximately  $10^\circ \text{C}$  higher than  $T_i$ ), and the results are usually extrapolated to zero difference; therefore it is doubtful that a valid comparison may be made because the temperature differences in the present case are as high as  $550^\circ \text{C}$ .
- (3) in a thermal conductivity cell the impinging molecules have random angles of incidence, whereas in the present experiment they are restricted to normal incidence; one might expect the accommodation to be more efficient at normal incidence, causing the values determined in this investigation to be larger than those of the thermal conductivity cell investigations.
- (4) most of the published values are for total energy transfer (i.e., translational plus internal molecular energy), but note that the total energy accommodation coefficient is identically equal to the translational energy accommodation coefficient in the case of monatomic gases (which cannot possess internal energy), and also in the case of gas molecules whose internal energies are unchanged by the particle-surface interaction.

#### 5.4.2 Tungsten Surfaces

A larger quantity of data was obtained for tungsten than for the other materials. The test conditions varied considerably and two balances and two slits were used. One test was made on a surface which was deliberately contaminated by painting it with diffusion pump oil; after an initial period of violent out-gassing, or evaporation, results were obtained which agree well with those for unpainted surfaces. This indicates that the nature of the surface contamination is not radically altered by additional quantities of oil.

From Figs. 11, 12, 17, and 18 it is possible to make the following estimates of  $\sigma''$  and  $\alpha_t$ :

Gas	Estimated Value of $\sigma''$	Estimated Value of $\alpha_t$	Approximate Range of $\alpha_t$	Values of $\alpha$ Measured by Others	Ref. No.
Helium	0.6	0.55	0.45 to 0.65	0.53	19
Hydrogen	0.7	0.60	0.4 to 0.8	0.48	16
Neon	0.75	0.70	0.65 to 0.75	~0.6	22
Nitrogen	1.0	1.0	--	--	--

The column "Values of  $\alpha$  Measured by Others" contains accommodation coefficients which have been determined by various investigators for contaminated tungsten surfaces. The helium and neon measurements were made with the thermal conductivity cell technique; the hydrogen accommodation coefficient of translational energy was evaluated from the damping of a vibrating hot filament (the accuracy of this technique is not known).

The extreme scatter in the hydrogen data is expected to be due to changes in the state of surface contamination as discussed previously.

#### 5.4.3 Blackened Tungsten Surfaces

The data for blackened tungsten surfaces was the most consistent obtained during the entire experimental program. The measurements were taken under varied test conditions with two different balances and source slits. Both the constant torque procedure and the constant pressure procedure were used and the agreement was excellent.

From Figs. 13 and 19 it is possible to make the following estimates of  $\sigma''$  and  $\alpha_t$ :

Gas	Estimated Value of $\sigma''$	Estimated Value of $\alpha_t$	Approximate Range of $\alpha_t$	Values of $\alpha$ Measured by Others	Ref. No.
Helium	0.85	0.8	0.75 to 0.85	0.91	1
Hydrogen	0.85	0.85	0.8 to 0.85	0.735	1
Carbon Dioxide	1.0	1.0	--	0.975	1

Since no data could be found in the literature for tungsten coated with platinum black, the present results have been compared to those obtained by Knudsen for platinum coated with platinum black. It is thought that this comparison is permissible because the properties of the substrate are probably obliterated by the platinum surface coating. The agreement is not entirely satisfactory; this may be due to experimental inaccuracies or to differences in the surface structure. It should be pointed out that for polyatomic molecules one might expect Knudsen's values to be smaller than the present values if the transfer of internal energy is less efficient than the transfer of translational energy.

#### 5.4.4 Aluminum Surfaces

Only one balance was used for the aluminum investigation, but it was tested on two separate occasions with different source slits, projector positions, and source pressure levels. Due to the limited amount of data obtained for neon and hydrogen, their values are not as well substantiated as those for helium and nitrogen.

From Figs. 14 and 20 it is possible to make the following estimates of  $\sigma''$  and  $\alpha_t$ :

Gas	Estimated Value of $\sigma''$	Estimated Value of $\alpha_t$	Approximate Range of $\alpha_t$
Helium	0.65	0.55	0.5 to 0.6
Hydrogen	0.75	0.65	0.6 to 0.7
Neon	0.85	0.85	--
Nitrogen	0.95	0.95	0.9 to 1.0

The only data which could be found for aluminum was that of Wiedmann and Trumpler<sup>23</sup> who determined  $\alpha$  to be between 0.87 and 0.95 for air on polished aluminum. The present result for nitrogen falls in the same range of values.

Baule's<sup>24</sup> classical analysis of the accommodation coefficient predicts that the value of  $\alpha$  for a specific gas should be larger for a surface of low molecular weight, such as aluminum, than for one of high molecular weight, such as tungsten. This tendency was not exhibited in the present experiment because surface contamination probably prevented the nature of the substrate from influencing the accommodation process.

#### 5.4.5 Platinum Surfaces

A smaller quantity of data was taken for platinum than for any other material; therefore the results are not as well substantiated. It should also be pointed out that the tests were restricted to the use of only one balance and one source slit. The limited amount of data which was obtained is fairly consistent, and the argon results are the most stable and reproducible of the entire experimental program.

From Figs. 15 and 21 it is possible to make the following estimates of  $\sigma''$  and  $\alpha_t$ :

Gas	Estimated Value of $\sigma''$	Estimated Value of $\alpha_t$	Approximate Range of $\alpha_t$	Values of $\alpha$ Measured by Others	Ref. No.
Helium	0.55	0.5	0.45 to 0.55	0.41	1
Hydrogen	0.65	0.55	0.55 to 0.65	0.32	1
Nitrogen	0.95	0.95	0.9 to 1.0	--	--
Carbon Dioxide	> 1.0	> 1.0	--	0.84	1

The results for carbon dioxide are especially interesting as they appear to indicate that  $\alpha_t$  is greater than unity. Since this is not a realistic value it is concluded that argon is not completely accommodated on platinum. Therefore it would be more appropriate to use carbon dioxide as the "reference gas"; this change would have an almost negligible effect on the values of  $\sigma''$  and  $\alpha_t$  for helium and hydrogen, but would give  $\alpha_t \approx 0.95$  for argon and  $\alpha_t \approx 0.9$  for nitrogen.

The present results are slightly higher than those of Knudsen. A possible explanation of this for hydrogen and carbon dioxide is that Knudsen's values are for  $\alpha$ , which may be smaller than  $\alpha_t$  due



to the inefficient transfer of internal energy. Other possibilities are that the present surfaces are more contaminated or rough, that neither carbon dioxide nor argon are completely accommodated, or it may be due to experimental inaccuracies.

#### 5.4.6 Overall Results and Conclusions

It is important to emphasize the fact that all of the test surfaces were probably coated with oxides, oil films and adsorbed gases. No special attempt was made to clean or "flash" the surfaces because they would have become immediately re-contaminated in the present apparatus. The results obtained are therefore applicable only to surfaces which are contaminated to the same extent as those in this experiment.

It appears that a specific gas is accommodated to approximately the same degree on each of the materials which have macroscopically smooth surfaces, i.e., tungsten, aluminum, and platinum. The "constant" accommodation coefficients are:

Gas	Approximate Value of $\sigma''$ for Smooth Surfaces	Approximate Value of $\alpha_t$ for Smooth Surfaces
Helium	0.6	0.55
Hydrogen	0.7	0.6
Nitrogen	0.95	0.95
Argon	1.0	1.0
Carbon Dioxide	1.0	1.0

It may be concluded that the chemical and physical natures of the materials have been almost completely obliterated by surface contamination, and therefore have little effect on the accommodation process.

The values of  $\sigma''$  and  $\alpha_t$  on the microscopically rough surface, blackened tungsten, are substantially higher than those on the smooth surfaces. If a classical model of the particle-surface interaction is assumed, this increase in accommodation may be thought of as being a result of the increase in the average number of collisions that a gas molecule will undergo on a rough surface<sup>1</sup>.

It should be noted that the values of  $\sigma''$  and  $\alpha_t$  appear to be relatively independent of surface temperature. This result is both interesting and convenient, and leads to the question: which parameter,  $\sigma''$  or  $\alpha_t$ , has more physical significance? (i.e., Is the accommodation process fundamentally one of constant energy transfer efficiency or one of constant momentum transfer efficiency, if either?) The present results are not sufficient to enable one to formulate a definite answer to this question.

#### 5.5 Experiments at Oblique Incidence: Results and Conclusions

As stated in Section 1.2, one of the objectives of the proposed investigation was to study the dependence of normal momentum transfer on the angle of incidence. This goal was not realized to a significant extent in the present program due to lack of time and experimental difficulties discussed below.

Several attempts were made to determine  $\alpha_t$  at an angle of incidence of  $45^\circ$  using the constant torque procedure. The data obtained for helium on blackened tungsten is summarized in Table IV. Equation (5.21) was used to calculate  $T_r$  for helium and  $T_w$  for argon, assuming that argon is completely accommodated. (It should be noted that this is a conservative assumption; if argon is not completely accommodated the

true value of  $\alpha_t$  for helium would be smaller than that reported in Table IV.) The results appear to indicate that the accommodation coefficient of helium at an angle of incidence of  $45^\circ$  may be slightly less than that at normal incidence.

The validity of these results is questionable because the magnitude of the estimated surface temperature at an angle of incidence of  $45^\circ$  appears to be as much as 13% less than the corresponding value (i.e., at the same projector voltage) at normal incidence. These temperatures were expected to be more nearly equal since the relative orientation of the projector and the test surface was approximately the same in both cases, the projector always being positioned so that its radiation is normal to the surface. This discrepancy may be due to incomplete accommodation of argon at  $45^\circ$ , or to deficiencies in the experimental apparatus, such as imperfect alignment of the balance with the source and defining slits (note that the alignment becomes more critical as the angle of incidence increases). It is not expected that inaccuracies in the determination of the angle of incidence cause this discrepancy because an error of  $\pm 5^\circ$  has very little effect on the magnitudes of  $T_r$  and  $\alpha_t$ .

Several other surface materials were investigated at  $45^\circ$  but the data was discarded because of its inconsistency. The source of this undesirable behavior was uncovered later: radiation from the projector had accidentally reached the source slit (slit #1, Section 4.4), causing thermal distortions which altered the dimensions of the aperture. Although these experimental results are unreliable, it is worthwhile to mention that helium appeared to be accommodated less efficiently

in the present case than at normal incidence. It would be possible to explain this behavior by the classical theory of particle-surface interactions, as it predicts that at oblique angles of incidence there is a higher probability for the occurrence of those collisions which transfer energy inefficiently, such as "glancing" encounters.

## 6.0 CONCLUDING CONSIDERATIONS AND COMMENTS

### 6.1 Precision and Sensitivity

In the present experiment an argon source pressure of 125 microns will cause a molecular beam intensity  $N$  of  $\sim 2 \times 10^{15}$  particles per second per  $\text{cm}^2$  on the test surface. At normal incidence the resulting force is  $\sim 1 \times 10^{-2}$  dynes (or  $\sim 1 \times 10^{-5}$  grams), meaning that the torque has a magnitude of  $\sim 5 \times 10^{-3}$  dyne-dm. Since the torsional rigidity of a 10 cm long, 0.0002 inch tungsten fiber is  $\sim 1 \times 10^{-3}$  dyne-cm per radian, the balance support shaft must be rotated through an angle of  $\theta \approx 5$  radians in order to apply a sufficient restoring torque.

It was occasionally possible to read the scale with a precision of  $\pm 1$  mm ( $5 \times 10^{-4}$  radians) meaning that torque increments of  $\sim 5 \times 10^{-7}$  dyne-cm (i.e., a 0.01% change) could be detected under ideal conditions. This corresponds to a force sensitivity of  $\sim 1 \times 10^{-9}$  grams per mm of scale deflection, a very respectable figure for a microbalance of any design<sup>10</sup>.

The angular position  $\theta$  of the balance support shaft is determined by the machine-divided wheel and vernier which can be read to  $\pm 1/16,000$  of a revolution, or  $\pm 4 \times 10^{-4}$  radians (Section 4.5.1). Therefore it is more precise than the scale reading, so the latter is the limiting measurement in the constant pressure procedure; the source pressure is the limiting measurement in the constant torque procedure since its reading precision is  $\sim \pm 0.5\%$  (Section 4.3.4).

### 6.2 Accuracy and Sources of Error

The preceding section indicates that the precision of reading the measurable quantities is very satisfactory: it is now necessary to

consider the accuracy, or validity, of the theoretical methods of interpretation which were used to convert these readings into meaningful results in terms of  $p_r$  or  $T_r$ , and  $T_w$ .

The interpretation of data obtained by the constant torque procedure at normal incidence is based on some assumptions which may not be completely valid under the present conditions. A critical evaluation of these assumptions follows:

- (1) Torque is caused only by the molecular beam. This statement includes the assumptions that radiometer effects and secondary effusion from the defining region are negligible, and that the distribution of radiant energy on the test surface was sufficiently uniform to prevent torque due to "radiation pressure" and non-uniform surface temperatures. Although it is expected that these assumptions are valid under the present conditions they have not been completely substantiated and may therefore be possible sources of error.
- (2) Heating the test surface produces no adverse side-effects. This statement assumes that the heating process does not cause any significant changes in the source chamber temperature  $T_i$ , in the torsional rigidity  $K$ , or in the dimensions and alignment of the geometry. No definite indications appeared during the experimental program to cause one to doubt the validity of these assumptions (except for the isolated case discussed in Section 5.5).

- (3) The molecular beam is normal to the test surface. This is not completely true because the particle paths are not exactly parallel (Appendix 2) and because it is difficult to determine precisely the orientation of the test surface relative to the molecular beam. Nevertheless, it is expected that resulting error is very small for normal incidence since the angular deviations cannot be very significant.
- (4) The intensity of the molecular beam is uniform over the test surface. The validity of this assumption for the case of normal incidence is indicated by a more detailed calculation appearing in Section A2.4 of Appendix 2.
- (5) The average velocity of the molecular beam is equal to the value given by simple kinetic theory. It is possible that this statement is slightly inaccurate since several investigations<sup>25</sup> have shown that the velocity distribution of a molecular beam may suffer a deficiency of low speed molecules. The resulting error is probably too small to have a strong influence in the present experiment.
- (6) The attenuation of the molecular beam is constant. The attenuation, or the fractional loss of beam intensity due to collisions with residual gas molecules or between the beam molecules themselves, is most likely negligible. On the other hand, if attenuation is significant it is probably valid to assume that it is constant under the present conditions.

- (7) The molecular beam intensity varies linearly with  $\xi P$ .

This assumption is based on results obtained by Liepmann<sup>9</sup> for near free molecule flow through circular apertures.

- (8) The ratio  $\xi/\xi_0$  is equal to unity for small changes in source pressure. The results of preliminary experiments (Section 2.5) and the excellent agreement of the constant pressure and constant torque results (Section 5.1.2) appear to verify this assumption.

- (9) The source pressure in the immediate neighborhood of the source slit is equal to that pressure measured by the McLeod Gauge. This statement may be broken down into three assumptions: 1) the McLeod gauge is an accurate means of measuring the pressure which exists in its volume; this was verified approximately by checking the gauge with a precision oil manometer; 2) the pressure in the McLeod is equal to that at the end of the sensing tube in the source chamber; an approximate check on this condition was made by varying the location of the sensing tube and altering the configuration of the external connecting tube and trap; 3) the pressure at the end of the sensing tube is equal to that in the immediate neighborhood of the source slit; it is not possible to verify this assumption accurately, and it may not be exactly true because of the small volume of the source chamber. It is expected that the ratio  $P_0/P$  will be fairly accurate even if the individual values of  $P$  and  $P_0$  are not exact; the excellent agreement of the constant



pressure and the constant torque results may be considered as an approximate indirect proof of this statement.

- (10) The reference gas, argon, is completely accommodated in the present experiment. This assumption appears to be fairly accurate (see Section 5.1). It should be noted that the estimated values of  $\sigma''$  and  $\alpha_t$  for helium and hydrogen would not be radically changed even if  $\alpha_t$  for argon were actually as low as 0.9.
- (11A) For an unheated surface (i.e.,  $T_w = T_1$ ), the test gases are re-emitted with the directional and velocity distributions of an equilibrium gas having the temperature of the surface. This is probably a valid supposition for the present conditions of normal incidence on contaminated metallic surfaces. It should be emphasized that the momentum interpretation (Section 5.3.1), contrary to the translational energy interpretation, makes no assumption concerning the nature of the re-emission when the surface is heated; therefore the value of  $p_r$  calculated from Eq. (5.3) is quite general since it is not based on a specific directional or velocity distribution function.
- (11B) For a heated surface, the test gases are re-emitted with the directional and velocity distributions of an equilibrium gas having the temperature  $T_r$  which is intermediate to  $T_w$  and  $T_1$ . The translational energy interpretation requires this assumption in addition to (11A). The present assumption is of questionable validity, although the results of experiments

concerning the directional<sup>21</sup> and velocity<sup>26,27</sup> distributions of re-emitted molecules may be considered as a partial verification.

As mentioned previously in Section 5.3.3, the interpretation of data obtained at oblique angles of incidence using the constant torque procedure does not require assumptions (3) and (4).

Although the interpretations of data obtained by the constant pressure procedure and the constant torque procedure employ the same equations (Section 3.3), they are not based on identical assumptions because of differences in their operational methods (see Sections 5.1.1 and 5.1.2). The interpretation of constant pressure data is based on assumptions (1) through (6) above, plus the assumptions that the torsional rigidity  $K$  is independent of the magnitude of the applied torque, and the eccentricity of the torsion fiber relative to the balance support shaft is negligible (see Section 2.5).

The general validity of those assumptions which are not common to both procedures was indirectly verified by the agreement of the constant torque and constant pressure results (Sections 5.1.2). One may consider the approximate agreement of the indirect estimates of the surface temperature with the "dummy surface" measurements (Section 5.2) as an indication of the general validity of the complete program, including both the experimental techniques and the theoretical interpretation schemes.

### 6.3 Proposed Future Investigations

A continuation of the investigation of normal momentum transfer at oblique angles of incidence is planned for the immediate future. A heated source chamber has been built and will probably be utilized in these studies. It will be most interesting to compare the results obtained with a heated gas to those obtained in the present investigation with a heated surface.

Another study which warrants attention is one employing a higher energy beam capable of simulating the conditions of high speed, high altitude flight. Such beams are being developed at the present time in various laboratories<sup>28</sup>.

All of the above-mentioned investigations would be of much greater value if conducted in a ultra-clean high vacuum system so that the contamination level of the test surface could be controlled. This constitutes a difficult and expensive improvement, but a very worthwhile one since the effect of the surface material on the particle-surface interaction could then be studied in more detail.

The work of Mitani, et.al.<sup>16</sup> introduces an experimental technique for evaluating both  $\alpha$  and  $\alpha_t$  (or  $\sigma''$ ) in the same apparatus; it combines the torsion balance with the thermal conductivity cell method which is commonly used for determining  $\alpha$ . This technique, or a similar one in which the torsion balance and conductivity cell are separate units but located in the same enclosure, could prove to be an effective means of investigating such problems as gas-surface reactions and catalysis.

A final remark should be made concerning possible improvements of the molecular beam-torsion balance system. Although the present

sensitivity appears to be more than adequate, it could be further increased by using a higher intensity beam with larger diffusion pumps, a longer torsion fiber, or a smaller diameter fiber. The last point is the most simple means of improving the sensitivity because the torsional rigidity  $K$  varies with the fourth power of the diameter. It is expected that substantial increases in sensitivity could be realized without exceeding the limit imposed by Brownian motion<sup>29</sup>.

#### 6.4 Comments on Particle-Surface Interaction Parameters Used in Rarefied Gas Dynamics

##### 6.4.1 Introductory Remarks

Calculations of lift, drag, and heat transfer rates for bodies moving through rarefied atmospheres require a knowledge of the particle-surface interactions. At the present time the aerodynamicist usually introduces the interaction effects into his analysis in terms of three macroscopic parameters, or "accommodation coefficients". These are  $\alpha$ , the thermal energy accommodation coefficient,  $\sigma'$ , the coefficient of normal momentum transfer, and  $\sigma$ , the coefficient of tangential momentum transfer. The defining equations are:<sup>20</sup>

$$\alpha = \frac{E_i - E_r}{E_i - E_w} \quad (6.1)$$

$$\sigma' = \frac{P_i - P_r}{P_i - P_w} \quad (6.2)$$

$$\sigma = \frac{\tau_i - \tau_r}{\tau_i} \quad (6.3)$$

where  $E_i$  is the energy transported to the surface per unit time by the

incident molecules,  $E_r$  is the energy transported from the surface per unit time by the re-emitted molecules,  $p_i$  and  $p_r$  are similarly defined for the incident and re-emitted normal momentum, and  $\tau_i$  and  $\tau_r$  for the incident and re-emitted tangential momentum. The quantities  $E_w$  and  $p_w$  are the energy and momentum which would be re-emitted by a maxwellian gas in thermal equilibrium with the surface, i.e., complete accommodation. (Note that  $\tau_w$  does not appear in Eq. (6.3) because it is identically zero.)

It is possible to obtain the following expressions from the defining equations given above:

$$E_r = \alpha E_w + (1 - \alpha) E_i \quad (6.1a)$$

$$p_r = \sigma' p_w + (1 - \sigma') p_i \quad (6.2a)$$

$$\tau_r = (1 - \sigma) \tau_i \quad (6.3a)$$

Several hypothetical models of the particle-surface interaction may be suggested from these relations. For example, from Eq. (6.1a) it may be suggested that the re-emitted molecules are divided into two classes, one consisting of the fraction  $\alpha$  of the molecules which are completely accommodated, the other consisting of the remaining fraction,  $(1 - \alpha)$ , which experiences no accommodation, i.e., the energies of these molecules are not changed by the interaction. A similar model may be assumed in terms of  $\sigma'$  from Eq. (6.2a), the only difference being that the re-emission of the unaccommodated class must now be defined more

specially as specular reflection. A model which has been associated with tangential momentum transfer (Eq. (6.3a)) is that a fraction  $(1 - \sigma)$  of the incident molecules are reflected specularly, and the remainder are re-emitted diffusely with a maxwellian distribution (therefore the re-emitted tangential momentum is zero for this fraction) at a temperature which is not necessarily equal to that of the surface<sup>20</sup>. None of these models are entirely realistic, as discussed in Section 5.3.1, but they are often useful as a point of departure in the formulation of more refined models.

Rather than being constants for a specific gas and surface material, the accommodation coefficients are most probably functions of the direction and velocity of the incident molecules, as well as the state of contamination, degree of smoothness, and temperature of the test surface. Therefore, it is not expected that the values determined for one set of conditions may be applied with certainty to other cases having different conditions. As stated in Section 5.3.1, the accommodation coefficients were designed primarily for near-equilibrium conditions and therefore may not be valid for situations involving flow or large temperature gradients.

The parameters defined in Eqs. (6.1) through (6.3) are not unique as it may be possible to formulate other parameters which will have more physical significance in certain cases (e.g., see Section 5.3.1). It is obvious that they are not completely independent parameters since all three are dependent on the velocity distribution functions of the incident and re-emitted molecules.

A desirable feature of a "well-behaved" parameter is that in the extreme or limiting cases, such as

(1) specular reflection, i.e.,  $E_r = E_i$ ,  $p_r = p_i$ , and

$$\tau_r = \tau_i$$

(2) complete accommodation, i.e.,  $E_r = E_w$ ,  $p_r = p_w$ , and

$$\tau_r = \tau_w = 0$$

(3) diffuse re-emission with no energy accommodation (see

Section 5.3.1); i.e.,  $E_r = E_i$ ,  $p_r = \frac{2}{3} p_i$  (Eq. (A1.10), valid only for normal incidence), and  $\tau_r = 0$

the parameter should have definite values, such as zero and unity, which are independent of the particular test conditions. It is also desirable that all of the physically possible values of the parameter be contained in the range which is bounded by the extreme, or limiting cases.

#### 6.4.2 The Energy Accommodation Coefficient

The energy coefficient defined in Eq. (6.1) appears to be a "well-behaved" parameter since it assumes a value of unity for the case of complete accommodation and a value of zero for the cases of specular reflection and diffuse re-emission with no energy accommodation. It is difficult, if not impossible, to hypothesize a physical situation in which the probable or expected values of  $\alpha$  would not be contained in the interval between zero and unity.

Consider a rarefied gas which is at rest with respect to the test surface and in a state of equilibrium with temperature  $T$ . If the temperature is not extremely high the gas molecules will possess only translational and rotational energies since the vibrational and electronic states will not be excited. In this case the average internal

energy per molecule is

$$\epsilon_{\text{int}} = \frac{j}{2} kT \quad (6.4)$$

where  $j$  is the number of rotational degrees of freedom for the molecule. The average translational energy of the molecules crossing an arbitrary surface (see Section (5.3.2)) is given by

$$\epsilon_t = 2 kT \quad (6.5)$$

It follows that the average total energy of the molecules crossing a surface is

$$\epsilon = \epsilon_t + \epsilon_{\text{int}} = \frac{4 + j}{2} kT \quad (6.6)$$

Now if the accommodation coefficient of internal energy is defined as\*

$$\alpha_{\text{int}} = \frac{(\epsilon_{\text{int}})_r - (\epsilon_{\text{int}})_i}{(\epsilon_{\text{int}})_w - (\epsilon_{\text{int}})_i} \quad (6.7)$$

Note that this definition is expressed in terms of average molecular energies rather than the macroscopic energy transport rates of Eq. (6.1); therefore it is based on the assumption that the number of molecules re-emitted per unit time is equal to the number incident (i.e., no condensation, chemical reaction, dissociation, etc.). By means of the above expressions one can show that average internal energy of the re-emitted molecules is

---

\*The energy coefficient  $\alpha$  may be divided into separate coefficients for the two classes of molecular energy, translational and internal.



$$(\epsilon_{int})_r = \frac{j}{2} k [\alpha_{int} (T_w - T_i) + T_i] \quad (6.8)$$

where  $T_i$  and  $T_w$  are the temperatures of the incident gas and the test surface, respectively. Similarly, the accommodation coefficient of translational energy is defined as

$$\alpha_t = \frac{(\epsilon_t)_r - (\epsilon_t)_i}{(\epsilon_t)_w - (\epsilon_t)_i} \quad (6.9)$$

so,

$$(\epsilon_t)_r = 2k [\alpha_t (T_w - T_i) + T_i] \quad (6.10)$$

The total energy accommodation coefficient (Eq. (6.1)) is equivalent to

$$\alpha = \frac{\epsilon_r - \epsilon_i}{\epsilon_w - \epsilon_i} \quad (6.11)$$

With Eqs. (6.6), (6.8), and (6.10) one can express Eq. (6.11) as

$$\alpha = \frac{4\alpha_t + j\alpha_{int}}{4 + j} \quad (6.12)$$

For a monatomic gas,  $j$  is equal to zero so Eq. (6.12) simplifies to

$$\alpha = \alpha_t \quad (6.13)$$

For a diatomic gas,  $j$  is equal to 2; therefore,

$$\alpha = \frac{2\alpha_t + \alpha_{int}}{3} \quad (6.14)$$

Note that  $\alpha_t$  has twice as much influence as  $\alpha_{int}$  on the magnitude of  $\alpha$ , and therefore on the heat transfer or energy exchange between a diatomic gas and the surface.

Consider now the case of a body, with surface temperature  $T_w$ , moving at velocity  $U$  through a rarefied gas which is in a state of equilibrium at temperature  $T_i$ ; it will be assumed that the thermal energy of the molecules is negligible compared to  $\frac{1}{2} m U^2$ , the kinetic energy of the mass motion.\* Fixing the frame of reference on the body, the gas molecules now strike the surface with an average translational energy of

$$(\epsilon_t)_i \approx \frac{1}{2} m U^2 \quad (6.15)$$

If it is assumed that  $(\epsilon_t)_w$  is also negligible compared to  $\frac{1}{2} m U^2$ , then  $\alpha_t$  is given by

$$\alpha_t \approx \frac{(\epsilon_t)_i - (\epsilon_t)_r}{(\epsilon_t)_i} \approx 1 - \frac{(\epsilon_t)_r}{\frac{1}{2} m U^2} \quad (6.16)$$

Therefore

$$(\epsilon_t)_r \approx \frac{1}{2} m U^2 (1 - \alpha_t)$$

and the total energy accommodation coefficient (Eq. (6.11)) may be expressed as\*\*

---

\* Such conditions generally exist for satellites; at an altitude of  $\sim 300$  km the major atmospheric constituent is atomic oxygen having a thermal energy of  $\sim 0.2$  eV, which is quite small compared to 4.8 eV, the approximate value of  $\frac{1}{2} m U^2$  for atomic oxygen.

\*\* The coefficient  $\alpha_{int}$  has not been utilized here because it may not be a "well-behaved" parameter in this case; it is physically possible that the energetic impact could excite the molecules to the extent that  $(\epsilon_{int})_r$  would be larger than both  $(\epsilon_{int})_i$  and  $(\epsilon_{int})_w$ , thereby causing  $\alpha_{int}$  to assume a value which is not contained in the interval between zero and unity. (The coefficients  $\alpha$  and  $\alpha_t$  are expected to be "well-behaved" in this case.)

$$\alpha \approx \frac{\epsilon_i - (\epsilon_{int})_i - (\epsilon_t)_i}{\epsilon_i} \approx \alpha_t - \frac{(\epsilon_{int})_i}{\frac{1}{2} m U^2} \quad (6.17)$$

where  $(\epsilon_{int})_i$  and  $(\epsilon_{int})_t$  have been neglected in addition to the corresponding thermal translational energies. For monatomic gases this equation reduces to\*

$$\alpha \approx \alpha_t \quad (6.18)$$

since the internal energy of the atoms is zero unless the quantity  $\frac{1}{2} m U^2$  is of sufficient magnitude to cause electronic excitation.

Equations (6.13), (6.14), and (6.18) illustrate the strong influence of the parameter  $\alpha_t$  on the magnitude of  $\alpha$ , and therefore on the heat transfer or energy exchange between gases and solids. It should be pointed out that the foregoing analysis, unlike that of Section 5.3.2, does not make any assumptions concerning the directions and velocities of the re-emitted molecules, and is therefore quite general.

#### 6.4.3 The Coefficient of Normal Momentum Transfer

A major fundamental difference between momentum and energy is that the former has both magnitude and direction (i.e., it is a vector quantity) while the latter has magnitude only (i.e., it is a scalar quantity). The result is that momentum transfer is equal to the sum  $p_i + p_r$ , whereas energy transfer is equal to the difference  $E_i - E_r$ . (Note:  $p_i$  and  $p_r$  are considered here to be the absolute magnitudes of the corresponding normal momentum components.) Another result is that  $p_r$ , unlike  $E_r$ , does not have the same limiting value for specular

---

\* At altitudes of more than 300 km at least 75% of the atmospheric constituents are completely dissociated (i.e., monatomic).

reflection as it has for diffuse re-emission with no energy accommodation (see Sections 5.3.1 and 6.4.1). Therefore it is difficult, if not impossible, to formulate or define an accommodation coefficient for normal momentum transfer which is both physically significant and "well-behaved" for various test conditions.

The general definition of the energy coefficient is of the form

$$\alpha = \frac{\text{actual energy transfer rate}}{\text{ideal energy transfer rate}} = \frac{E_i - E_r}{E_i - E_w} \quad (6.19)$$

which may theoretically have values from zero (no energy accommodation;  $E_r = E_i$ ) to unity (complete accommodation;  $E_r = E_w$ ). An analogous expression for normal momentum would have the following form:

$$\frac{\text{actual normal momentum transfer rate}}{\text{ideal normal momentum transfer rate}} = \frac{p_i + p_r}{p_i + p_w} \quad (6.20)$$

An undesirable feature of this parameter is that its values are not theoretically restricted to the range zero to unity, but to the range  $2 p_i / (p_i + p_w)$  (specular reflection) to unity (complete accommodation). The specular reflection value is not a convenient, or "well-behaved" limit because it is dependent on the test conditions, e.g., on  $T_i$  and  $T_w$ .

The generally accepted parameter for normal momentum transfer is defined in Eq. (6.2) and may be shown to have a value of zero for specular reflection, unity for complete accommodation, and  $\frac{(1/3)p_i}{p_i - p_w}$  for the case of diffuse re-emission with no energy accommodation. It is this last value which prevents  $\sigma'$  from being a "well-behaved"

parameter; note that the quantity  $\frac{(1/3)p_i}{p_i - p_w}$  is a function of the test conditions and may therefore assume values which are not contained in the interval between zero and unity (e.g., see Section 5.3.1).

The parameter  $\sigma''$  introduced in Section 5.3.1 circumvents the above-mentioned undesirable characteristic of  $\sigma'$ , but does so at the expense of the specular reflection limit; the value of  $\sigma''$  is  $\frac{(1/3)p_i}{p_w - (2/3)p_i}$  for specular reflection. Therefore the problem has been shifted from one limiting case to another, but the improvement which is gained may be significant since  $\sigma''$  is probably a more realistic parameter for most gases, surfaces, and angles of incidence (the possible exceptions are discussed in the following paragraph).

Wave mechanics predicts that the specular reflection and diffraction of atoms or molecules by surfaces will occur when the de Broglie wave length<sup>\*</sup> of the incident particles is large enough to be of the same order of magnitude as the characteristic dimension of the surface, i.e., the surface roughness for specular reflection and the lattice spacing for diffraction. In practice such conditions are achieved only for light atoms or molecules (H, He, H<sub>2</sub>) at grazing incidence on smooth surfaces and crystal lattices (see reference 30 for a more detailed discussion). On the basis of classical mechanics one might expect a re-emission similar to that of specular reflection to occur for gases on smooth, clean surfaces which have a close-packed structure; this hypothesis has been verified experimentally for various liquid metal and crystalline surfaces.<sup>31</sup>

---

\*The de Broglie wave length is equal to  $h/mv$ , where  $h$  is Planck's constant, and  $m$  and  $v$  are the mass and speed of the particles.

#### 6.4.4 The Coefficient of Tangential Momentum Transfer

There are several fundamental differences between tangential momentum transfer and normal momentum transfer:

- (1) The vector component  $p_r$  has only one possible direction, i.e., away from the surface; the component  $\tau_r$  has more than one possibility but it is generally assumed to have the same direction as  $\tau_i$  (in general this assumption is physically a realistic one; therefore the present discussion will be based on it). Note that due to these directional restrictions the tangential momentum transfer is equal to the difference  $\tau_i - \tau_r$ , whereas the normal momentum transfer is equal to the sum  $p_i + p_r$ .
- (2) If the re-emission is diffuse and maxwellian, the magnitude of  $\tau_r$  will be zero regardless of the degree of energy accommodation; this is not true for  $p_r$ , as discussed previously in Sections 5.3.1 and 6.4.3.

The coefficient of tangential momentum transfer defined in Eq. (6.3) appears to be a "well-behaved" parameter in flow situations since it has a limiting value of zero for the case of specular reflection, and unity for both complete accommodation and diffuse re-emission with no energy accommodation; it is difficult to imagine a physical situation in which the value of  $\sigma$  would not be contained in the interval bounded by these limits.

#### 6.4.5 Concluding Remarks on Accommodation Coefficients

The complete description of a particle-surface interaction requires a theoretical or experimental determination of the velocity distribution function of the re-emitted molecules for a given incident distribution. This represents an arduous task, one which is not likely to be accomplished in the immediate future except possibly for special cases. Therefore, at present it is necessary to accept simplified descriptions of the interaction using various parameters and hypothetical models which are of questionable validity. In the preceding sections the attributes of several accommodation coefficients were discussed briefly, and a modified coefficient of normal momentum transfer was introduced.

APPENDIX 1. AN ANALYSIS OF NORMAL MOMENTUM TRANSFER BASED ON  
AN "IDEAL MODEL". (Normal Incidence)

A1.1 Summary

A highly idealized and simplified theoretical analysis of the normal momentum transfer rate is considered in this appendix; the results will be summarized below and used to derive an expression for the applied torque. The analysis is not expected to be entirely accurate or realistic, but should provide valuable insight into the problem; it utilizes an "ideal model" of the particle-surface interaction which is based on the following assumptions (a more complete list of assumptions is discussed in Section 6.2):

- (1) The molecular beam is "ideal" (see Section 2.2), meaning that its properties may be calculated by means of simple kinetic theory.
- (2) The test surface is located on, and is perpendicular to, the normal drawn from the plane of the source slit (see Fig. 1).
- (3) The distance from the source slit to the test surface is sufficiently large (and the test surface is sufficiently small) that the molecules striking each element of surface area are equal in number and parallel in direction (i.e., the molecular beam has parallel particle paths and uniform intensity at the test surface).
- (4) The re-emitted molecules behave as though they had come from a gas which is at rest and in a state of



equilibrium with temperature  $T_r$ ; therefore the directional distribution is diffuse and the velocity distribution maxwellian.

Note that this model is restricted to the special case where the direction of the molecular beam is normal to the test surface (i.e., normal incidence). A more detailed analysis which does require assumptions (2) and (3), and is therefore applicable at oblique angles of incidence, is presented in Appendix 2.

Consider the following simplified model of the particle-surface interaction: a gas molecule of mass  $m$  and velocity  $v_i$  strikes the test surface and is scattered, or re-emitted, with a velocity  $v_r$ . If  $N$  represents the number of molecules striking the surface per unit time, then

$$P_i = N m \bar{v}_{ni} \quad (A1.1)$$

$$P_r = N m \bar{v}_{nr} \quad (A1.2)$$

$$p = N m (\bar{v}_{ni} + \bar{v}_{nr}) \quad (A1.3)$$

$$\tau = R p = R N m (\bar{v}_{ni} + \bar{v}_{nr}) \quad (A1.4)$$

where  $\bar{v}_{ni}$  and  $\bar{v}_{nr}$  are the time-averaged normal velocities of the incident and scattered molecules. It has been assumed that the quantities  $N$  and  $m$  for the scattered particles are equal to the corresponding values for the incident particles (i.e., no dissociation, chemical reaction, condensation, etc.)

A theoretical expression of  $N$  has been derived in Section A1.2 using assumptions (1) through (3) of this section:

$$N = \frac{P S S'}{2 \pi l^2} \left[ \frac{2}{m \pi k T_1} \right]^{1/2} \quad (\text{A1.5})$$

where  $P$  and  $T_1$  are the pressure and temperature of the gas in the source chamber,  $S$  is the area of the source slit,  $S'$  is that area of the test surface which is exposed to the molecular beam, and  $l$  is the distance from the source slit to the test surface.

The mean speed of molecules in an "ideal" beam is (see Eq. (A1.28)):

$$\bar{v}_1 = \frac{3}{4} \left[ \frac{2 \pi k T_1}{m} \right]^{1/2} \quad (\text{A1.6})$$

Using assumption (4) it is possible to derive the following expression for  $\bar{v}_{nr}$  (see Eq. (A1.35)):

$$\bar{v}_{nr} = \frac{1}{2} \left[ \frac{2 \pi k T_r}{m} \right]^{1/2} \quad (\text{A1.7})$$

Therefore the ratio of  $p_r$  to  $p_1$  at normal incidence is

$$\frac{p_r}{p_1} = \frac{\bar{v}_{nr}}{\bar{v}_1} = \frac{2}{3} \sqrt{T_r/T_1} \quad (\text{A1.8})$$

This relation may also be derived from Eqs. (A1.33) and (A1.39). For a gas which is completely accommodated (i.e., the gas attains a state of thermal equilibrium with the surface temperature  $T_w$  before being re-emitted), Eq. (A1.8) has the form

$$\frac{p_w}{p_i} = \frac{2}{3} \sqrt{T_w/T_i} \quad (A1.9)$$

where  $p_w$  is defined as the rate at which normal momentum is transported from the surface by a completely accommodated gas. Note that when the test surface and the source gas are at the same temperature, Eq. (A1.8) and Eq. (A1.9) both reduce to

$$\frac{p_r}{p_i} = \frac{p_w}{p_i} = \frac{2}{3} \quad (A1.10)$$

if it is assumed that  $T_r = T_i$  when  $T_w = T_i$ .

With Eqs. (A1.5) through (A1.7) it is possible to express Eq. (A1.4) as

$$\tau = C P \left[ \frac{3}{2} + \sqrt{T_r/T_i} \right] \quad (A1.11)$$

where  $C$  is a constant for a given geometrical configuration:

$$C = \frac{R S S'}{2 \pi \ell^2} \quad (A1.12)$$

When the source gas and the test surface are at the same temperature, Eq. (A1.11) simplifies to

$$\tau_{(T_w=T_i)} = \frac{5}{2} C P \quad (A1.13)$$

if again it is assumed that  $T_r = T_i$  when  $T_w = T_i$ .

### A1.2 The Intensity of an "Ideal" Molecular Beam

Consider a volume of gas which is at rest and in a equilibrium state at pressure  $P$  and temperature  $T$ . Its number density is given by the perfect gas law:

$$n = \frac{P}{k T} \quad (A1.14)$$

where  $k$  is the Boltzmann constant. The number of molecules crossing an arbitrary surface  $dS$  per unit time with speeds in the range  $dv$  and in a direction contained in the solid angle  $d\omega$  which is inclined at an angle  $\phi$  relative to the surface normal is<sup>3</sup>

$$n \Lambda v^3 e^{-\beta^2 v^2} dv d\omega dS \cos \phi \quad (A1.15)$$

where

$$\Lambda = \frac{\beta^3}{\pi^{3/2}} \quad (A1.16)$$

and

$$\beta = \sqrt{\frac{m}{2 k T}} \quad (A1.17)$$

and  $m$  is the mass of the molecule. Now assume that  $dS$  is a source slit which permits the gas to effuse into an evacuated chamber. Assume also that the effusing stream of molecules is collision-free and the equilibrium conditions of the source chamber are not disturbed by the effusion.

If  $d\omega$  intersects a surface  $dS'$  (see Fig. 23) at a distance  $r$  from  $dS$ , and  $r$  is inclined at an angle  $\phi'$  relative to the surface normal of  $dS'$ , then  $d\omega$  may be expressed geometrically as

$$d\omega = \frac{dS' \cos \varphi'}{r^2} \quad (\text{A1.18})$$

The substitution of this into Eq. (A1.15) gives the following expression for the number of molecules striking  $dS'$  per unit time which come from  $dS$  having speeds in the range  $dv$ :

$$n \Lambda v^3 e^{-\beta^2 v^2} dv \frac{dS' \cos \varphi'}{r^2} dS \cos \varphi \quad (\text{A1.19})$$

Integrating over  $v$  from zero to infinity gives  $dN$ , the total number of molecules from  $dS$  which strike  $dS'$  per unit time:

$$dN = \frac{n \Lambda dS dS' \cos \varphi \cos \varphi'}{2 \beta^4 r^2} \quad (\text{A1.20})$$

An alternate form is obtained by substituting Eqs. (A1.16) and (A1.17) for  $\Lambda$  and  $\beta$ :

$$dN = \frac{n \bar{c}_1}{4 \pi r^2} dS dS' \cos \varphi \cos \varphi' \quad (\text{A1.21})$$

where  $\bar{c}_1$  is the mean random molecular speed of the source chamber gas at equilibrium with temperature  $T_1$ :

$$\bar{c}_1 = \sqrt{\frac{8 k T_1}{m \pi}} \quad (\text{A1.22})$$

Consider a special case of normal incidence where:

- (1)  $dS'$  is located on, and is perpendicular to, the normal drawn from the plane of  $dS$ . (See Fig. 1 for an example of this condition.)

- (2) the distance  $r$  is sufficiently large (and  $dS'$  is sufficiently small) that the particle paths of the beam molecules are parallel at  $dS'$ .

In this case  $\phi$  and  $\phi'$  are zero so Eq. (A1.21) simplifies to

$$dN = \frac{n \bar{c}_1}{4 \pi l^2} dS dS' \quad (\text{A1.23})$$

where  $l$  is the perpendicular distance from  $dS$  to  $dS'$ . Now if  $dS$  and  $dS'$  are integrated over the areas  $S$  and  $S'$ , respectively, an expression is obtained for  $N$ , the rate at which molecules from  $S$  strike  $S'$ :

$$N = \frac{n \bar{c}_1}{4 \pi l^2} S S' \quad (\text{A1.24})$$

An alternate form is obtained by substituting the proper expressions for  $n$  and  $\bar{c}_1$ :

$$N = \frac{P S S'}{2 \pi l^2} \left[ \frac{2}{m \pi k T_1} \right]^{1/2} \quad (\text{A1.25})$$

### A1.3 The Mean Speed of an "Ideal" Molecular Beam

If Eq. (A1.15) is integrated over  $v$  from zero to infinity, one obtains an expression for the total number of molecules which cross  $dS$  per unit time in a direction contained in the solid angle  $d\omega$ :

$$\frac{n \Lambda \cos \phi}{2 \beta^4} d\omega dS \quad (\text{A1.26})$$

Dividing Eq. (A1.15) by Eq. (A1.26) gives the probability  $P$  that a molecule crossing  $dS$  in  $d\omega$  will have a speed in the range  $dv$ :

$$P = 2 \beta^4 v^3 e^{-\beta^2 v^2} dv \quad (A1.27)$$

Note that this probability is independent of the angle  $\phi$ . The mean speed  $\bar{v}_1$  of the molecules in the beam is calculated by multiplying  $v$  by  $P$  and then integrating  $v$  from zero to infinity. The result is conveniently expressed in the form

$$\bar{v}_1 = \frac{3}{4} \left[ \frac{2 \pi k T_1}{m} \right]^{1/2} = \frac{3 \pi}{8} \bar{c}_1 \quad (A1.28)$$

where  $\bar{c}_1$  is defined by Eq. (A1.22). The magnitude of  $\bar{v}_1$  is slightly larger than  $\bar{c}_1$  because the faster molecules obviously stand a better chance of crossing the surface in a given time interval.

#### A1.4 The Momentum Transported by an "Ideal" Molecular Beam

The rate at which momentum is transported to the surface  $dS'$  by molecules from  $dS$  having velocities in the range  $dv$  is expressed by multiplying Eq. (A1.19) by  $m v$ , the momentum of a single molecule:

$$n m \Lambda v^4 e^{-\beta^2 v^2} dv \frac{dS' \cos \phi'}{r^2} dS \cos \phi \quad (A1.29)$$

Integrating this over  $v$  from zero to infinity gives  $dp_1$ , the rate at which momentum is transported to  $dS'$  by molecules of all speeds from  $dS$ :

$$dp_1 = \frac{3 \sqrt{\pi} n m \Lambda \cos \phi \cos \phi'}{8 \beta^5 r^2} \quad (A1.30)$$

An alternate form is obtained by substituting Eqs. (A1.14), (A1.16) and (A1.17) for  $n$ ,  $\Lambda$ , and  $\beta$ :

$$dp_1 = \frac{3 P \cos \varphi \cos \varphi'}{4 \pi r^2} dS dS' \quad (A1.31)$$

Note that this equation predicts that the momentum transported by a molecular beam to a surface is independent of the mass of the molecules and the temperature of the source chamber.

For the special case of  $\varphi = \varphi' = 0$ , Eq. (A1.31) reduces to

$$dp_1 = \frac{3 P}{4 \pi l^2} dS dS' \quad (A1.32)$$

where  $l$  is the perpendicular distance from  $S$  to  $S'$ . Now if  $dS$  and  $dS'$  are integrated over the areas  $S$  and  $S'$ , respectively, an expression is obtained for  $p_1$ , the rate at which momentum is transported to  $S'$  by molecules from  $S$ :

$$p_1 = \frac{3 P S S'}{4 \pi l^2} \quad (A1.33)$$

The above equation may also be derived by multiplying the mean momentum per molecule,  $m \bar{v}_1$ , by  $N$ , the rate at which molecules from  $S$  strike  $S'$ :

$$p_1 = N m \bar{v}_1 \quad (A1.34)$$

One may prove that Eqs. (A1.33) and (A1.34) are identical by substituting the proper expressions for  $N$  and  $\bar{v}_1$ .



### A1.5 The Mean Normal Velocity Component for Re-Emission from an Equilibrium Gas

In order to obtain an explicit expression for the mean normal velocity component of the re-emitted molecules,  $\bar{v}_{nr}$ , one must assign a directional and velocity distribution function. Here it is assumed that the re-emitted molecules behave as though they had come from an equilibrium gas at temperature  $T_r$  and number density  $n_r$ , which means the directional distribution is diffuse and the velocity distribution is maxwellian; therefore the equations of the preceding sections are applicable.

One may obtain an expression for  $\bar{v}_{nr}$  by multiplying Eq. (A1.27), expressed in terms of  $v_r$ , by  $v_r \cos \phi'$ , the normal component of the molecular velocity, and then integrating over  $v_r$  from zero to infinity. The result is

$$\bar{v}_{nr} = \frac{1}{2} \left[ \frac{2 \pi k T_r}{m} \right]^{1/2} = \frac{\pi}{4} \bar{c}_r \quad (\text{A1.35})$$

where

$$\bar{c}_r = \sqrt{\frac{8 k T_r}{m \pi}} \quad (\text{A1.36})$$

$\bar{c}_r$  being the mean random molecular speed of an equilibrium gas at temperature  $T_r$ .

### A1.6 The Re-Emitted Normal Momentum for an Equilibrium Gas

The re-emission model of Section A1.5 will be employed here also. The rate at which normal momentum is transported from the surface by the re-emitted particles is obtained by multiplying Eq. (A1.15), expressed in terms of  $n_r$ ,  $v_r$ , and  $\phi'$ , by  $m v_r \cos \phi'$ , the normal

momentum of a single molecule, and then integrating  $v_r$  from zero to infinity,  $\phi'$  and  $\omega$  over a hemisphere, and  $dS'$  over  $S'$ . The result is simply

$$p_{nr} = \frac{1}{2} n_r k T_r S' \quad (A1.37)$$

If the rate at which the molecules are re-emitted from  $S'$ ,  $\frac{1}{4} n_r \bar{c}_r S'$  (obtained by integrating Eq. (A1.15)), is assumed to be equal to  $N$ , the rate at which molecules strike  $S'$ , one can derive the following expression for  $n_r$ :

$$n_r = \frac{n S}{\pi \lambda^2} \sqrt{T_1/T_r} \quad (A1.38)$$

Substituting this into Eq. (A1.37) gives

$$p_r = \frac{p S S'}{2 \pi \lambda^2} \sqrt{T_r/T_1} \quad (A1.39)$$

where  $n$  has been replaced by Eq. (A1.14). An equivalent statement of the above equation is

$$p_r = N m \bar{v}_{nr} \quad (A1.40)$$

This constitutes a simple alternate method for deriving Eq. (A1.39). One may easily prove that Eqs. (A1.39) and (A1.40) are identical by substituting the proper expressions for  $N$  and  $\bar{v}_{nr}$ .

## APPENDIX 2. THE APPLIED TORQUE AT ARBITRARY ANGLE OF INCIDENCE

### A2.1 Introduction

The theoretical expression for applied torque which was derived in Section A1.1 is based on the assumptions that the molecular beam is normal to the surface and has a uniform intensity over the surface. A derivation which is independent of these assumptions is presented in this appendix, along with calculations of the applied torque for various angles of incidence.

### A2.2 Theoretical Formulation of the Problem

Consider the torque which results from a molecular beam striking the test surface at an "angle of attack"  $\psi$  (the angle of attack is defined as the angle between the plane of the surface and the primary direction of the molecular beam; note that the "angle of incidence" is equal to  $90^\circ - \psi$ ). The rate at which particles cross the elemental area  $dS$  and strike  $dS'$  is given by Eq. (A1.21) to be

$$dN = \frac{n \bar{c}_1}{4 \pi r^2} dS dS' \cos \varphi \cos \varphi' \quad (A2.1)$$

Substituting this into Eq. (A1.4) it is possible to express the resulting elemental torque as

$$d\tau = R \frac{n \bar{c}_1}{4 \pi r^2} dS dS' \cos \varphi \cos \varphi' m (\bar{v}_1 \cos \varphi' + \bar{v}_{nr}) \quad (A2.2)$$

where  $\bar{v}_1 \cos \varphi'$  is the normal component of  $\bar{v}_1$ . From the geometry shown in Fig. 24 it is evident that

$$R = \frac{y'}{\sin \psi} \quad (\text{A2.3})$$

$$dS = w dz \quad (\text{A2.4})$$

$$dS' = \frac{dy'}{\sin \psi} dz \quad (\text{A2.5})$$

$$r = [(\ell + y' \cot \psi)^2 + (z' - z)^2 + (y')^2]^{1/2} \quad (\text{A2.6})$$

$$\cos \varphi = \frac{\ell + y' \cot \psi}{r} \quad (\text{A2.7})$$

$$\cos \varphi = \frac{\ell \sin \psi}{r} \quad (\text{A2.8})$$

Note that it has been assumed that the slit width  $w$  is sufficiently small so that  $dy = w$ . This is equivalent to considering the slit to be a line source; it simplifies the following equations by eliminating the necessity of integrating over  $y$ .

Using the above expressions it is possible to obtain an integral equation for the applied torque:

$$\tau = A (\sin \psi I_1 + \frac{1}{\ell} \frac{\bar{v}_{nr}}{\bar{v}_1} I_2) \quad (\text{A2.9})$$

where

$$A = \frac{n m \bar{c}_1 \bar{v}_1 w \ell^2}{4 \pi} \quad (\text{A2.10})$$

$$I_1 = \int_{-\frac{1}{2}h}^{+\frac{1}{2}h} dz \int_{-\frac{1}{2}Z}^{+\frac{1}{2}Z} dz' \int_0^{Y/\sin \psi} dy' \frac{y'(\ell + y' \cot \psi)}{[(\ell + y' \cot \psi)^2 + (z' - z)^2 + (y')^2]^{5/2}} \quad (\text{A2.11})$$

$$I_2 = \int_{-\frac{1}{2}h}^{+\frac{1}{2}h} dz \int_{-\frac{1}{2}Z}^{+\frac{1}{2}Z} dz' \int_0^{Y/\sin \psi} dy' \frac{y'(\ell + y' \cot \psi)}{[(\ell + y' \cot \psi)^2 + (z' - z)^2 + (y')^2]^2} \quad (A2.12)$$

Note that  $h$  is the height of the source slit and  $Z$  and  $Y$  are the dimensions of the surface  $S'$ . The results of integrating over  $z$  and  $z'$  are

$$I_1 = \frac{2}{3} \int_0^{Y/\sin \psi} dy' \frac{y'(\ell + y' \cot \psi)}{\xi^4} \left\{ \frac{\frac{1}{2}(Z+h)^2 + \xi^2}{\left[\frac{1}{4}(Z+h)^2 + \xi^2\right]^{1/2}} - \frac{\frac{1}{2}(Z-h)^2 + \xi^2}{\left[\frac{1}{4}(Z-h)^2 + \xi^2\right]^{1/2}} \right\} \quad (A2.13)$$

$$I_2 = \frac{1}{2} \int_0^{Y/\sin \psi} dy' \frac{y'(\ell + y' \cot \psi)}{\xi^3} \left[ (Z+h) \tan^{-1} \frac{(Z+h)}{2\xi} - (Z-h) \tan^{-1} \frac{(Z-h)}{2\xi} \right] \quad (A2.14)$$

where  $\xi$  is a function of  $y'$ :

$$\xi = \left[ (y')^2 + (\ell + y' \cot \psi)^2 \right]^{1/2} \quad (A2.15)$$

It was not possible to integrate these equations directly in their present form; an approximate solution was obtained by the technique described in the next section.

### A2.3 An Approximate Solution

It is possible to obtain approximate solutions of Eqs. (A2.13) and (A2.14) by transforming the integrals into summations. Consider the surface  $S'$  to be divided into  $v$  equal strips of width  $Y/v$  and height  $Z$ . In this case  $y_i''$ , the distance from the  $z$ -axis to the center

of the  $i^{\text{th}}$  strip, is given by

$$y_i'' = \frac{i - \frac{1}{2}}{v} Y \quad (\text{A2.16})$$

and if  $v$  is sufficiently large,

$$dy'' = \Delta y'' = \frac{Y}{v} \quad (\text{A2.17})$$

From Fig. 24 it is evident that

$$y' = y'' \sin \psi \quad (\text{A2.18})$$

$$\text{Therefore,} \quad y' = \frac{i - \frac{1}{2}}{v} Y \sin \psi \quad (\text{A2.19})$$

$$dy' = dy'' \sin \psi = \frac{Y}{v} \sin \psi \quad (\text{A2.20})$$

Substitution of the last two equations into Eqs. (A2.13) and (A2.14) produces the following approximate expressions of the integrals:

$$I_1 = \frac{2Y^2 \sin \psi}{3v} \sum_{i=1}^{i=v} \frac{1}{\xi_i^4} \left( \frac{i - \frac{1}{2}}{v} \right) \left[ 1 + \left( \frac{i - \frac{1}{2}}{v} \right) Y \cos \psi \right] \left\{ \frac{\frac{1}{2}(Z+h)^2 + \xi_i^2}{\left[ \frac{1}{4}(Z+h)^2 + \xi_i^2 \right]^{1/2}} - \frac{\frac{1}{2}(Z-h)^2 + \xi_i^2}{\left[ \frac{1}{4}(Z-h)^2 + \xi_i^2 \right]^{1/2}} \right\} \quad (\text{A2.21})$$

$$I_2 = \frac{Y^2 \sin \psi}{2} \sum_{i=1}^{i=v} \frac{1}{\xi_i^3} \left( \frac{i - \frac{1}{2}}{v} \right) \left[ 1 + \left( \frac{i - \frac{1}{2}}{v} \right) Y \cos \psi \right] \left\{ (Z+h) \tan^{-1} \frac{(Z+h)}{2\xi_i} - (Z-h) \tan^{-1} \frac{(Z-h)}{2\xi_i} \right\} \quad (\text{A2.22})$$

where

$$\xi_1 = \left[ \ell^2 + 2\ell \left( \frac{1 - \frac{1}{2}}{v} \right) Y \cos \psi + \left( \frac{1 - \frac{1}{2}}{v} \right)^2 Y^2 \right]^{1/2} \quad (\text{A2.23})$$

An IBM 704 computer was used to evaluate these summations for various values of  $\psi$ . The surface  $S'$  was divided into 40 strips. The dimensions of the present apparatus with source slit #2 were used (i.e.,  $h = 0.35$  cm,  $\ell = 6.50$  cm, and  $Y = Z = 1.00$  cm). The results appear in Table V along with the torque ratio  $\tau/\tau_{90^\circ}$  which is calculated by means of Eq. (A2.9); a graph of  $\tau/\tau_{90^\circ}$  versus  $\psi$  is shown in Fig. 22.

#### A2.4 Results and Conclusions

If Eqs. (A1.14), (A1.22), (A1.28), and (A1.35) are applied to Eq. (A2.9), the resulting expression is

$$\tau = \frac{3 \zeta P w \ell^2}{4 \pi} \left[ \sin \psi I_1 + \frac{2}{3\ell} \sqrt{T_r/T_1} I_2 \right] \quad (\text{A2.24})$$

where the flow coefficient  $\zeta$  has also been introduced (see Section 2.5). Using the dimensions and data which appear in Table V, it is possible to obtain the following form of Eq. (A2.24) for the case of  $\psi = 90^\circ$ :

$$\tau = 1.122 \times 10^{-5} \zeta P \left[ 1.490 + \sqrt{T_r/T_1} \right] \quad (\text{A2.25})$$

It is of interest to compare this expression to the corresponding one derived by a more simple technique in Section A1.1. For the present dimensions, Eq. (A1.11) may be expressed as

$$\tau = 1.154 \times 10^{-5} \zeta P \left[ \frac{3}{2} + \sqrt{T_r/T_1} \right] \quad (\text{A2.26})$$

The degree of agreement of the above equations leads one to the conclusion that assumptions (2) and (3) of Section A1.1 are quite valid in the present case. It should be noted that the numerical constant,  $1.154 \times 10^{-5}$ , appearing in Eq. (A2.26) has no influence on relative measurements because it may be cancelled when the ratios  $P_o/P$  and  $\theta/\theta_o$  are formed.

The application of Eq. (A2.24) to experimental results obtained at oblique angles of incidence is described in Section 5.3.3; an experimental verification of the equation is also discussed.



# REFERENCES

1. M. Knudsen      The Kinetic Theory of Gases, Methuen, London, (1934).
2. L.B.Loeb        The Kinetic Theory of Gases, McGraw-Hill, New York,  
(1934).
3. E.H.Kennard     Kinetic Theory of Gases, McGraw-Hill, New York,  
(1938).
4. F.C.Hurlbut     "Recent Studies of Particle-Surface Interactions,"  
Proc. of the Atomic and Molecular Beams Conference,  
Univ. of Denver, (1960).  
  
F.C.Hurlbut       "A Survey of Particle-Surface Interactions,"(paper  
in preparation).
5. R.A.Millikan    "Coefficients of Slip in Gases and the Law of  
Reflection of Molecules from the Surfaces of Solids  
and Liquids," Phys. Rev., 21, 217, (1923).  
  
E. Blankenstein "Coefficients of Slip and Momentum Transfer in  
Hydrogen, Helium, Air, and Oxygen," Phys. Rev.,  
22, 582, (1923).  
  
F.C.Hurlbut       "Influence of Pressure History on Momentum Transfer  
in Rarefied Gas Flows," Phys. Fluids, 3, 541, (1960).  
(Note: this paper summarizes the results of rotating  
cylinder experiments performed at the Univ. of Calif.  
Aero. Sciences Lab.)
6. F.C.Hurlbut     "Notes on Surface Interaction and Satellite Drag,"  
Project RAND Report R-339, Aerodynamics of the  
Upper Atmosphere, (1959).

7. D.W.Bassett "The Development of a New Technique for the Investigation of Energy Transfer at the Gas-Solid Interface,"  
Ph.D. thesis, Dept. of Chemistry, Univ. of London,  
(1958). (also Brit.J.Appl.Phys., 10, 534, (1959).)
8. N.F.Ramsey Molecular Beams, Oxford Univ. Press, (1956).
9. H.W.Liepmann "Gaskinetics and Gasdynamics of Orifice Flow," J.  
Fluid Mechanics, 10, Part 1, 65, (1961).
10. K.Behrndt "Die Mikrowaagen in ihrer Entwicklung seit 1886,"  
Z. angew. Physik, 8, 453, (1956).
11. H.Mayer,  
K.Behrndt "Eine neue Mikrowaage aus Quarz fur Arbeiten im  
Hochstvakuum," A. Physik, 147, 499, (1957).
12. B.B.Cunningham "Microchemical Methods Used in Nuclear Research,"  
Nucleonics, p. 62, (November, 1949).
13. M.J.Copley,  
V.Deitz "A Torsion Manometer for the Measurement of the  
Force of a Molecular Ray," Rev. Sci. Instr., 8,  
314, (1937).
14. W.Paul,  
G.Wessel "Messung von Dichte und mittlerer Molekulargesch-  
windigkeit in einen Atomstrahl," Z. Physik, 124,  
691, (1948).
- J.L.Costa,  
H.D.Smyth,  
K.T.Compton "A Mechanical Maxwell Demon," Phys. Rev., 30, 349,  
(1927).
15. H.Mayer "Uber eine experimentelle Methode zur Messung von  
Molekularstrahlung," Z. Physik, 52, 235, (1928).
16. N.Sasaki,  
N.Taku,  
K.Mitani "The Exchange Efficiencies of the Translational and  
Internal Energy of Gas Molecules on Solid Surfaces,"  
Mem. Coll. Sci., Univ. of Kyoto, A22, No. 2, 75, (1949).

- (also J. Chem. Soc. Japan, 70, 425, (1949); *ibid*,  
71, 9, (1950); *ibid*, 71, 100, (1950).)
17. G.S.Holister,  
R.T.Brackmann,  
W.L.Fite      "The Use of Modulated Atomic-Beam Techniques for the  
Study of Space-Flight Problems," AFOSR TN 59-1033,  
General Atomic Corp. GA-1024, (1959).
  18. L.G.Carpenter      (private communication) Royal Aircraft Establishment,  
England.
  19. W.C.Michels      "Accommodation Coefficient of Helium and Argon against  
Tungsten," Phys.Rev., 40, 472, (1932).
  20. S.A.Schaaf,  
P.L.Chambre'      "Flow of Rarefied Gases," Vol. III, Part H, High Speed  
Aerodynamics and Jet Propulsion Series, Princeton Univ.  
Press, (1958).
  21. F.C.Hurlbut      "An Experimental Molecular Beam Investigation of the  
Scattering of Molecules from Surfaces," Univ. of Calif.  
Eng. Proj. Report HE-150-118, (1953). (also J. Appl.  
Phys., 28, 8, 844, (1957).)
  22. J.K.Roberts      "The Exchange of Energy between Gas Atoms and Solid  
Surfaces; III. The Accommodation Coefficient of Neon,"  
Proc. Roy. Soc., A142, 518, (1933).
  23. M.Wiedmann,  
P.Trumpler      "Thermal Accommodation Coefficients," Trans. Am. Soc.  
Mech. Engrs., 68, 57, (1946).
  24. B.Baule      "Theoretische Behandlung der Erscheinungen in  
verduunten Gasen," Ann. Physik, 44, 145, (1914).
  25. I.Estermann,  
O.C.Simpson,  
O.Stern      "The Free Fall of Atoms and the Measurement of Velocity  
Distribution in a Molecular Beam of Cesium Atoms,"  
Phys. Rev., 71, 238, (1947).

- V.W.Cohen,  
A.Ellet "Velocity Analysis by Means of the Stern-Gerlach Effect," Phys. Rev., 52, 502, (1937).
26. J.H.McFee,  
P.M.Marcus "Velocity Distributions in Direct and Reflected Atomic Beams," Carnegie Inst. of Tec., Dept. of Physics Tech. Report No.1, (1960). (also see p. 178, Proc. Atomic and Molecular Beams Conference, Univ. of Denver, (1960).)
27. A.Ellett,  
V.W.Cohen "Velocity Analysis of Potassium Atoms Scattered by Magnesium Oxide," Phys. Rev., 52, 509, (1937).
28. F.M.Devienne,  
J.Souquet "Production of a Molecular Beam at a Very High Speed and Relatively Great Density; Development of a Molecular Gun," Rarefied Gas Dynamics, Academic Press, (1961).
- R.N.Zapata,  
H.M.Parker,  
J.H.Bodine "Performance of a Supersonic Molecular Beam," Rarefied Gas Dynamics, Academic Press, (1961).
- A.J.Moncrieff-  
Yeates "A Neutral Beam Generator," Proc. Atomic and Molecular Beams Conference, Univ. of Denver, (1960).
- R.M.Drake, Jr. (private communication) Dept. of Mech. Eng., Princeton Univ.
- E.Knuth (private communication) Engr. Dept., Univ. of Calif. at Los Angeles.
29. J.Strong Procedures in Experimental Physics, Prentice-Hall, New York, (1938).
30. I.Estermann "Molecular Beam Technique," Revs. Modern Phys., 18, 3, 300, (1946).

31. F.C.Hurlbut, "New Studies of Molecular Scattering at the Solid  
D.E.Beck Surface," Univ. of Calif. Eng. Proj. Report HE-150-  
166, (1959).

TABLE I. TYPICAL DATA SHEET FOR THE CONSTANT TORQUE PROCEDURE

Date: 10-26-61  
 Surface Material: Platinum  
 Period of Balance: 39.6 sec  
 Room Temperature: 24° C

Zero Point Scale Reading: 75.0  
 Zero Point Wheel Reading  $W'$ : 55.9  
 Constant Wheel Reading  $W$ : 129.0

$$\theta \left[ \theta = 2\pi \left( \frac{W - W'}{100} \right) \right] : 0.459 \text{ radians}$$

Gas	Time	Average Scale Reading	Projector Voltage	Projector Amps.	Source Pressure P, microns	$P_o/P$
Argon	8:03 PM	74.2	0	0	94.5	-
	12	75.0	80	5.00	74.9	1.261
	28	75.7	50	3.80	79.8	1.185
	39	74.7	20	2.26	86.3	1.095
	55	75.5	0	0	94.4	-
	9:03	75.5	20	2.25	86.2	1.096
	11	76.0	50	3.79	78.9	1.198
	18	74.7	80	5.00	75.1	1.258
	28	75.0	0	0	94.5	-
Helium	9:43 PM	75.0	0	0	96.2	-
	51	75.5	80	5.00	84.8	1.134
	10:00	74.7	50	3.80	87.7	1.095
	08	74.2	20	2.25	91.3	1.053
	18	75.0	0	0	96.2	-
	26	74.5	20	2.24	90.5	1.062
	37	75.0	50	3.78	86.3	1.114
	48	75.0	80	5.00	83.5	1.151
	59	76.0	0	0	96.0	-

AVERAGED DATA:

Projector Voltage	Average Value of $P_o$ , microns		Average Value of $P_o/P$	
	Argon	Helium	Argon	Helium
0	94.5	96.1	-	-
20			1.096	1.057
50			1.192	1.105
80			1.259	1.143

TABLE II - TYPICAL DATA SHEET FOR THE CONSTANT PRESSURE PROCEDURE

Date: 10-12-61  
 Surface Material: Blackened Tungsten  
 Period of Balance: 41.7 sec  
 Room Temperature: 26° C

Zero Point Scale Reading: 75.0  
 Zero Point Wheel Reading W': 68.3  
 Argon Source Pressure: 132.4 microns  
 Helium Source Pressure: 142.7 microns

<u>Gas</u>	<u>Time</u>	<u>Average Scale Reading</u>	<u>Projector Voltage</u>	<u>Projector Amps</u>	<u>Wheel Reading, W</u>
Argon	8:56 PM	75.0	0	0	174.1
	9:12	75.0	80	5.00	196.8
	19	75.0	60	4.28	192.3
	28	75.0	50	3.83	189.5
	36	75.0	40	3.40	186.8
	41	75.0	30	2.89	183.5
	45	75.0	20	2.30	179.8
	50	75.0	10	1.60	175.8
	10:04	75.0	0	0	174.4
	08	74.8	10	1.60	175.8
	14	75.0	20	2.30	179.7
	19	75.2	30	2.89	183.3
	24	75.0	40	3.35	186.4
	30	75.0	50	3.83	189.5
	36	75.0	60	4.27	192.1
	43	75.0	80	5.00	196.7
	53	75.0	0	0	174.5
Helium	1:10 AM	75.0	0	0	180.5
	23	75.0	80	5.00	200.7
	28	75.0	60	4.29	196.7
	34	75.0	50	3.83	194.3
	39	75.0	40	3.37	191.6
	46	75.0	30	2.88	188.8
	52	75.0	20	2.30	185.5
	2:00	75.0	10	1.60	182.0
	12	75.0	0	0	180.7
	19	75.0	10	1.60	181.9
	26	75.0	20	2.30	185.3
	32	75.0	30	2.88	188.5
	37	75.0	40	3.37	191.2
	44	75.0	50	3.82	193.8
	50	75.0	60	4.28	196.2
	57	75.0	80	5.00	200.1
	3:10	75.0	0	0	180.5

See next page for averaged data.

TABLE II - Continued

AVERAGED DATA:

Projector Voltage	Average Wheel Reading W		Average Wheel Displacement W - W'		Ratio of Average Angular Displacement, $\frac{\theta}{\theta_0} = \frac{W-W'}{W_0-W'}$	
	Argon	Helium	Argon	Helium	Argon	Helium
0	174.3	180.6	106.0	112.3	1.000	1.000
10	175.8	181.95	107.5	113.65	1.014	1.011
20	179.75	185.4	111.45	117.1	1.052	1.042
30	183.4	188.65	115.1	120.35	1.087	1.071
40	186.6	191.4	118.3	123.1	1.117	1.096
50	189.5	194.05	121.2	125.75	1.144	1.119
60	192.2	196.45	123.9	128.15	1.171	1.140
80	196.75	200.4	128.45	132.1	1.212	1.175



TABLE III (A) - SUMMARY OF DATA FOR TUNGSTEN SURFACES

Date	Gas	Symbol	$(P_o)_{ave}$ in microns	Projector Voltage	$(P_o/P)_{ave}$	Notes
7-20-61	Argon		138.5	10	1.030	Target #1 Slit #1 Period ~ 40.6 sec
				20	1.100	
				30	1.143	
				40	1.175	
				50	1.203	
				75	1.252	
	Helium	○	142.0	10	1.020	
				20	1.057	
				30	1.080	
				40	1.107	
				50	1.125	
				75	1.156	
7-24-61	Argon		135.5	20	1.088	Target #1 Slit #1
				44	1.168	
				88	1.244	
	Helium	○	138.0	20	1.057	
				44	1.105	
				88	1.160	
	Nitrogen	◇	135.3	20	1.089	
				44	1.166	
				88	1.236	
8-25-61	Argon		102.3	20	1.089	Target #2 Slit #1
				44	1.143	
				88	1.182	
	Helium	○	104.3	20	1.044	
				44	1.073	
				88	1.098	
	Hydrogen	△	104.8	20	1.044	
				44	1.082	
				88	1.106	
8-26-61	Argon		101.6	20	1.086	Target #2
				44	1.152	
				88	1.192	
	Neon	□		20	1.062	
				44	1.105	
				88	1.134	
	Nitrogen	◇		20	1.091	
				44	1.151	
				88	1.192	

TABLE III (A) - Continued

<u>Date</u>	<u>Gas</u>	<u>Symbol</u>	<u>(P<sub>o</sub>)<sub>ave</sub> in microns</u>	<u>Projector Voltage</u>	<u>(P<sub>o</sub>/P)<sub>ave</sub></u>	<u>Notes</u>
9-27-61	Argon		123.6	10	1.049	Target #2 Slit #2
				20	1.112	
				30	1.149	
				50	1.200	
				80	1.253	
	Helium	Q	125.5	10	1.030	
				20	1.064	
				30	1.087	
				50	1.120	
				80	1.156	
	Hydrogen	A	125.0	10	1.034	
				20	1.081	
				30	1.110	
				50	1.152	
				80	1.193	
10-2-61	Argon		123.8	10	1.042	Target #2 Slit #2
				20	1.104	
				30	1.140	
				50	1.199	
				80	1.252	
	Hydrogen	A	126.0	10	1.034	
				20	1.083	
				30	1.104	
				50	1.143	
				80	1.179	
10-3-61	Argon		123.8	10	1.042	
				30	1.138	
				80	1.236	
	Hydrogen	A	126.6	10	1.025	
				30	1.083	
				80	1.144	
10-4-61	Argon		123.6	10	1.047	Target #2 Slit #2
				30	1.145	
				80	1.230	
	Helium	O	126.2	10	1.026	
				30	1.082	
				80	1.143	

TABLE III (A) - Continued





Date	Gas	Symbol	(P <sub>O</sub> ) <sub>ave</sub> in microns	Projector Voltage	(P <sub>O</sub> /P) <sub>ave</sub>	Notes
10-5-61	Argon		198.7	10	1.042	Target #2 Slit #2
				30	1.135	
				80	1.224	
	Helium		204.5	10	1.026	
				30	1.071	
				80	1.121	
10-6-61	Argon		62.2	10	1.050	Target #2 Slit #2
				30	1.144	
				80	1.236	
	Helium		63.2	10	1.020	
				30	1.072	
				80	1.121	
	Hydrogen		63.5	10	1.019	
				30	1.074	
				80	1.131	
10-7-61	Argon		123.4	10	1.046	Target #2 Slit #2
				30	1.140	
				80	1.241	
	Neon		125.2	10	1.033	
				30	1.099	
				80	1.181	
10-9-61	Argon		123.4	10	1.046	Target #2 Slit #2
				20	1.110	
				30	1.145	
				50	1.192	
				80	1.233	
	Neon		124.8	10	1.040	
				20	1.075	
				30	1.109	
				50	1.147	
				80	1.188	

TABLE III (B) - SUMMARY OF DATA FOR BLACKENED TUNGSTEN SURFACES

Date	Gas	Symbol	$(P_o)_{ave}$ in microns	Projector Voltage	$(P_o/P)_{ave}$	Notes
8-12-61	Argon		124.3	20	1.044	Target #1 Slit #1
				44	1.109	
				88	1.189	
				115	1.220	
	Helium	O	127.2	20	1.042	
				44	1.092	
				88	1.153	
				115	1.178	
10-10-61	Argon		139.0	10	1.021	Target #2 Slit #2
				30	1.088	
				80	1.215	
	Helium	O	144.0	10	1.011	
				30	1.074	
				80	1.182	
10-11-61	Argon		136.9	20	1.050	Target #2 Slit #2
				50	1.145	
				80	1.214	
	Helium	O	141.2	20	1.037	
				50	1.111	
				80	1.174	
	Hydrogen	$\Delta$	140.0	20	1.041	
				50	1.126	
				80	1.188	
10-12-61	Argon		~ 145	10	1.014	Constant Pressure Procedure Target #2 Slit #2
				20	1.052	
				30	1.087	
				40	1.117	
				50	1.144	
				60	1.171	
				80	1.212	
	Helium	O	~ 150	10	1.011	
				20	1.042	
				30	1.071	
				40	1.096	
				50	1.119	
				60	1.140	
				80	1.175	

TABLE III (B) - Continued

Date	Gas	Symbol	$(P_o)_{ave}$ in microns	Projector Voltage	$(P_o/P)_{ave}$	Notes
10-14-61	Argon		157.9	20	1.052	Target #2 Slit #2
				50	1.143	
				80	1.208	
	Hydrogen	$\Delta$	162.6	20	1.041	
				50	1.120	
				80	1.183	
10-17-61	Argon		~ 140	10	1.014	Constant Pressure Procedure Target #2
				20	1.052	
				30	1.087	
				40	1.117	
				50	1.146	
				60	1.172	
				80	1.213	
	Carbon Dioxide	$\nabla$	~ 140	10	1.015	
				20	1.052	
				30	1.088	
				40	1.118	
				50	1.146	
				60	1.170	
				80	1.212	

TABLE III (C) - SUMMARY OF DATA FOR ALUMINUM SURFACES

Date	Gas	Symbol	$(P_o)_{ave}$ in microns	Projector Voltage	$(P_o/P)_{ave}$	Notes
8-4-61	Argon		106.0	20	1.045	Target #1 Slit #1
				44	1.143	
				88	1.263	
	Helium	○	107.5	20	1.029	
				44	1.082	
				88	1.152	
	Neon	□	107.5	20	1.045	
				44	1.122	
				88	1.227	
	Nitrogen	◇	106.5	20	1.044	
				44	1.136	
				88	1.244	
8-5-61	Argon		54.2	20	1.046	Target #1 Slit #1
				44	1.144	
				88	1.266	
	Helium	○	55.8	20	1.026	
				44	1.086	
				88	1.170	
	Nitrogen	◇	54.2	20	1.044	
				44	1.138	
				88	1.258	
10-20-61	Argon		109.2	20	1.065	Target #1 Slit #2
				50	1.178	
				80	1.259	
	Helium	○	111.1	20	1.034	
				50	1.109	
				80	1.161	
10-23-61	Argon		126.9	20	1.065	Target #1 Slit #2
				50	1.167	
				80	1.236	
	Hydrogen	△	130.0	20	1.042	
				50	1.115	
				80	1.178	

TABLE III (C) - Continued

<u>Date</u>	<u>Gas</u>	<u>Symbol</u>	<u>(P<sub>o</sub>)<sub>ave</sub> in microns</u>	<u>Projector Voltage</u>	<u>(P<sub>o</sub>/P)<sub>ave</sub></u>	<u>Notes</u>
10-24-61	Argon		96.4	20	1.056	Target #1 Slit #2
				50	1.166	
				80	1.247	
	Helium	⊙	98.3	20	1.033	
				50	1.104	
				80	1.163	
	Hydrogen	△	98.9	20	1.038	
				50	1.126	
				80	1.183	
	Nitrogen	◇	96.2	20	1.046	
				50	1.159	
				80	1.230	

TABLE III (D) - SUMMARY OF DATA FOR PLATINUM SURFACES

Date	Gas	Symbol	$(P_o)_{ave}$ in microns	Projector Voltage	$(P_o/P)_{ave}$	Notes
10-25-61	Argon		94.6	20	1.095	Target #1 Slit #2
				50	1.189	
				80	1.253	
	Helium	○	96.4	20	1.052	
				50	1.099	
				80	1.135	
10-26-61	Argon		94.5	20	1.095	Target #1 Slit #2
				50	1.192	
				80	1.259	
	Helium	○	96.1	20	1.057	
				50	1.105	
				80	1.143	
	Hydrogen	△	96.3	20	1.056	
				50	1.114	
				80	1.159	
	Nitrogen	◇	94.8	20	1.096	
				50	1.178	
				80	1.242	
10-27-61	Argon		94.1	20	1.078	Target #1 Slit #2
				50	1.161	
				80	1.224	
	Helium	○	96.4	20	1.038	
				50	1.091	
				80	1.133	
	Hydrogen	△	96.4	20	1.045	
				50	1.109	
				80	1.144	
	Carbon Dioxide	▽	94.3	20	1.079	
				50	1.167	
				80	1.232	
	Nitrogen	◇	95.0	20	1.076	
				50	1.153	
				80	1.218	



TABLE IV. RESULTS FOR HELIUM ON BLACKENED TUNGSTEN AT AN ANGLE OF INCIDENCE OF 45°

Projector Voltage	Argon Results		Helium Results	
	Average Value of $P_o/P$	Calculated Value of $T_r, ^\circ K$	Average Value of $P_o/P$	Calculated Value of $T_r, ^\circ K$
20	1.057	369	1.049	359
50	1.153	507	1.120	457
80	1.211	600	1.169	532

Note:  $T_r = 298 (1.988 \frac{P_o}{P} - 0.988)^2$  [Eq. (5.21)]

THE ACCOMMODATION COEFFICIENT OF HELIUM

Projector Voltage	Calculated Value of $\alpha$
20	0.86
50	0.76
80	0.78

NOTES: 1)  $\alpha = \frac{T_r - T_i}{T_w - T_i}$  [Eq. (5.15)]

2)  $T_i$  is approximately equal to 298° K.

3)  $T_w$  is assumed to be equal to  $T_r$  for argon (i.e., argon is assumed to be completely accommodated).

TABLE V - THEORETICAL RESULTS FOR APPLIED TORQUE AT  
OBLIQUE ANGLES OF INCIDENCE

(Refer to Appendix 2)

Angle of Attack, $\psi$	$I_1$	$\tau_i/A$	$I_2$	$(\tau_r/A)_{T_w=T_i}$	$(\tau/\tau_{90^\circ})_{T_w=T_i}$
120	$1.018 \times 10^{-4}$	$8.816 \times 10^{-5}$	$6.313 \times 10^{-4}$	$6.475 \times 10^{-5}$	0.966
110	$1.028 \times 10^{-4}$	$9.660 \times 10^{-5}$	$6.489 \times 10^{-4}$	$6.655 \times 10^{-5}$	1.031
100	$1.001 \times 10^{-4}$	$9.858 \times 10^{-5}$	$6.439 \times 10^{-4}$	$6.604 \times 10^{-5}$	1.040
90	$9.470 \times 10^{-3}$	$9.470 \times 10^{-5}$	$6.198 \times 10^{-4}$	$6.357 \times 10^{-5}$	1.000
80	$8.716 \times 10^{-3}$	$8.584 \times 10^{-5}$	$5.802 \times 10^{-4}$	$5.951 \times 10^{-5}$	0.918
70	$7.813 \times 10^{-3}$	$7.342 \times 10^{-5}$	$5.283 \times 10^{-4}$	$5.418 \times 10^{-5}$	0.806
60	$6.808 \times 10^{-3}$	$5.896 \times 10^{-5}$	$4.668 \times 10^{-4}$	$4.788 \times 10^{-5}$	0.675
50	$5.736 \times 10^{-3}$	$4.394 \times 10^{-5}$	$3.981 \times 10^{-4}$	$4.083 \times 10^{-5}$	0.536
45	$5.183 \times 10^{-3}$	$3.665 \times 10^{-5}$	$3.616 \times 10^{-4}$	$3.709 \times 10^{-5}$	0.466
40	$4.622 \times 10^{-3}$	$2.971 \times 10^{-5}$	$3.240 \times 10^{-4}$	$3.323 \times 10^{-5}$	0.398
30	$3.482 \times 10^{-3}$	$1.741 \times 10^{-5}$	$2.461 \times 10^{-4}$	$2.524 \times 10^{-5}$	0.270
20	$2.327 \times 10^{-3}$	$7.958 \times 10^{-6}$	$1.654 \times 10^{-4}$	$1.696 \times 10^{-5}$	0.158
10	$1.165 \times 10^{-3}$	$2.022 \times 10^{-6}$	$8.308 \times 10^{-5}$	$8.521 \times 10^{-6}$	0.067

NOTES:  $\tau_i$  = torque due to incident momentum =  $A \sin \psi I_1$

$\tau_r$  = torque due to re-emitted momentum =  $A \frac{\bar{v}_{nr}/\bar{v}_i}{l} I_2$

$\tau$  = total applied torque =  $\tau_i + \tau_r$

$$A = \frac{n m \tau_i \bar{v}_i w l^2}{4 \pi} = \frac{3 w l^2}{4 \pi} \zeta P$$

For the special case of an unheated test surface (i.e.,  $T_w=T_i=T_r$ ) and  
 $l = 6.50$  cm;

$$\tau/\tau_{90^\circ} = \frac{\sin \psi I_1 + 0.1026 I_2}{1.583 \times 10^{-4}}$$

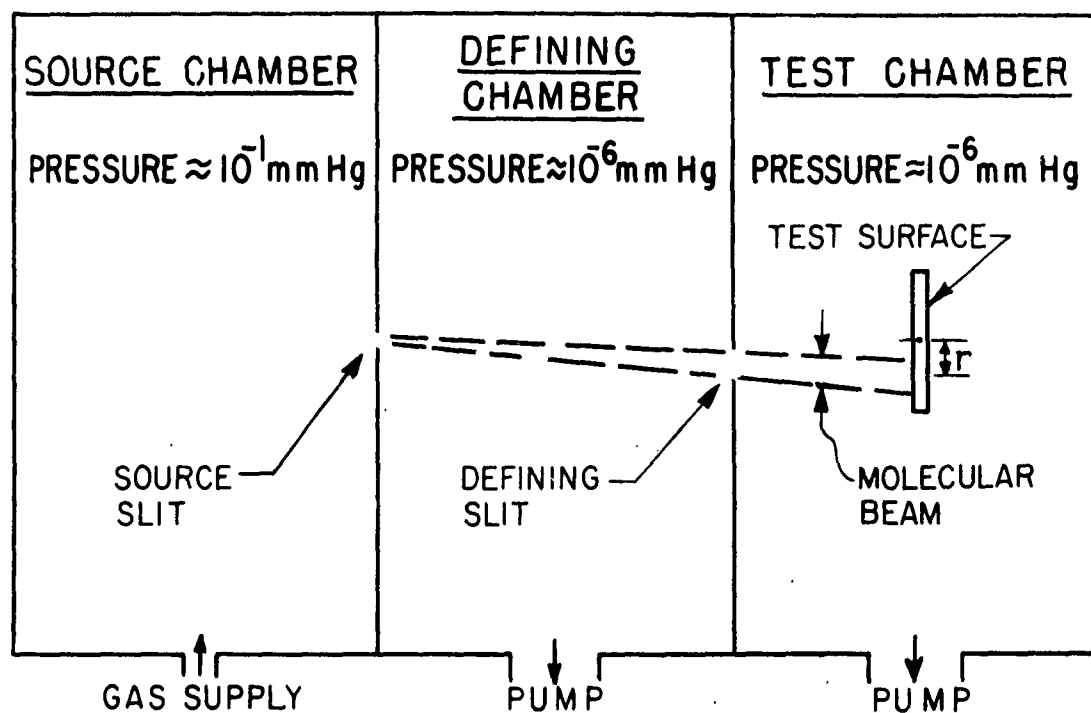


FIG. 1a SCHEMATIC OF THE CONVENTIONAL MOLECULAR BEAM DESIGN

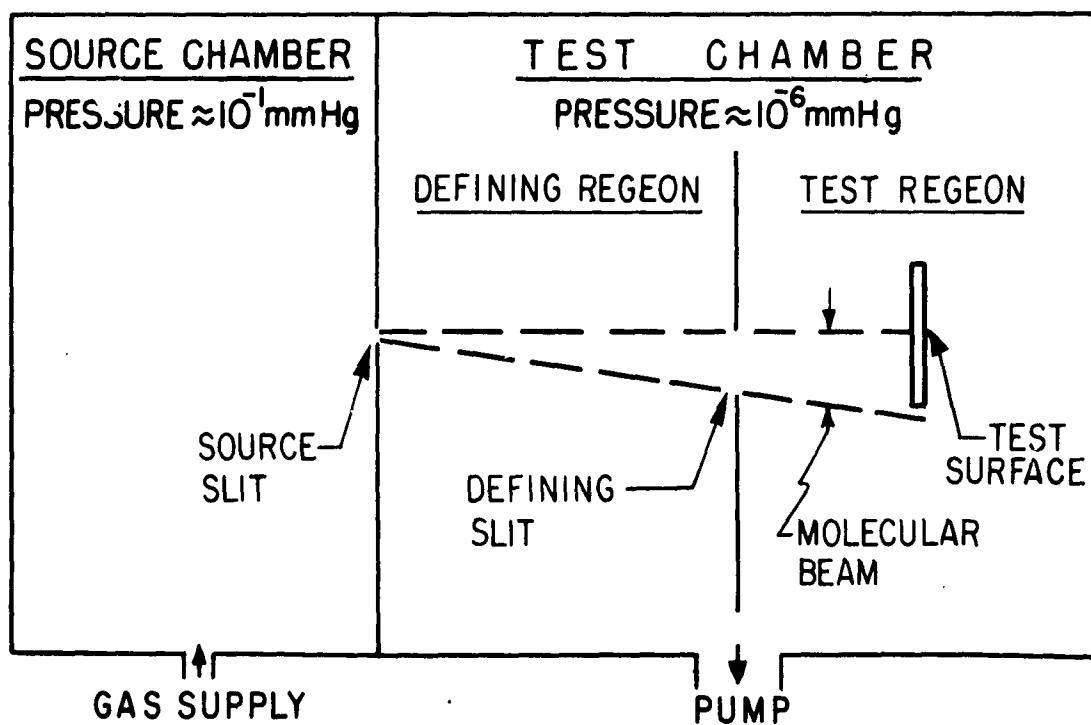


FIG. 1b SCHEMATIC OF THE PRESENT MOLECULAR BEAM DESIGN

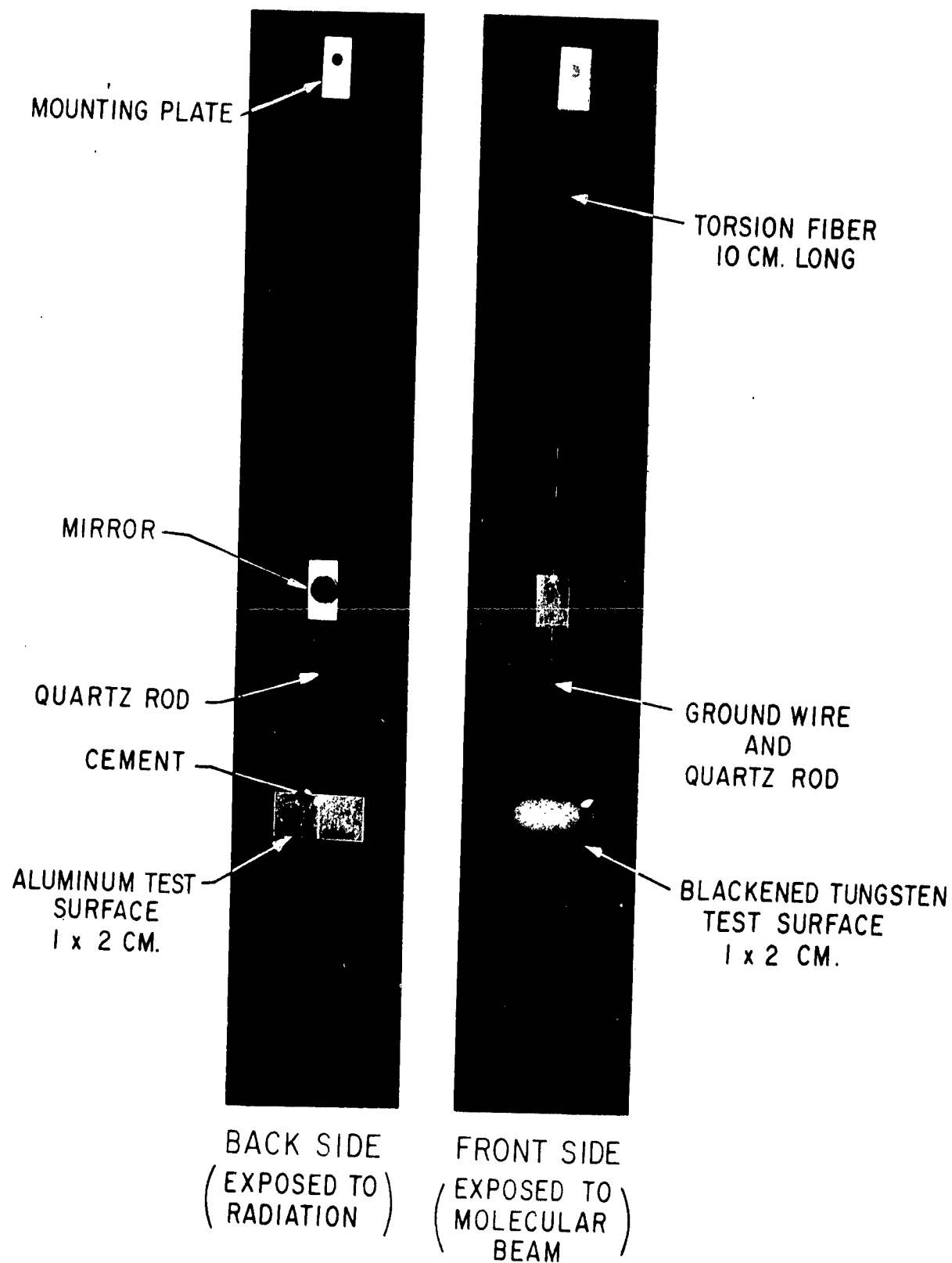


FIG. 2 TYPICAL TORSION BALANCES

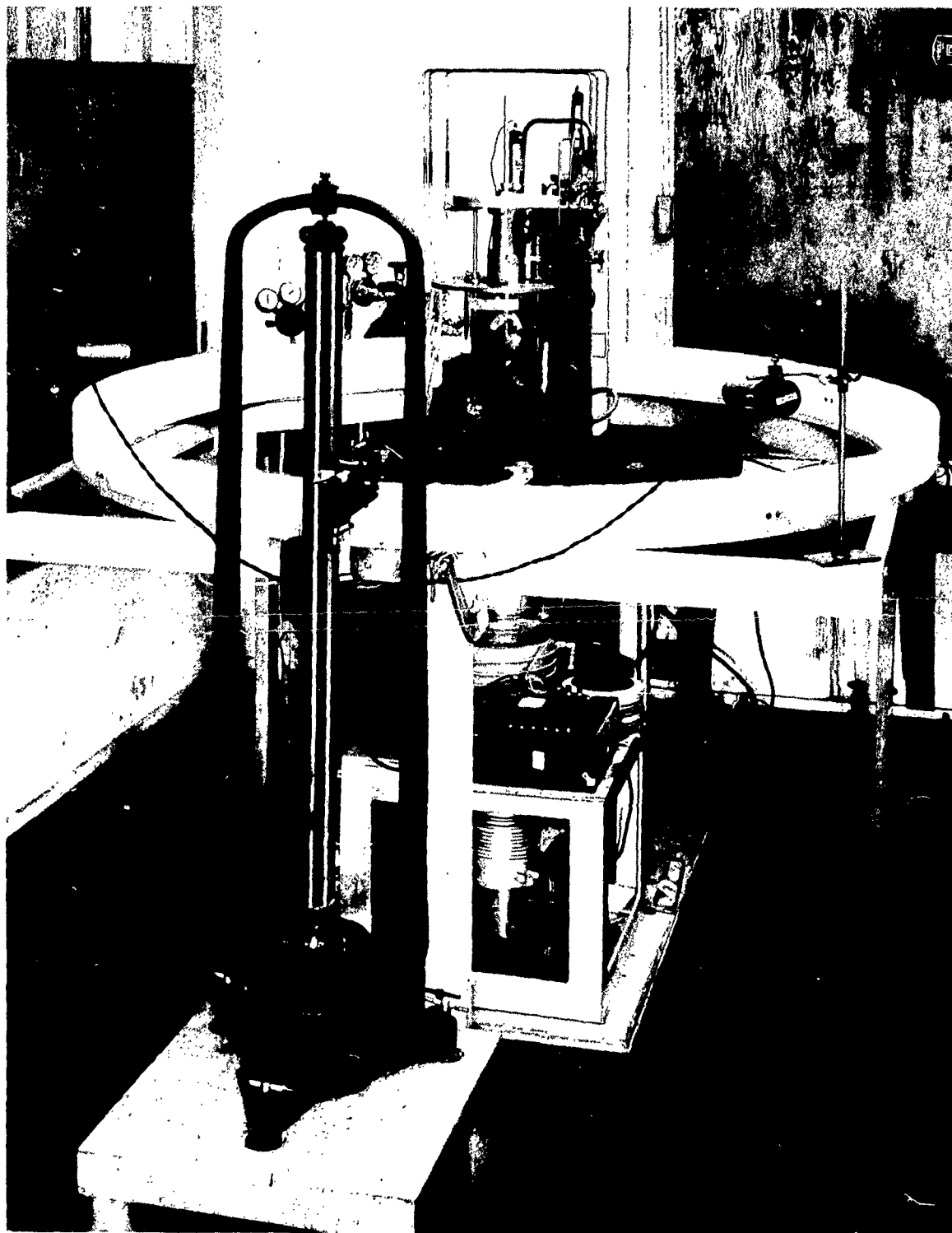


FIG. 3 OVERALL VIEW OF THE APPARATUS

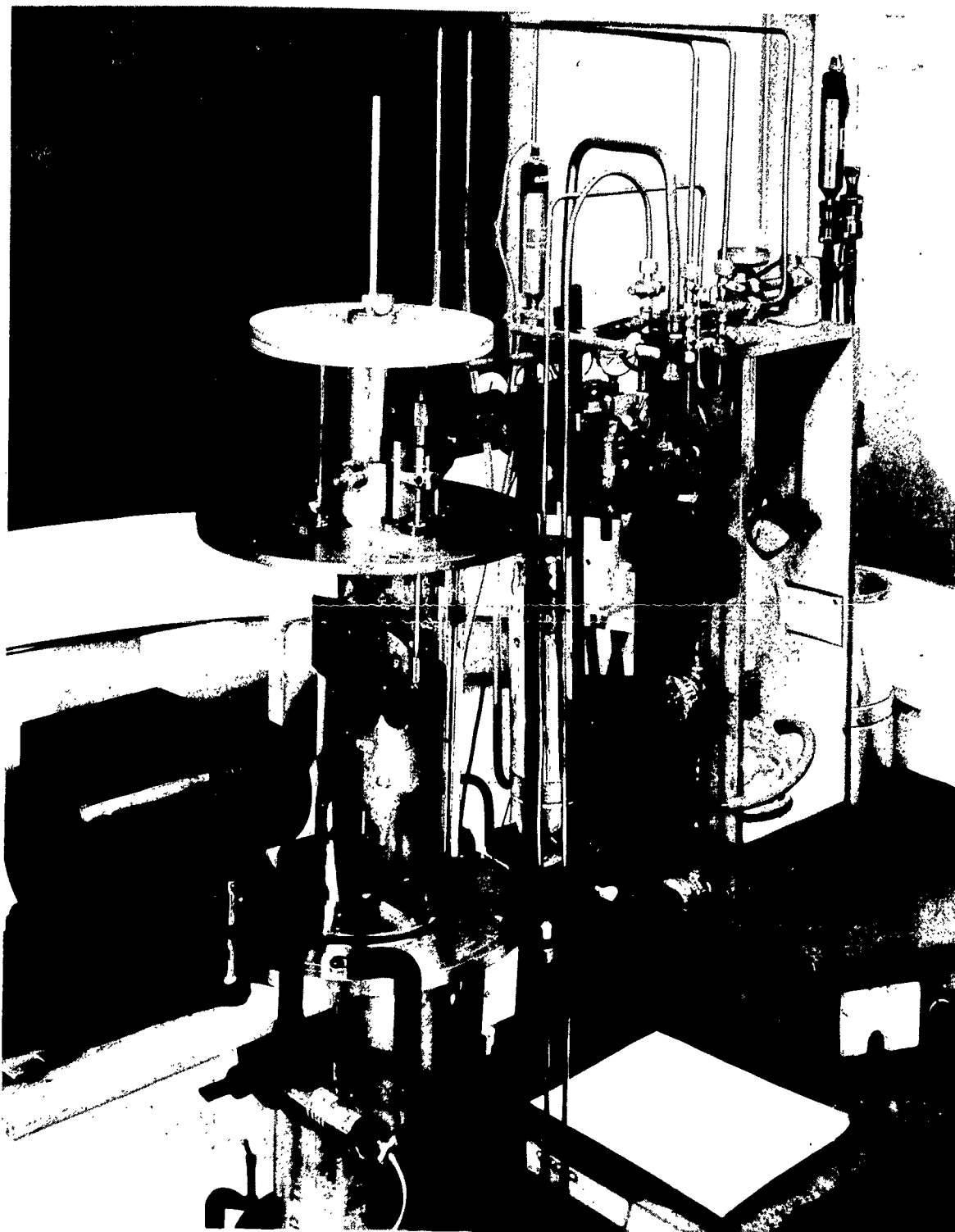


FIG. 4 THE TEST CHAMBER AND RELATED APPARATUS

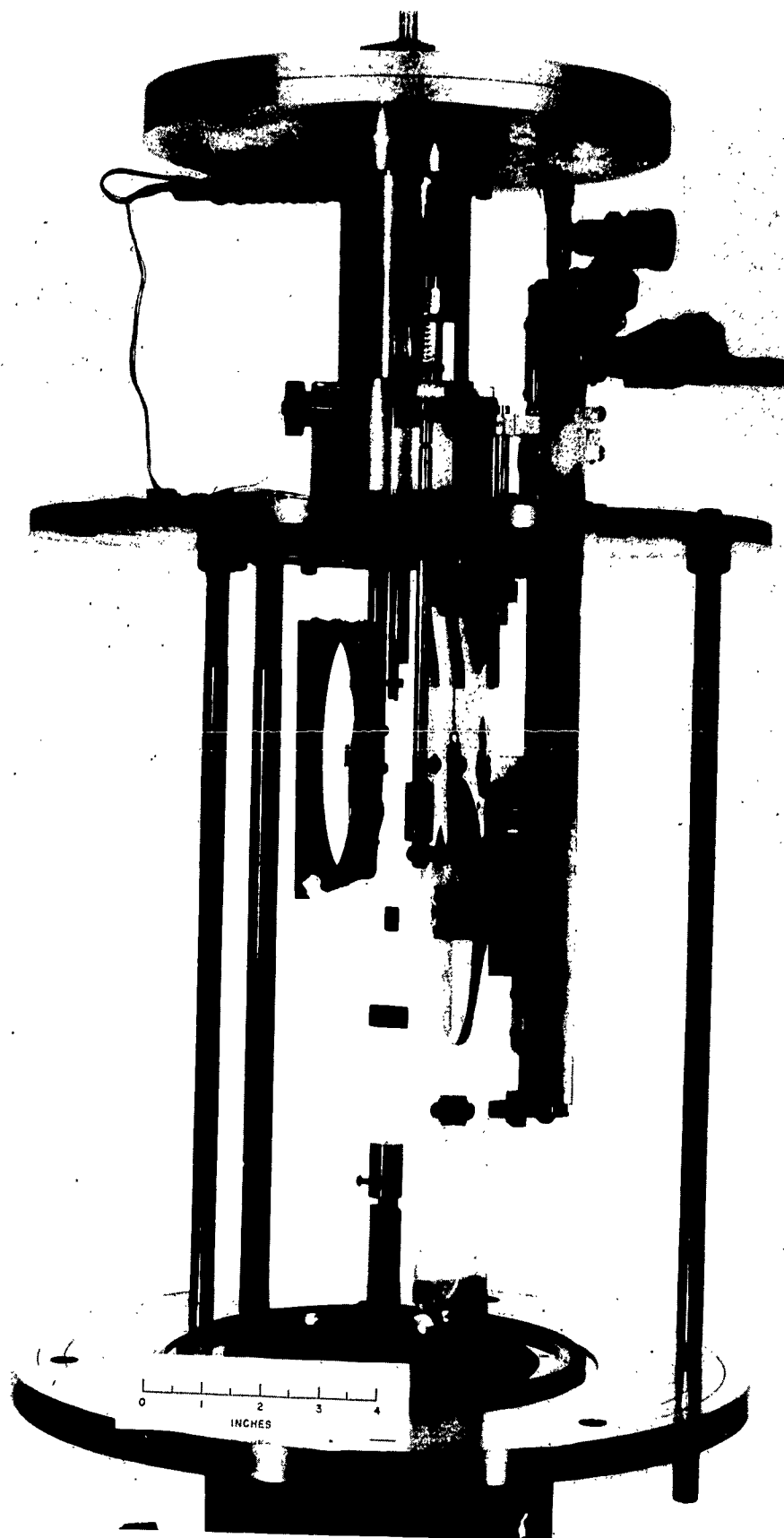


FIG. 5 THE TEST SECTION WITH THE GLASS CYLINDER REMOVED

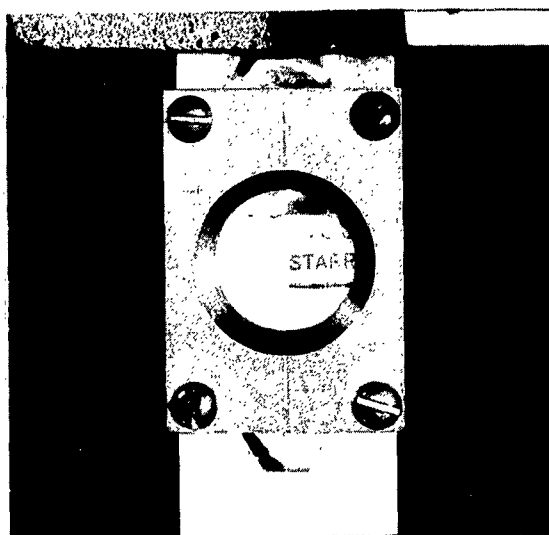


FIG. 6a SOURCE SLIT No. 1

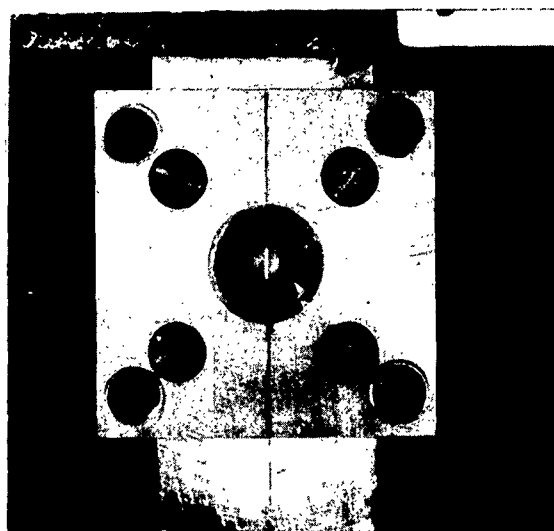


FIG. 6b SOURCE SLIT No. 2



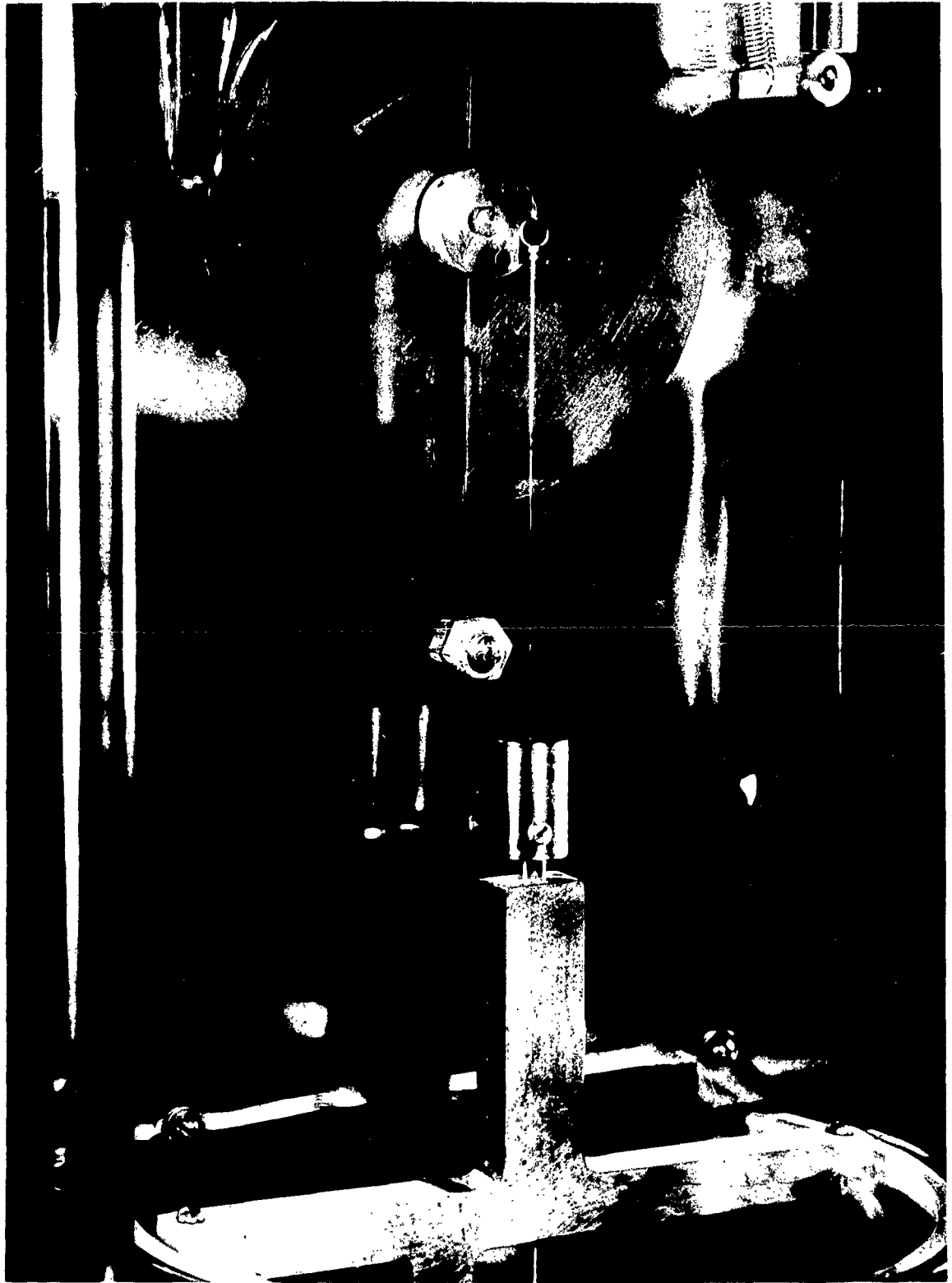


FIG. 7 CLOSE-UP OF TEST SECTION

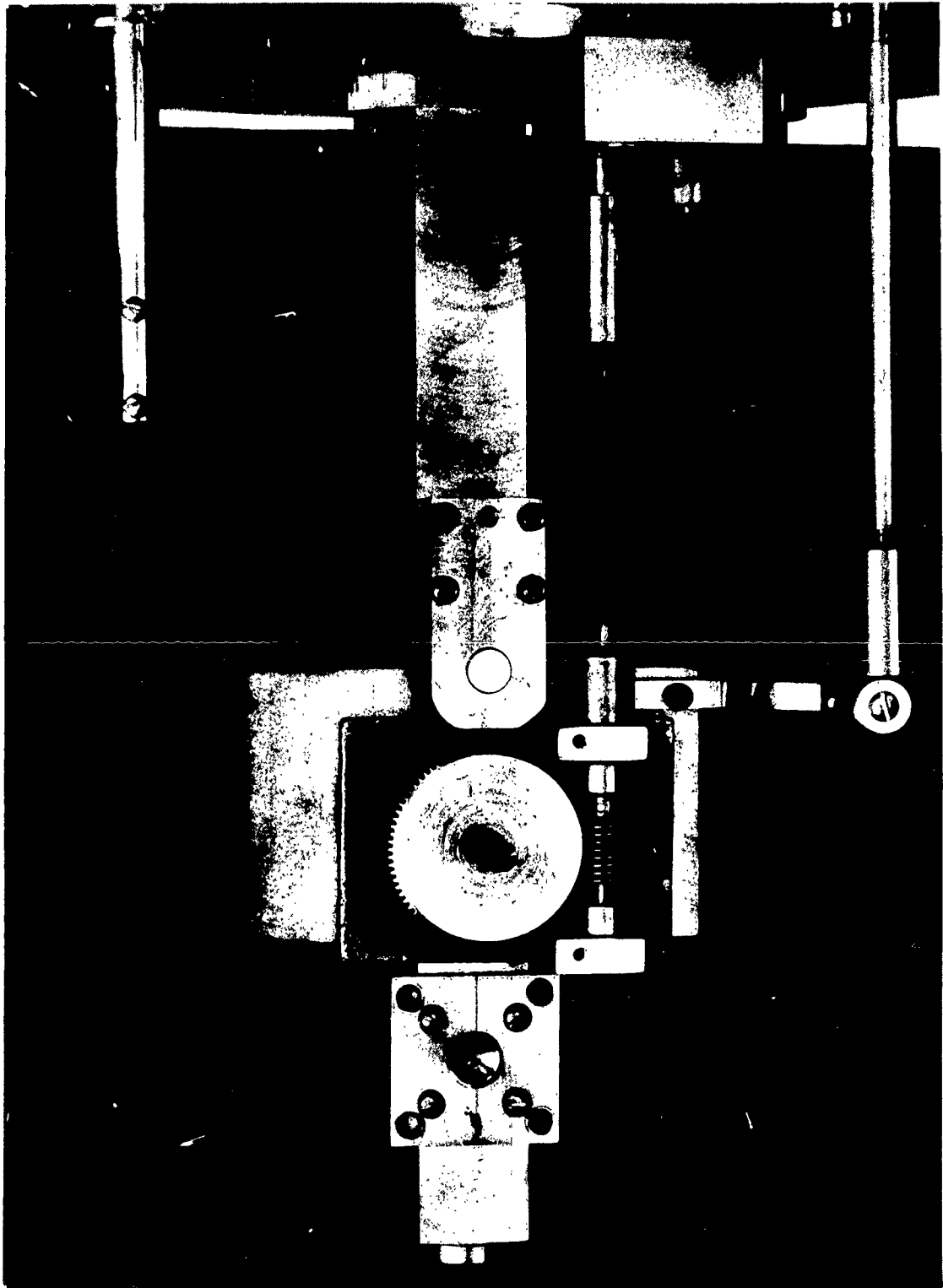


FIG. 8 ALIGNING MECHANISM FOR DEFINING SLIT  
(DEFINING SLIT HAS BEEN REMOVED)

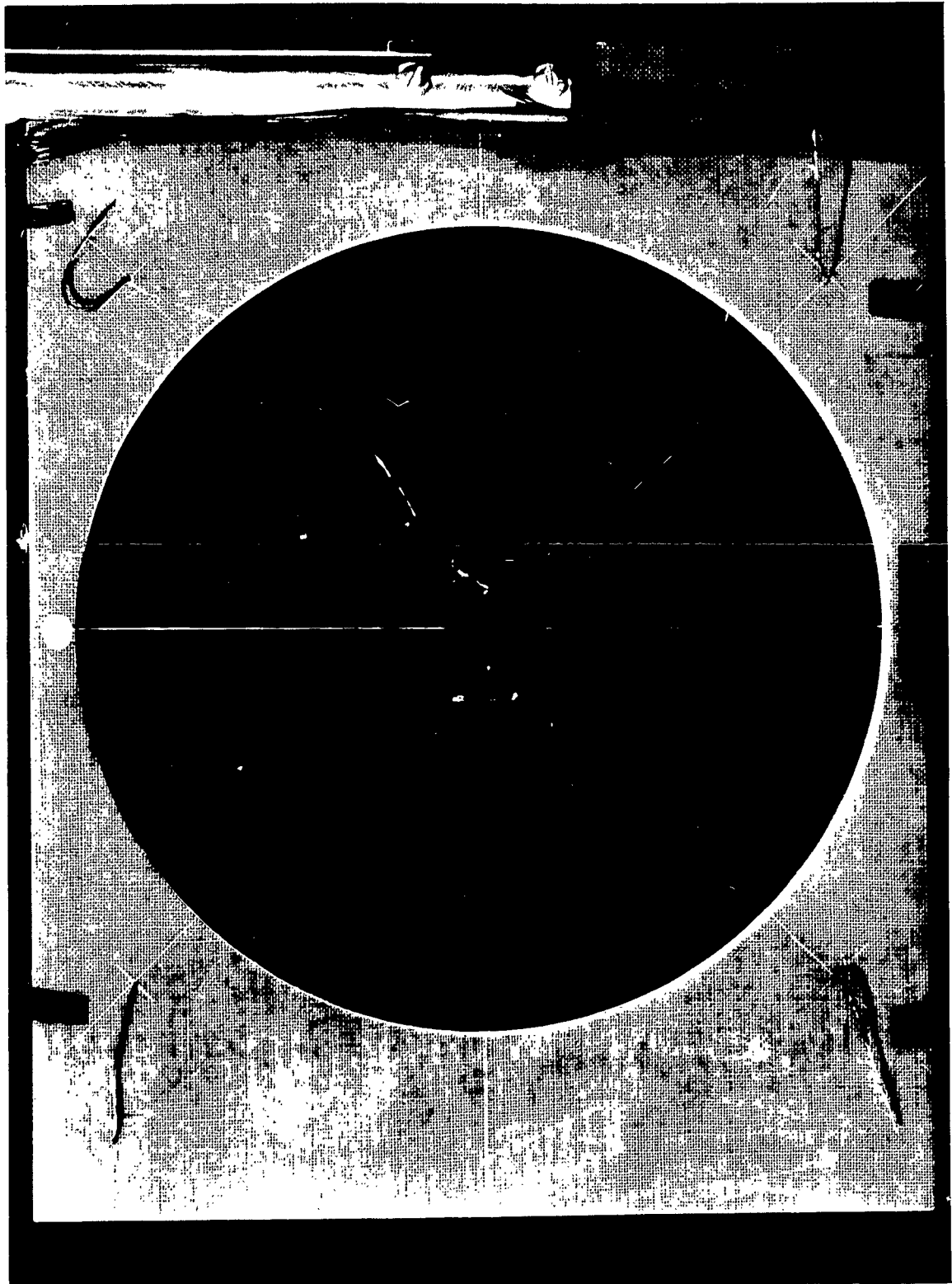


FIG. 9 THE DUMMY SURFACE

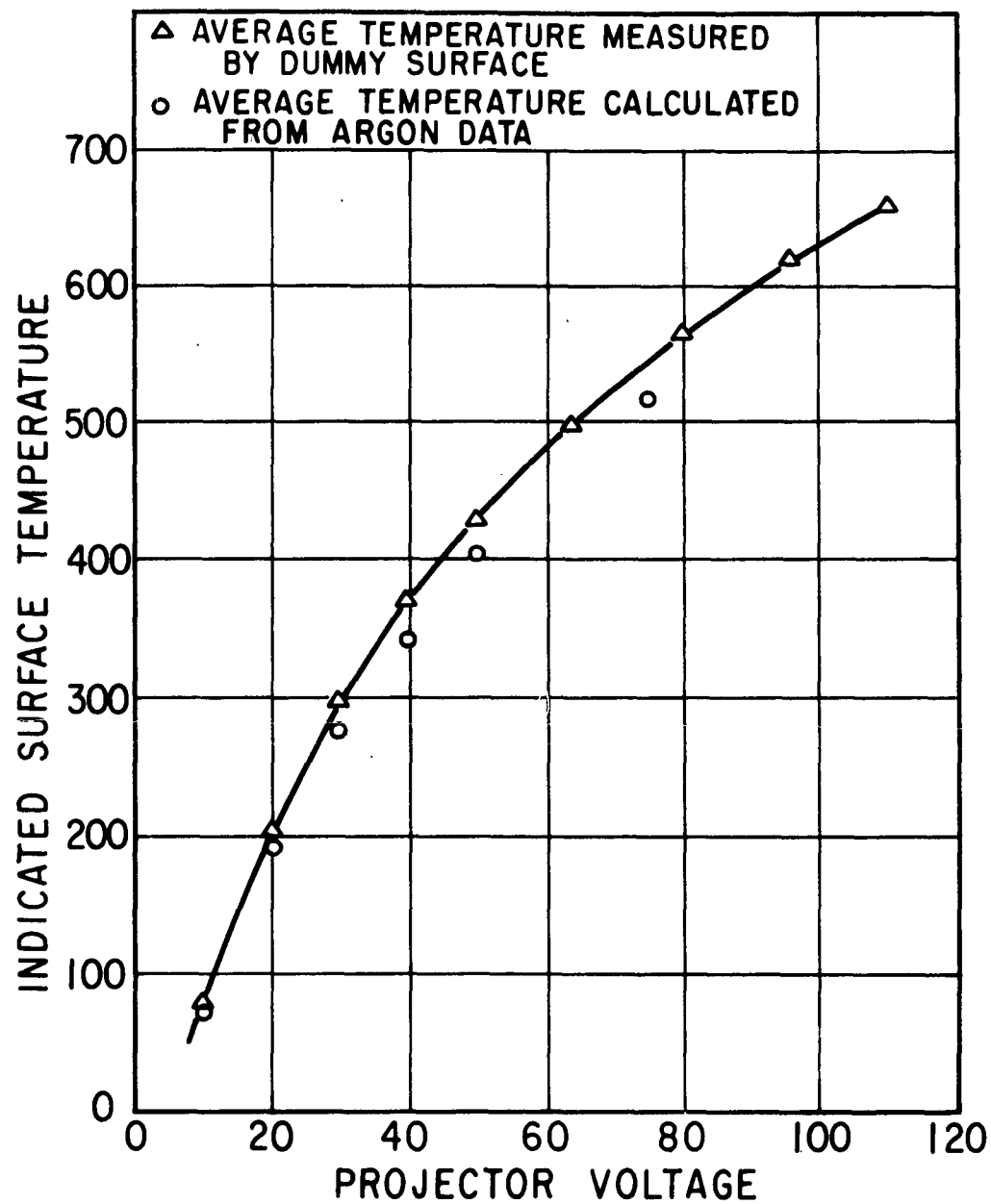


FIG. 10 A COMPARISON OF SURFACE TEMPERATURE TECHNIQUES MEASURING

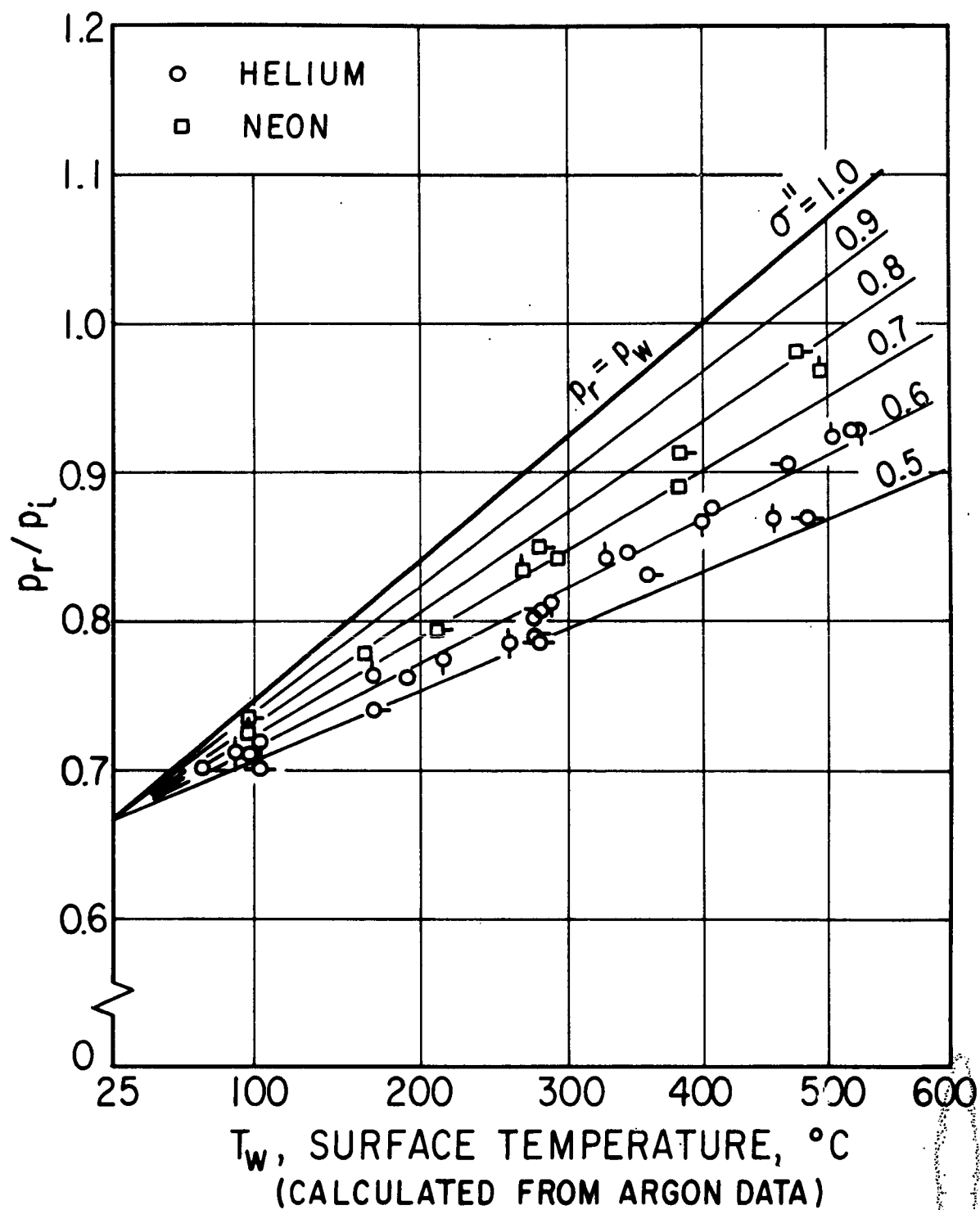


FIG. II EXPERIMENTAL RESULTS FOR HELIUM AND NEON ON TUNGSTEN

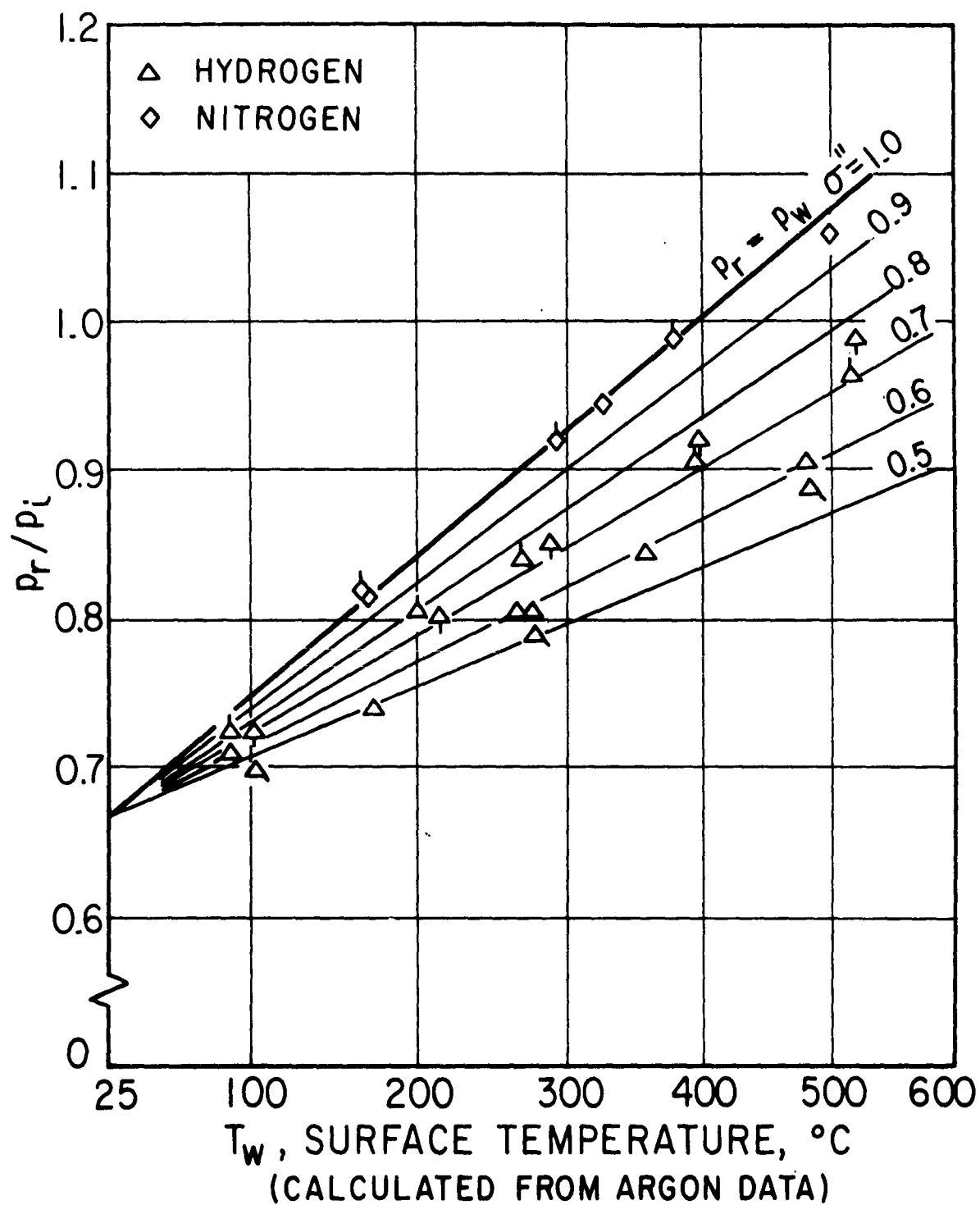


FIG. 12 EXPERIMENTAL RESULTS FOR HYDROGEN AND NITROGEN ON TUNGSTEN

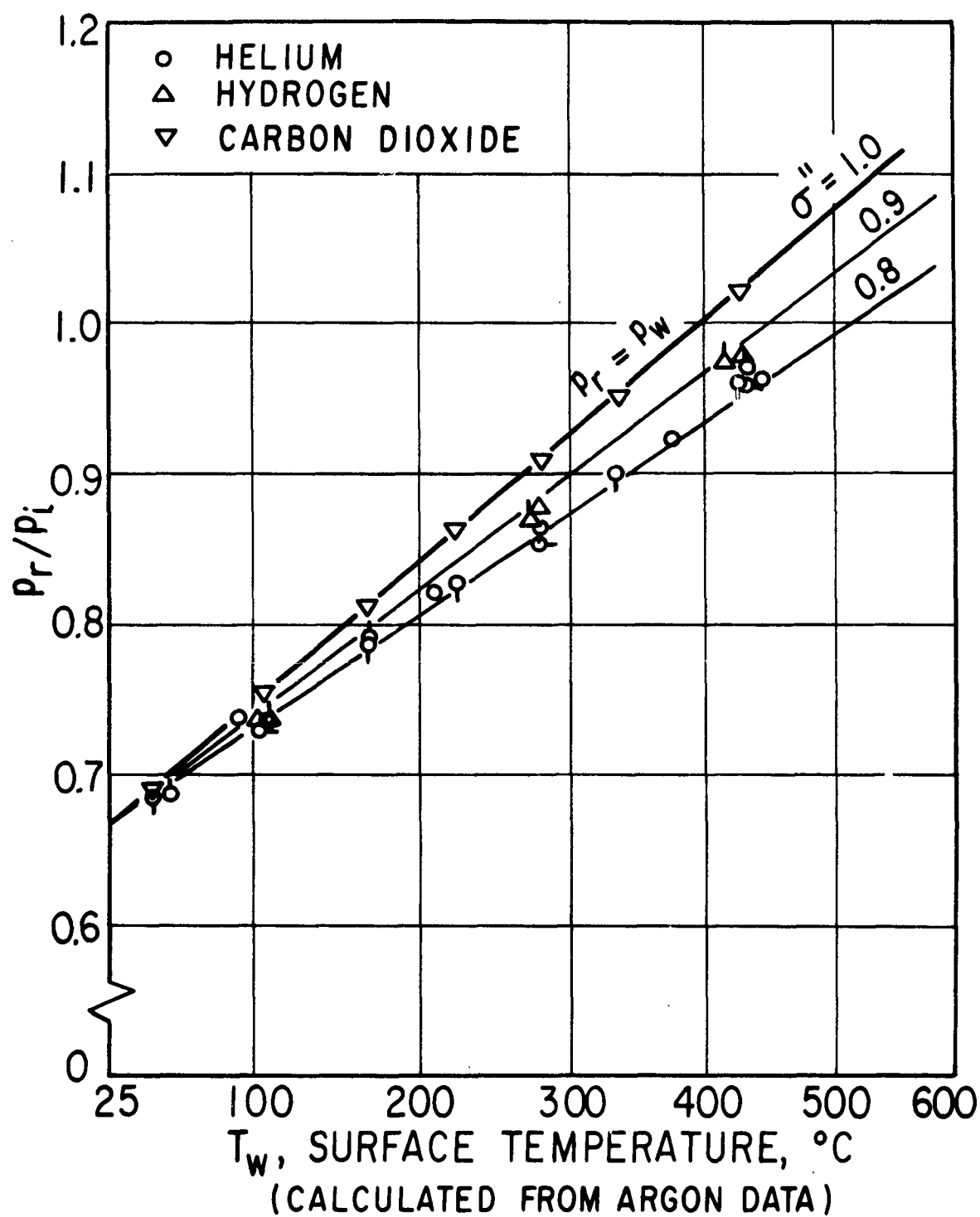


FIG. 13 EXPERIMENTAL RESULTS FOR HELIUM, HYDROGEN, AND CARBON DIOXIDE ON BLACKENED TUNGSTEN.

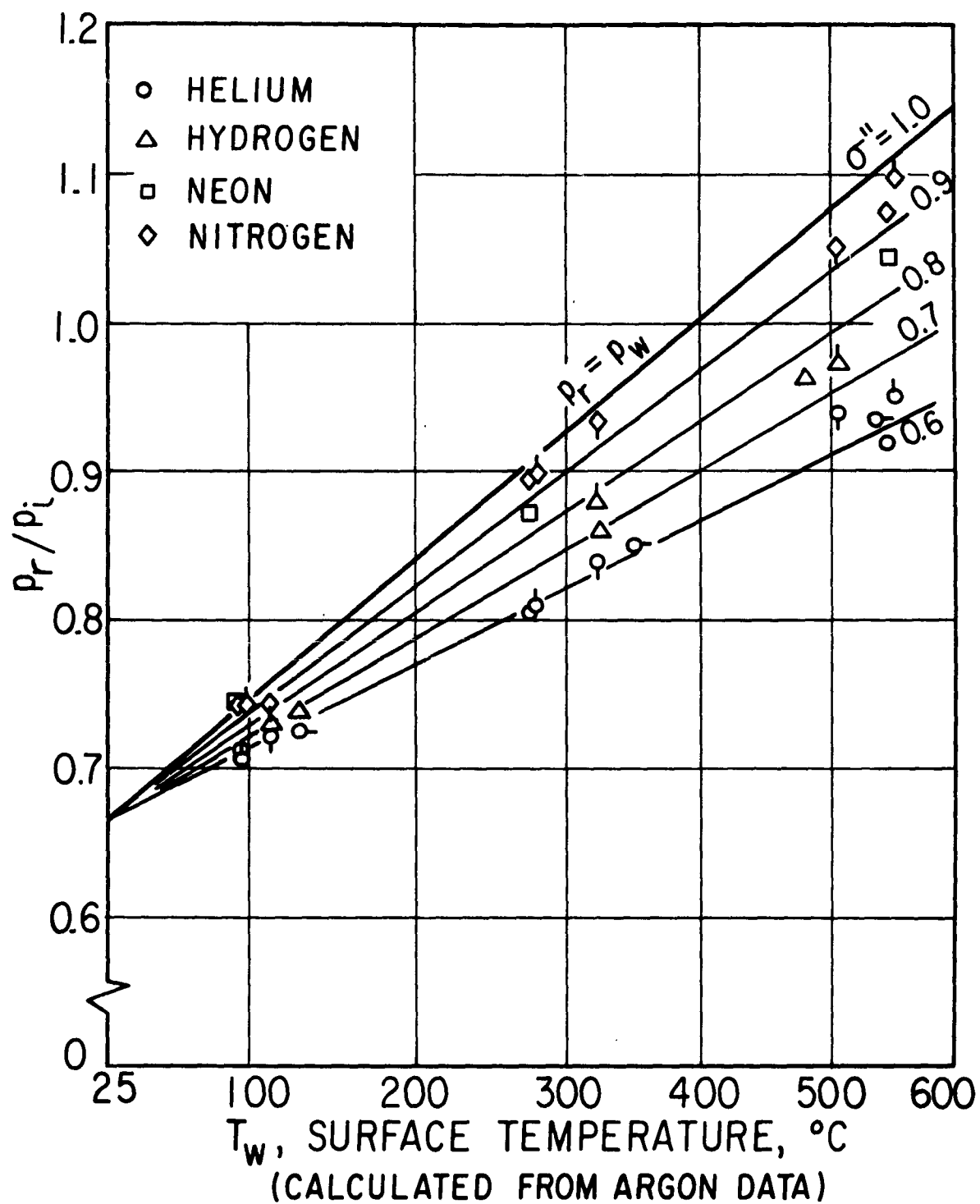


FIG.14 EXPERIMENTAL RESULTS FOR HELIUM, HYDROGEN, NEON, AND NITROGEN ON ALUMINUM



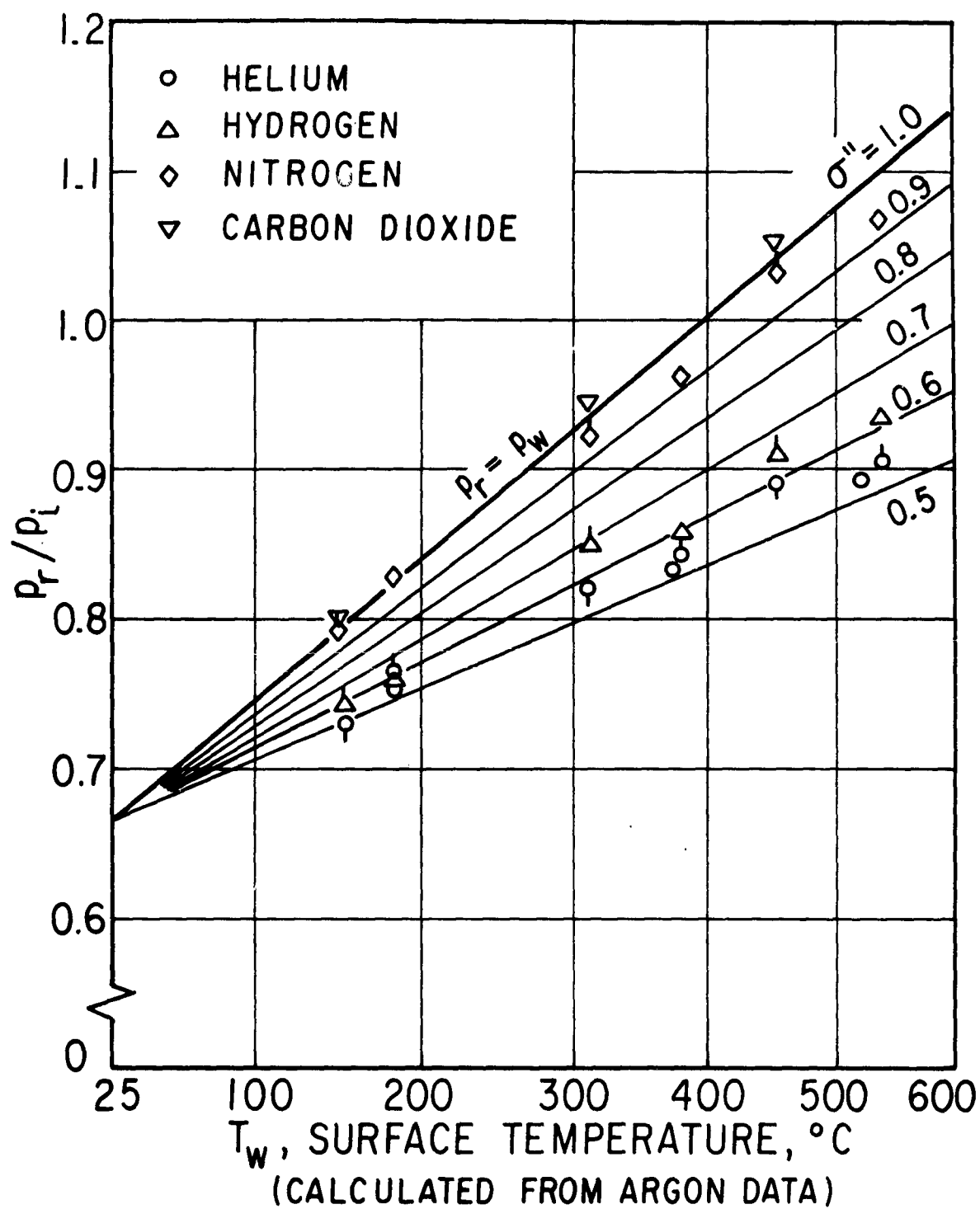


FIG. 15 EXPERIMENTAL RESULTS FOR HELIUM, HYDROGEN, NITROGEN, AND CARBON DIOXIDE ON PLATINUM.

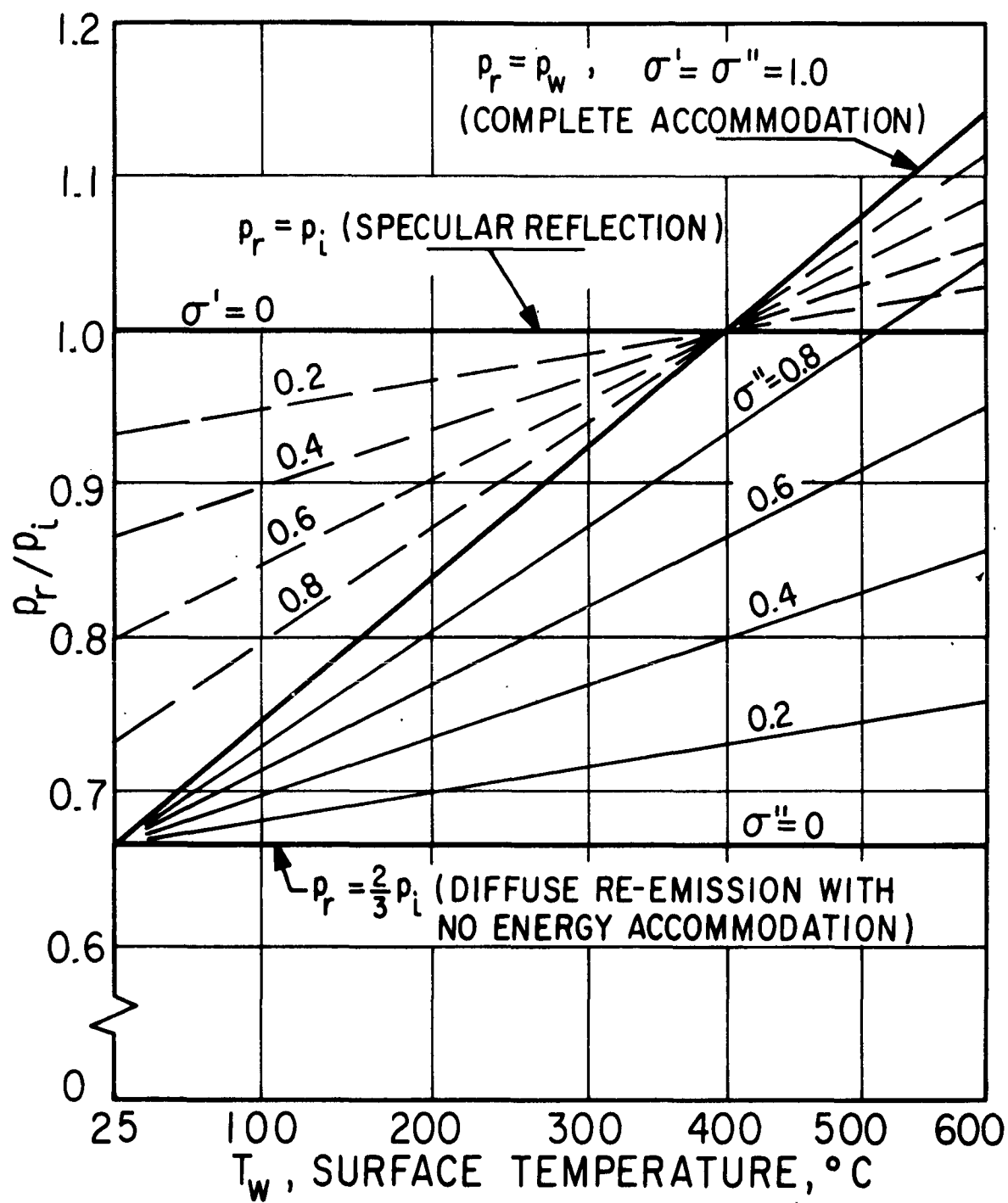


FIG. 16 RE-EMITTED NORMAL MOMENTUM vs SURFACE TEMPERATURE

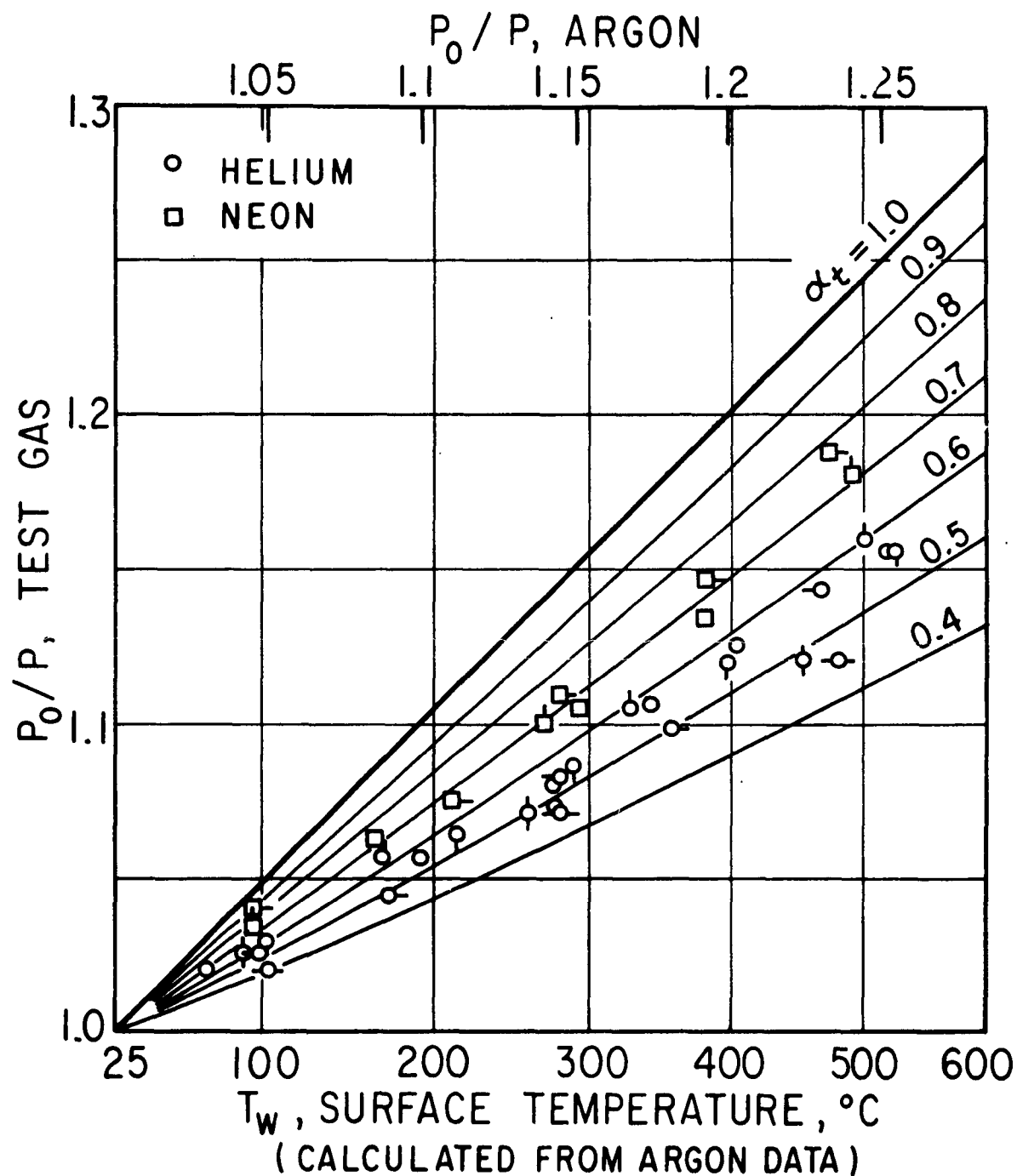


FIG. 17 EXPERIMENTAL RESULTS FOR HELIUM AND NEON ON TUNGSTEN

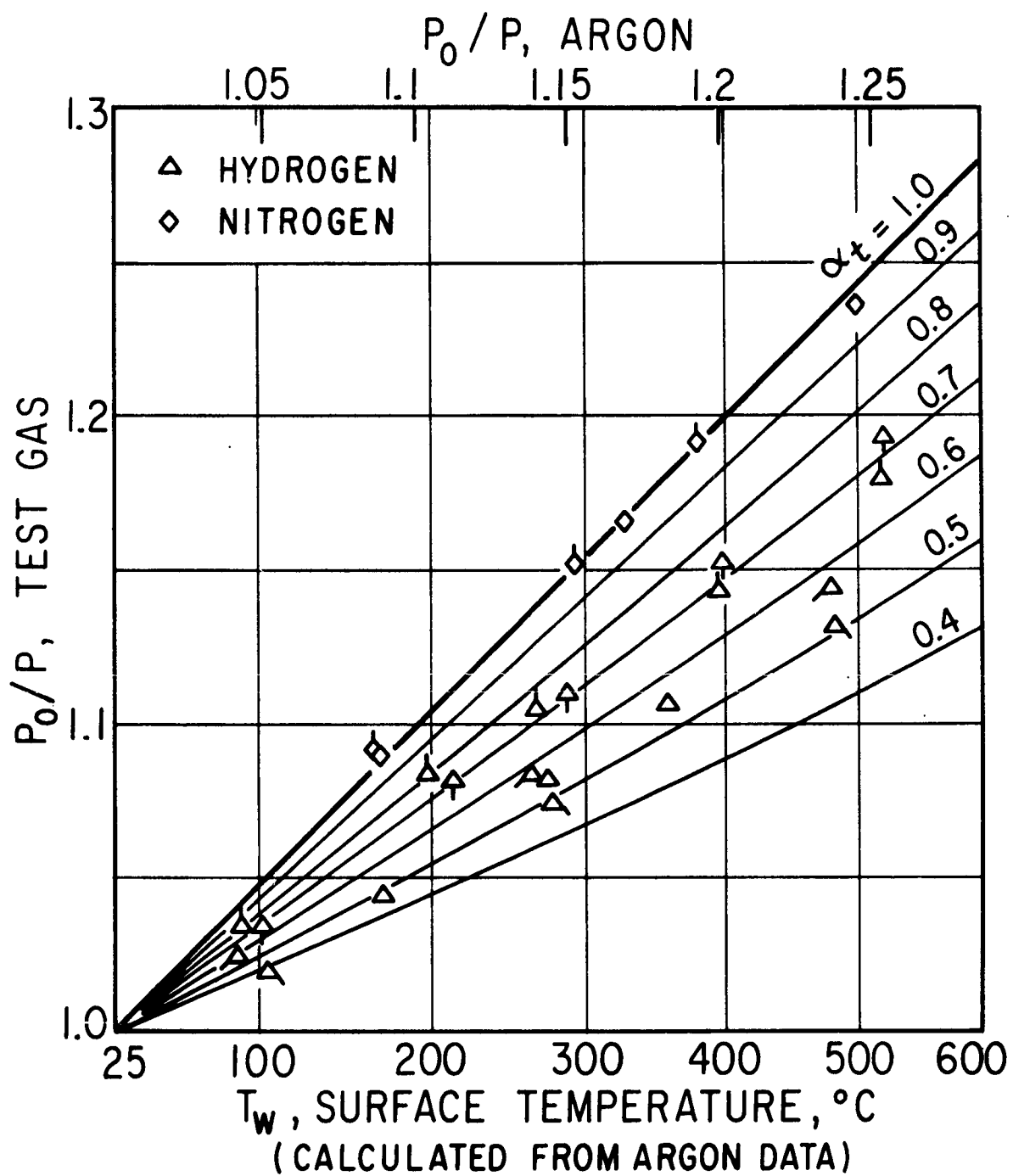


FIG. 18 EXPERIMENTAL RESULTS FOR HYDROGEN AND NITROGEN ON TUNGSTEN

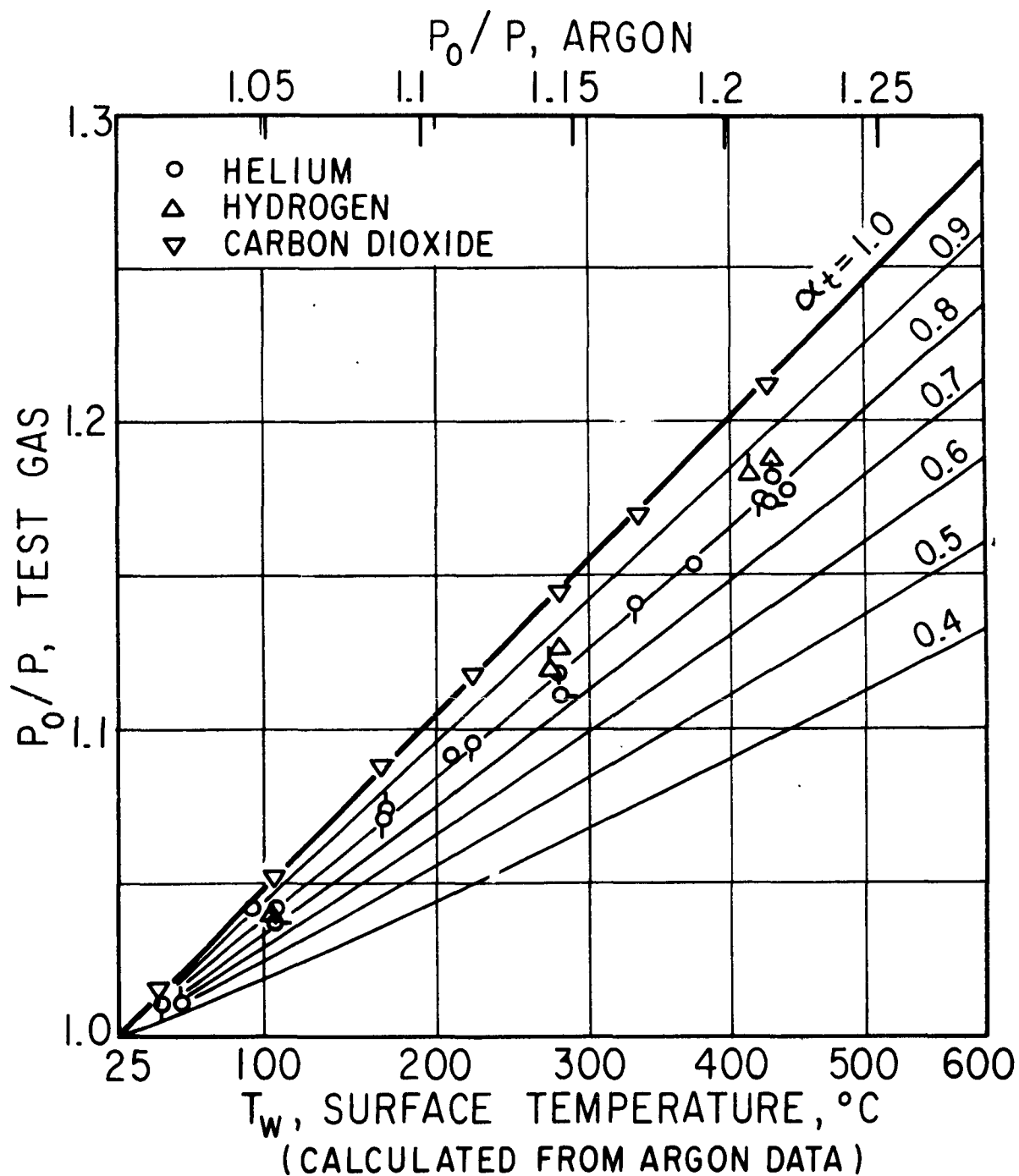


FIG. 19 EXPERIMENTAL RESULTS FOR HELIUM, HYDROGEN, AND CARBON DIOXIDE ON BLACKENED TUNGSTEN

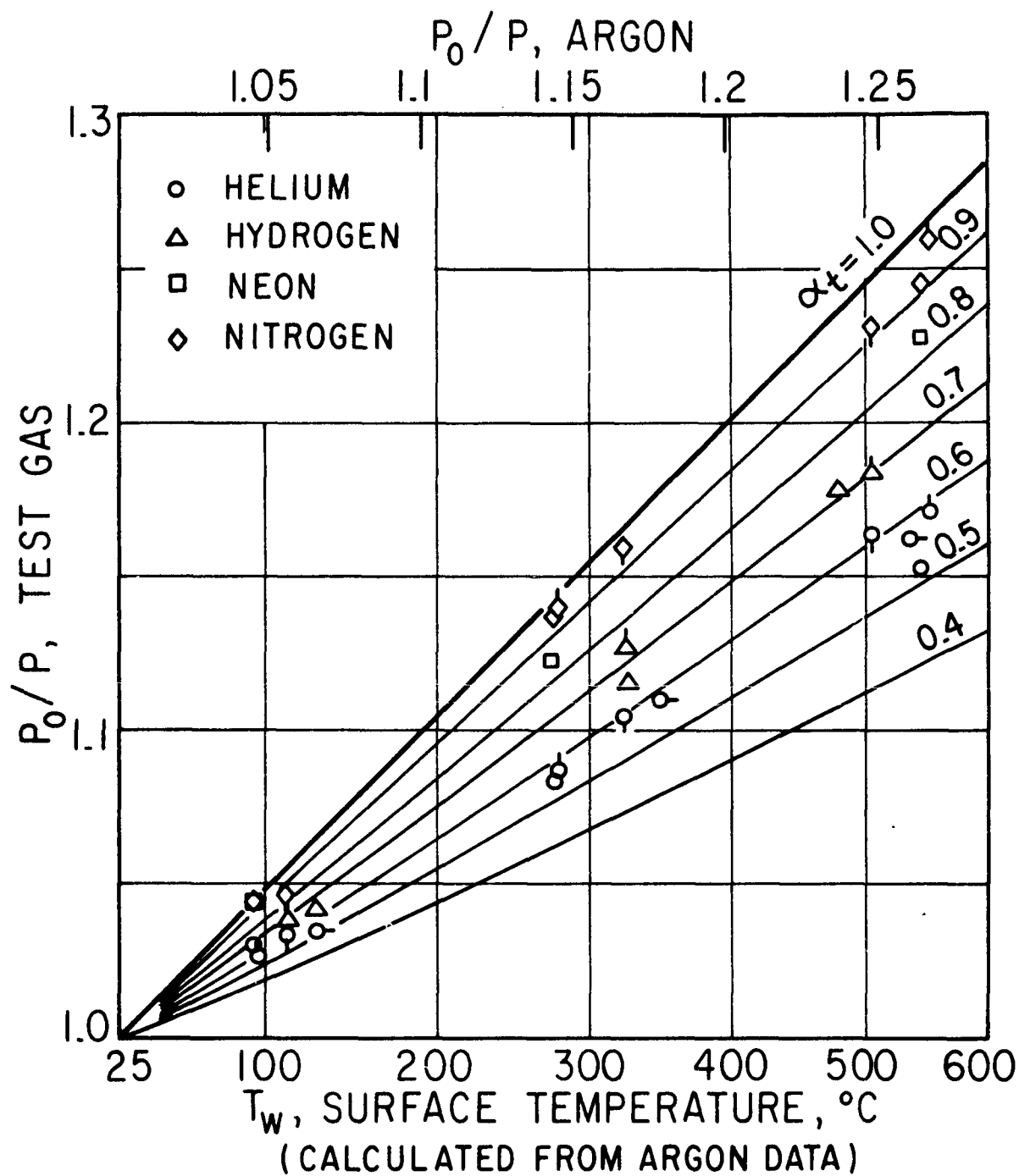


FIG. 20 EXPERIMENTAL RESULTS FOR HELIUM, NEON, HYDROGEN AND NITROGEN ON ALUMINUM

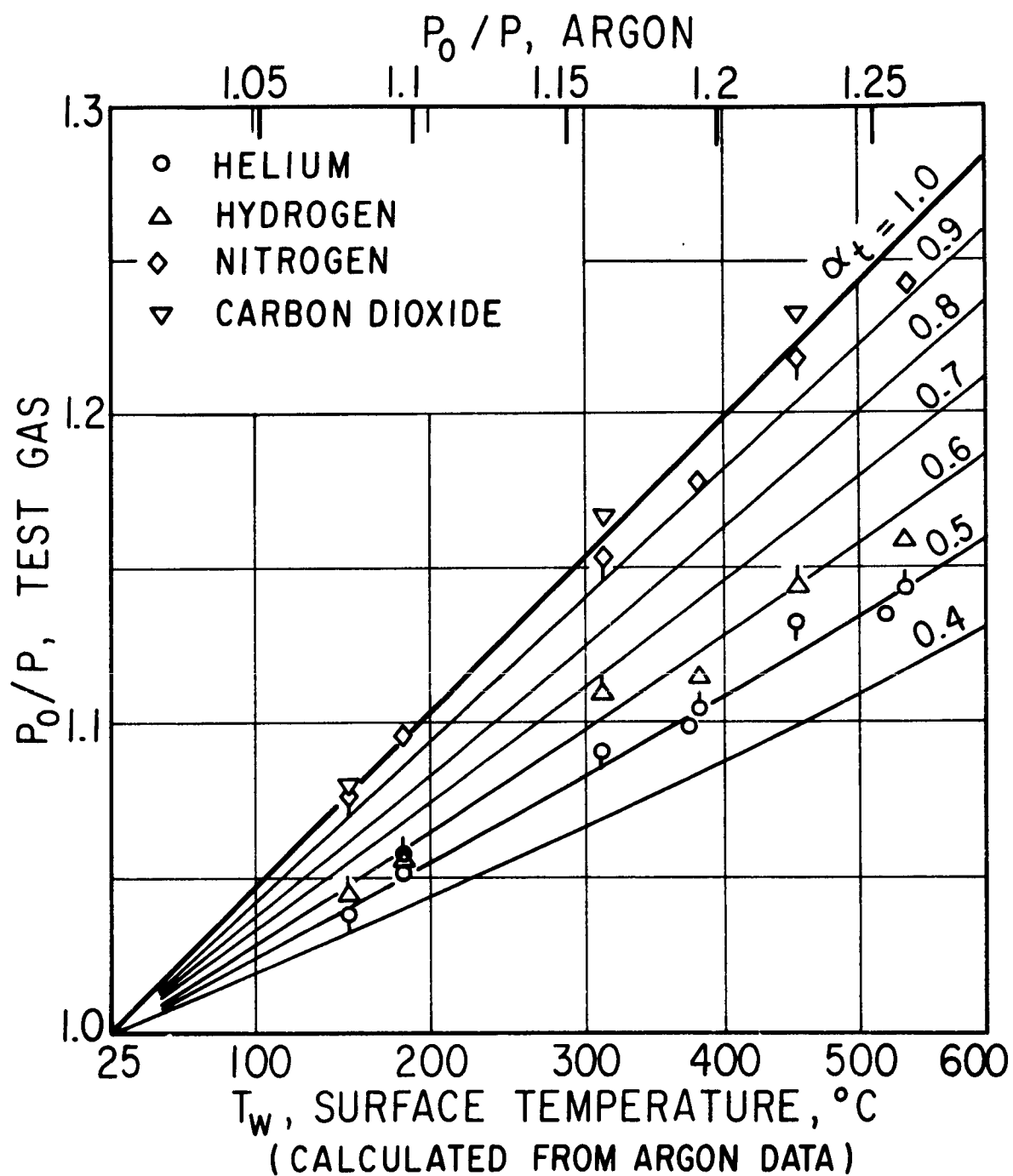


FIG. 21 EXPERIMENTAL RESULTS FOR HELIUM, HYDROGEN, NITROGEN, AND CARBON DIOXIDE ON PLATINUM

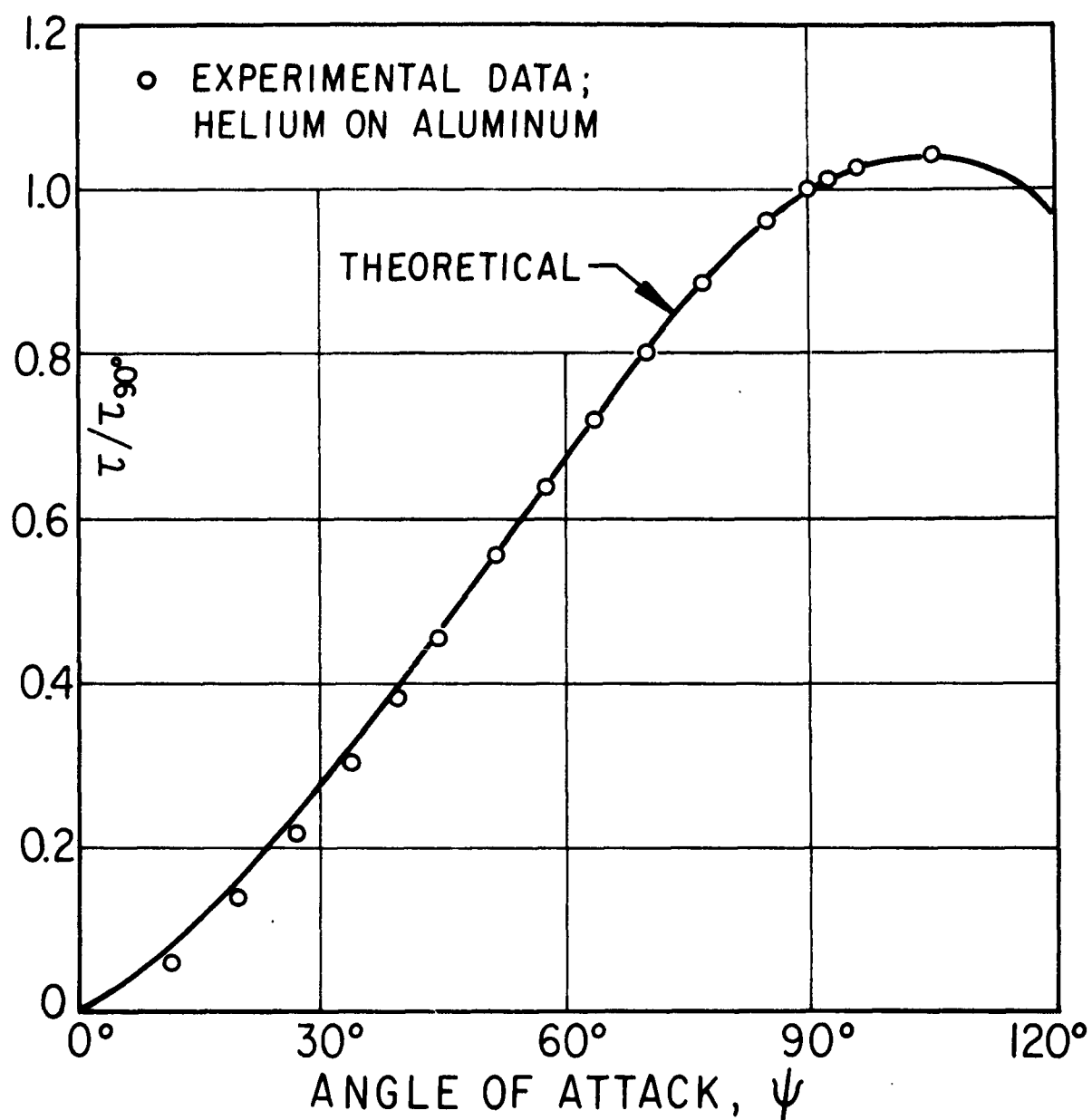


FIG. 22 TORQUE vs ANGLE OF ATTACK FOR UNHEATED TEST SURFACE



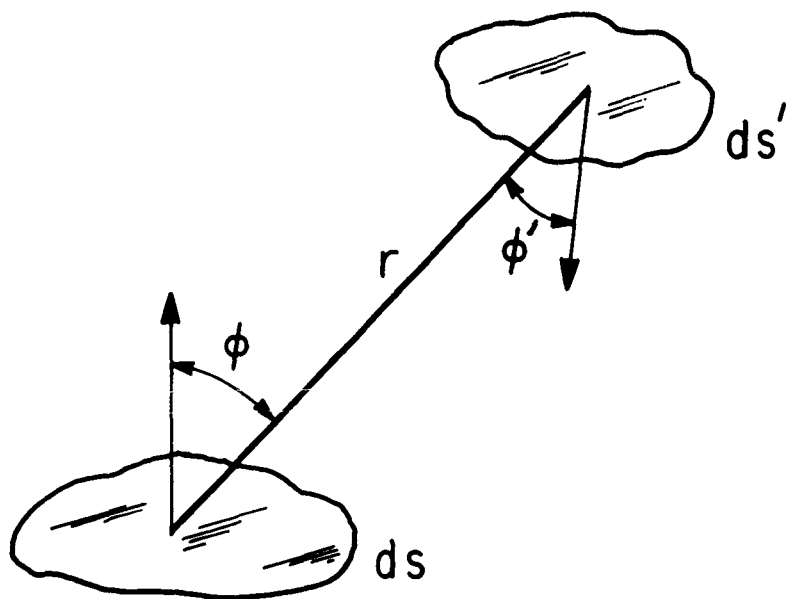


FIG. 23 MOLECULAR BEAM-TEST SURFACE GEOMETRY

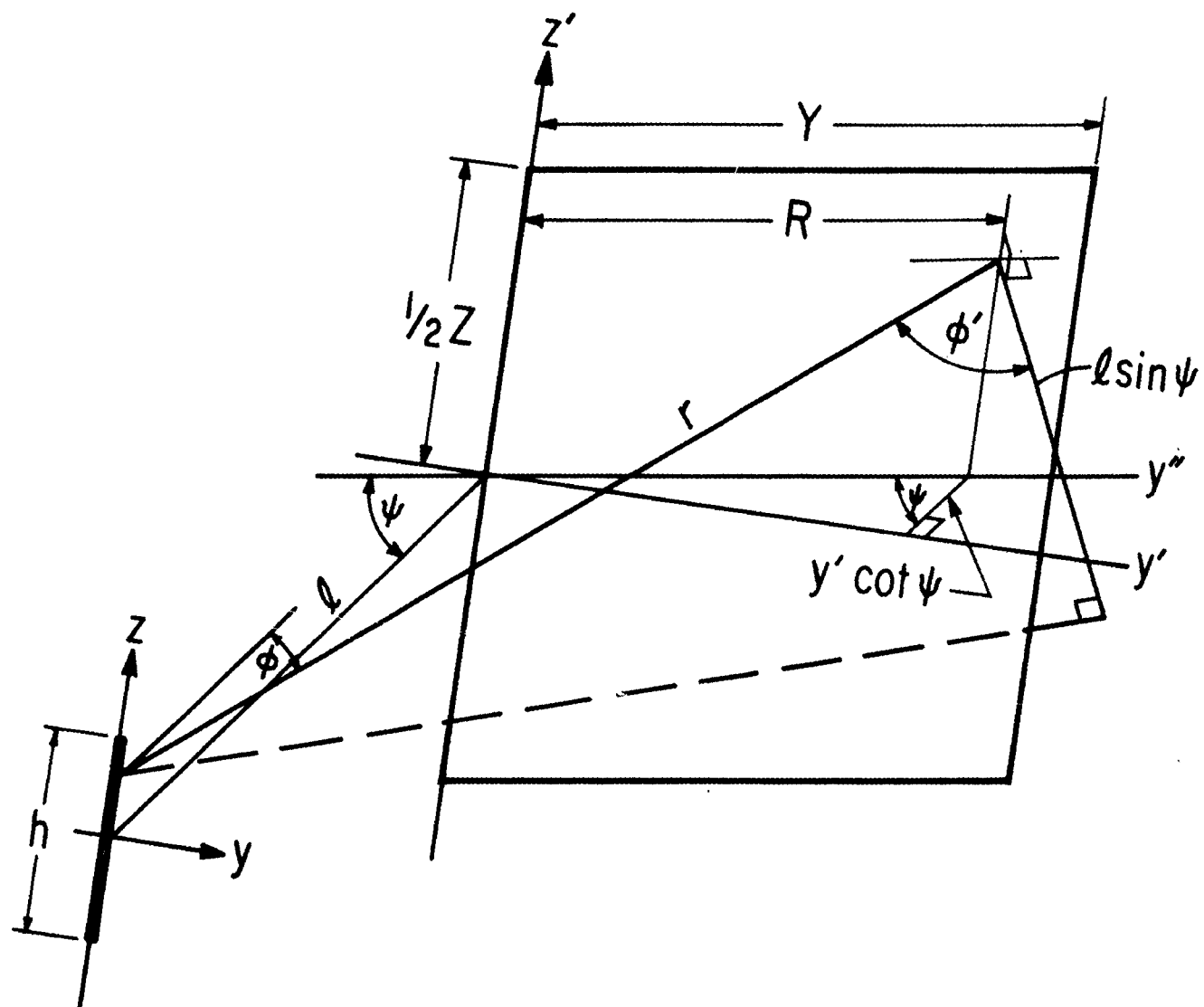


FIG. 24 GEOMETRY FOR APPLIED TORQUE AT  
OBLIQUE ANGLES OF INCIDENCE

**AUTOMATIC DISTRIBUTION LIST FOR UNCLASSIFIED  
TECHNICAL REPORTS - 2/18/59**

**NAVY**

Chief of Naval Research Department of the Navy Washington 25, D. C. Attn: Code 438 (2) Code 419 (1) Code 461 (1)	Chief, Bureau of Aeronautics Department of the Navy Washington 25, D. C. Attn: Research Division Aero & Hydro Branch (2)
Commanding Officer Office of Naval Research Branch Office 150 Causeway Street Boston, Massachusetts (1)	Commanding Officer and Director David Taylor Model Basin Carderock, Maryland Attn: Aerodynamics Laboratory (1)
Commanding Officer Office of Naval Research Branch Office The John Crerar Library Building 86 East Randolph Street Chicago 1, Illinois (1)	Chief, Bureau of Ordnance Department of the Navy Washington 25, D. C. Attn: Code Re 0 (1) Code Re S1-e (1)
Commanding Officer Office of Naval Research Branch Office 346 Broadway New York 13, New York (1)	Commander Dahlgren Proving Ground Dahlgren, Virginia Attn: Technical Library (1)
Commanding Officer Office of Naval Research Branch Office 1030 East Green Street Pasadena 1, California (1)	Commander Naval Ordnance Test Station Inyokern, China Lake, California Attn: Technical Library (1) Code 501 (1)
Commanding Officer Office of Naval Research Fleet Post Office Navy No. 100, Box 39 New York, New York (15)	Commander Naval Ordnance Laboratory White Oak, Maryland Attn: Hyperballistics Division (1) Aeroballistics Division (1) Aerophysics Division (1)
Commanding Officer Office of Naval Research Branch Office 1000 Geary Blvd. San Francisco 9, California (2)	Commander Office of Scientific Research Air Research & Development Command P.O. Box 1395 Baltimore 3, Maryland (1)
Director Naval Research Laboratory Washington 25, D. C. Attn: Code 2021 (6)	Chief, Bureau of Yards & Docks Department of the Navy Washington 25, D. C. Attn: Plans & Research Section (1)
	Superintendent Naval Postgraduate School Monterey, California (1)

NAVY (cont.)

U.S. Naval Air Material Test  
Center  
Point Mugu, California  
Attn: Chief Scientist (1)

AIR FORCE

Commander  
Air Force Office of Scientific  
Research  
Washington 25, D. C.  
Attn: Mechanics Division

Director  
Office for Advanced Studies  
Air Force Office of Scientific  
Research  
Box 2035  
Pasadena 2, California (1)

Commander  
Western Development Division  
Air Research & Development Command  
P.O. Box 262  
Inglewood, California (1)

Commander  
Air Force Cambridge Research  
Center  
230 Albany Street  
Cambridge 39, Massachusetts  
Attn: Geo-Phys. Research Library (1)

Arnold Engineering Development  
Center Library  
P.O. Box 162  
Tullahoma, Tennessee  
Attn: Dr. J. Lukasiewicz (2)

Commander  
Wright Air Development Center  
Wright-Patterson Air Force Base  
Dayton, Ohio  
Attn: Aeronautical Research Lab (1)  
Aircraft Laboratory (1)

ARMY

Office of Ordnance Research  
Department of the Army  
Duke Station  
Durham, North Carolina (1)

Ballistics Research Laboratory  
Aberdeen Proving Ground  
Aberdeen, Maryland  
Attn: Dr. R.H. Kent (1)  
Dr. F.D. Bennett (1)

Internal Ballistics Laboratory  
Aberdeen Proving Ground  
Aberdeen, Maryland  
Attn: Dr. J.H. Frazer (1)

Commanding General  
Redstone Arsenal, U.S. Army  
Redstone Arsenal, Alabama  
Attn: Technical Library (1)

NACA

Director of Research  
National Aeronautics and Space  
Administration  
1512 H Street, N.W.  
Washington 25, D. C. (5)

Director  
Langley Research Center, NASA  
Langley Field  
Hampton, Virginia (1)

Director  
Ames Research Center, NASA  
Moffett Field, California (1)

Director  
Lewis Research Center, NASA  
21000 Brookpark Road  
Cleveland 35, Ohio (1)

Western Coordination Office  
National Aeronautics and Space  
Administration  
7660 Beverly Blvd.  
Los Angeles, California (1)

DEPARTMENT OF DEFENSE

Chief  
Armed Forces Special Weapons Project  
P.O. Box 2610  
Washington 25, D. C. (1)

DEPARTMENT OF DEFENSE (cont.)

Executive Secretary  
Weapons System Evaluation Group  
Office of Secretary of Defense  
The Pentagon  
Washington 25, D. C. (1)

OTHER GOVERNMENT AGENCIES

Director  
National Bureau of Standards  
Washington 25, D. C.  
Attn: Fluid Mechanics Section (1)  
Electron Physics Section (1)

U.S. Atomic Energy Commission  
Technical Information Service  
Washington 25, D.C.  
Attn: Technical Librarian (1)

National Science Foundation  
Division of Mathematical, Physical  
and Engineering Sciences  
Washington 25, D. C. (1)

Documents Service Center  
Armed Services Technical  
Information Agency  
Arlington Hall Station  
Arlington 12, Virginia (5)

Office of Technical Services  
Department of Commerce  
Washington, D. C. (1)

EDUCATIONAL INSTITUTIONS

Prof. R.F.Probstein  
Division of Engineering  
Brown University  
Providence 12, Rhode Island (1)

Aeronautical Laboratory  
Division of Engineering  
Brown University  
Providence 12, Rhode Island  
Attn: Dr. Maeder (1)

Metcalf Laboratory  
Brown University  
Providence 12, Rhode Island  
Attn: Prof. D.F.Hornig (1)

Los Alamos Scientific Laboratory  
University of California  
Los Alamos, New Mexico  
Attn: Theoretical Division,  
Dr. J.L.Tuck (1)  
Dr. R.G.Shreffler (1)  
J-1 Division,  
Dr's. Duff and Graves (1)

Jet Propulsion Laboratory  
California Institute of Technology  
Pasadena 4, California  
Attn: Dr. P. Wegener (1)

Guggenheim Aeronautical Laboratory  
California Institute of Technology  
Pasadena 4, California  
Attn: Prof.C.B.Millikan,Director (1)  
Prof. Lester Lees (1)  
Prof. H.W.Liepmann (1)  
Prof. J. Cole (1)

Department of Physics  
California Institute of Technology  
Pasadena 4, California  
Attn: Prof. F. Zwicky (1)

Radiation Laboratory  
University of California  
Livermore, California  
Attn: Dr. S. A. Colgate (1)  
Dr. R. Post (1)

Department of Aerodynamics  
Case Institute of Technology  
Cleveland 6, Ohio  
Attn: Prof. G. Kuerti (1)

Yerkes Observatory  
University of Chicago  
Williams Bay, Wisconsin  
Attn: Prof. S. Chandrasekhar (1)

Graduate School of Aeronautical  
Engineering  
Cornell University  
Ithaca, New York  
Attn: Prof. W. Sears (1)  
Prof. E. L. Resler, Jr. (1)

Cornell Aeronautical Laboratory  
4455 Genesee Street  
Buffalo, New York  
Attn: Dr. A. Hertzberg (1)

Department of Engineering Sciences  
Harvard University  
Cambridge 38, Massachusetts  
Attn: Prof. G. Carrier (1)  
Prof. H. Emmons (1)

Harvard Observatory  
Harvard University  
Cambridge, Massachusetts  
Attn: Prof. F. Whipple (1)

Department of Aeronautical  
Engineering  
University of Illinois  
Urbana, Illinois  
Attn: Prof. H. S. Stillwell,  
Chairman (1)

Armour Research Foundation  
Illinois Institute of Technology  
Chicago 16, Illinois  
Attn: Dr. A. Ritter (1)

Department of Aeronautics  
Johns Hopkins University  
P.O. Box 244 - Rt. 1  
Laurel, Maryland  
Attn: Dr. F. N. Frenkiel  
Technical Reports Office (2)

Department of Physics  
Lehigh University  
Bethlehem, Pennsylvania  
Attn: Prof. R. J. Emrich (1)

Institute for Fluid Mechanics  
and Applied Mathematics  
University of Maryland  
College Park, Maryland  
Attn: Prof. Burgers (1)

Department of Aeronautical  
Engineering  
Massachusetts Institute of Technology  
Cambridge 39, Massachusetts  
Attn: Prof. H. G. Stever (1)  
Prof. L. Trilling (1)

Department of Mathematics  
Massachusetts Institute of Technology  
Cambridge 39, Massachusetts  
Attn: Prof. C. C. Lin (1)

Department of Mechanical Engineering  
Massachusetts Institute of Technology  
Cambridge 39, Massachusetts  
Attn: Prof. J. Kaye (1)

Department of Aeronautical Engineering  
University of Michigan  
Ann Arbor, Michigan  
Attn: Prof. W. C. Nelson (1)

Engineering Research Institute  
University of Michigan  
Ann Arbor, Michigan  
Attn: Prof. O. Laporte (1)  
Prof. G. Uhlenbeck (1)

Department of Astronomy  
University of Michigan  
Ann Arbor, Michigan  
Attn: Prof. L. Goldberg (1)

Department of Aeronautical Engineering  
University of Minnesota  
Minneapolis, Minnesota  
Attn: Prof. J. D. Akerman, Chairman (1)

Institute of Meteoritics  
University of New Mexico  
Albuquerque, New Mexico  
Attn: Prof. L. LaPaz (1)

Institute for Mathematics and  
Mechanics  
New York University  
25 Waverly Place  
New York 3, New York  
Attn: Prof. R. Courant, Director (1)  
Prof. J. Stoker (1)

Guggenheim School of Aeronautics  
New York University  
New York 53, New York  
Attn: Prof. J. F. Ludloff (1)

Department of Mechanical Engineering  
Northwestern University  
Evanston, Illinois  
Attn: Prof. A. B. Cambel (1)

Department of Physics  
University of Oklahoma  
Norman, Oklahoma  
Attn: R. G. Fowler (1)

Distribution List  
February 18, 1959

Page 5.

Dr. Loren E. Bollinger  
The Ohio State University  
Rocket Research Laboratory  
2240 Olentangy River Road  
Columbus 10, Ohio (1)

Aerodynamics Laboratory  
Polytechnic Institute of Brooklyn  
Freeport, L.I., New York  
Attn: Prof. A. Ferri (1)

Palmer Physical Laboratory  
Princeton University  
Princeton, New Jersey  
Attn: Prof. W. Bleakney (1)  
Prof. W.C.Griffith (1)

Department of Aeronautical Engineering  
Princeton University  
Princeton, New Jersey  
Attn: Prof. S. Bogdonoff (1)  
Prof. W. Hayes (1)

Princeton University Observatory  
Princeton, New Jersey  
Attn: Prof. L. Spitzer, Jr. (1)

Department of Aeronautical Engineering  
Rensselaer Polytechnic Institute  
Troy, New York  
Attn: Prof's. Harrington & Foa (1)

Engineering Center  
University of Southern California  
University Park  
Los Angeles 7, California  
Attn: Dr's R.Chuan & C.L.Daily (1)

Guggenheim Aeronautical Laboratory  
Stanford University  
Stanford, California  
Prof. W. Vincenti (1)

Defense Research Laboratory  
University of Texas  
P.O.Box 8029  
Austin, Texas  
Attn: M.J.Thompson (1)

College of Engineering  
Univ. of Calif., Los Angeles  
Los Angeles 24, California  
Attn: Dean L.M.K.Boelter (1)

Department of Physics  
Univ. of Calif., Los Angeles  
Los Angeles 24, California  
Attn: Prof. J. Kaplan (1)

Experimental Research Group  
University of Utah  
Salt Lake City, Utah  
Attn: Prof. M.A.Cook, Director (1)

Department of Aeronautical Engineering  
University of Washington  
Seattle 5, Washington  
Attn: Department Librarian (1)

Department of Chemistry  
University of Wisconsin  
Madison, Wisconsin  
Attn: Prof. J.O.Hirschfelder (1)

Sterling Chemistry Laboratory  
Yale University  
New Haven, Connecticut  
Attn: Prof. J.G.Kirkwood (1)

CANADA

Institute of Aerophysics  
University of Toronto  
Toronto 5, Canada  
Attn: Dr.G.N.Patterson,Director (1)

Division of Mechanical Engineering  
National Research Laboratories  
Ottawa, Canada  
Attn: Dr.K.Orlik,Dr.Ruckemann (1)

INDUSTRIAL ORGANIZATIONS

Aerojet Engineering Corporation  
6352 North Irwindale Avenue  
Box 296  
Azusa, California (1)

ARO, Inc.  
Tullahoma, Tennessee  
Attn: Dr's R.W.Perry & R.Smelt (1)

Miss Spence, Librarian  
AVCO Manufacturing Company  
Research Laboratories  
2385 Revere Beach Parkway  
Everett 49, Massachusetts  
Attn: Dr's Kantrowitz & Lin (2)

INDUSTRIAL ORGANIZATIONS (cont.)

AVCO Manufacturing Company Lycoming Division Stratford, Connecticut Attn: Dr. J. C. Keck (1)	The Glenn L. Martin Company Department 520, Mail No. 3072 Baltimore 3, Maryland Attn: Mr. L. Cooper (1)
Bell Aircraft Corporation Box 1 Buffalo 5, New York Attn: Dr. J.F.Isenberg (1)	Gruen Applied Science Laboratories Meadowbrook National Bank Building 60 Hempstead Avenue Hempstead, New York Attn: J. Kindestin, Librarian (1)
Boeing Airplane Company Box 3107 Seattle 14, Washington (1)	Grumman Aircraft Engineering Corp. Bethpage, L.I., New York (1)
Borg-Warner Corporation Research Center Applied Physics Group Des Plaines, Illinois Attn: Mr. Roy J. Heyman (1)	Hughes Aircraft Corporation Research and Development Laboratory Culver City, California Attn: Dr. A.E.Puckett (1)
Chance-Vought Aircraft Corporation Dallas, Texas (1)	Dr. Louis N. Ridenour Director of Research Lockheed Missiles & Space Division P.O. Box 504 Sunnyvale, California (1)
CONVAIR San Diego Division San Diego 12, California Attn: Dr. W.H.Dorrance (1)	Marquardt Aircraft Corporation 7801 Havehurst Van Nuys, California (1)
Douglas Aircraft Company, Inc. 3000 Ocean Park Blvd. Santa Monica, California (1)	Midwest Research Institute Department of Physics 4049 Pennsylvania Avenue Kansas City, Missouri Attn: Mr. K.L.Sandefur (1)
Fairchild Engine & Aircraft Company Guided Missiles Division Wyandanch, L.I., New York (1)	North American Aviation, Inc. Aerophysics Department 12214 Lakewood Blvd. Downey, California Attn: Dr. van Driest (1)
Fairchild Engine & Aircraft Company Fairchild Engine Division Farmingdale, L.I., New York Attn: Mrs. C.Minck, Librarian (1)	Northrop Aircraft, Inc. Northrop Field Hawthorne, California (1)
General Electric Company Research Laboratory P.O.Box 1088 Schenectady, New York Attn: Dr's Nagamatsu, White, and Alpher (1)	Technical Librarian Ramo-Wooldridge Corporation 8820 Bellance Avenue Los Angeles 45, California Attn: Dr's M.U.Clauser, Doll, & J. Logan (2)
General Electric Company Special Defense Projects Department 3198 Chestnut Street Philadelphia 4, Pennsylvania Attn: Aerophysics Lab. Operation Dr. J. Farber (2)	



INDUSTRIAL ORGANIZATIONS (cont.)

Rand Corporation  
1700 Main Street  
Santa Monica, California  
Attn: E.P. Williams and  
C. Gazley, Jr. (1)

Republic Aviation Corporation  
Farmingdale, L.I., New York (1)

Sandia Corporation  
Sandia Base  
Albuquerque, New Mexico  
Attn: Dr's C.C. Hudson,  
M.L. Merritt, & J.D. Shreve, Jr. (1)

Stanford Research Institute  
Poulter Laboratories  
Palo Alto, California  
Attn: Dr's Poulter and Duvall (1)

United Aircraft Corporation  
Research Department  
362 Main Street  
East Hartford 8, Connecticut (1)

SPECIAL ADDITIONAL LIST FOR  
THEORETICAL PAPERS

Professor M. Holt  
Division of Applied Mathematics  
Brown University  
Providence 12, Rhode Island (1)

Professor H. Lewy  
Applied Mathematics Group  
Mathematics Department  
University of California  
Berkeley 4, California (1)

Professor D. Gilbarg  
Graduate School for Applied  
Mathematics  
Indiana University  
Bloomington, Indiana (1)

Librarian  
Graduate School for Applied  
Mathematics  
Indiana University  
Bloomington, Indiana (1)

Dr. G. Griderley  
P.O. Box 186  
Fairborn 4, Ohio (1)

SPECIAL ADDITIONAL LIST FOR  
RAREFIED GASES

Mr. K. M. Siegel  
Upper Atmosphere Section  
Willow Run Research Center  
University of Michigan  
Ypsilanti, Michigan (1)

Professor A. H. Kuhlthau  
Department of Physics  
University of Virginia  
Charlottesville, Virginia (1)

Australian Weapons Research  
Establishment  
c/o Defence Research and  
Development Representative  
Australian Joint Service Staff  
P.O. Box 4837  
Washington 8, D. C. (1)